UNIVERSITAT DE BARCELONA

Molecular mechanisms of resistance to therapy in glioblastoma

Leire Pedrosa Eguílaz

UNIVERSITAT DE BARCELONA

Molecular mechanisms of resistance to therapy in glioblastoma

Tesis presentada per

Leire Pedrosa Eguílaz

Tesis dirigida per

Dra. Núria de la Iglesia Zaragoza

Tesis realitzada a

Institut d'Investigacions Biomèdiques August Pi i Sunyer (IDIBAPS)

Leire Pedrosa Eguílaz
Doctoranda

Núria de la Iglesia Zaragoza
Directora de la tesi

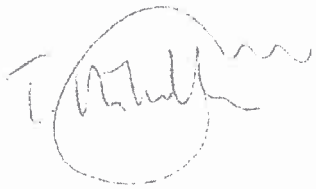

Teresa Ribalta Farrés
Tutora de la tesi

Programa de doctorat en Biomedicina

Facultat de Medicina

Universitat de Barcelona 2020

CONTENTS

ABBREVIATIONS

ANOVA: Analysis of Variance

ASO: Antisense Oligonucleotide

ATRX: Alpha-Thalassemia/Mental Retardation Syndrome X-Linked

BANCR: (BRAF)-Activated Noncoding RNA

bFGF: Basic Fibroblast Growth Factor

C/EBPβ: CCAAT/Enhancer-Binding Protein Beta

CD109: Cluster of Differentiation 109

CD44: Cluster of Differentiation 44

CDKN2A: Cyclin-Dependent Kinase Inhibitor 2A

ceRNA: Competing For Endogenous RNA

CHART: Capture Hybridization Analysis Of RNA Targets

CHI3L1: Chitinase-3-Like Protein 1

CI: Confidence Interval

CIC: Cancer Initiating Cell

CL: Classical

CNAG: Centro Nacional de Análisis Genómico

CNS: Central Nervous System

CTRL: Control

CRISPR: Clustered Regularly Interspaced Short Palindromic Repeats

CRNDE: Colorectal Neoplasia Differentially Expressed

CSC: Cancer Stem Cells

CTGF: Connective Tissue Growth Factor

DDI: Distilled De-Ionized

DMEM: Dulbecco's Modified Eagle Medium

DMSO: Dimethyl Sulfoxide

DNA: Deoxyribonucleic Acid

DNMT1: DNA Methyl Transferase 1

DSBs: Double-Strand Breaks

DTT: Dithiothreitol

ECM: Extracellular Matrix

EGF: Epidermal Growth Factor

EGFR: Epidermal Growth Factor Receptor

EMT: Epithelial To Mesenchymal Transition

ERBB2: Erb-B2 Receptor Tyrosine Kinase 2

ESC: Embryonic Stem Cell

FACS: Fluorescence Activated Cell Sorting

FBS: Fetal Bovine Serum

FDA: Food Drug Administration

FFPE: Paraffin-Embedded

FN1: Fibronectin 1

GBM: Glioblastoma or Glioblastoma Multiforme

G-CIMP: Glioma-Cpg Island Methylator Phenotype

GEP: Gene Expression Profiling

GF: Growth Factor

GFP: Green Fluorescent Protein

GIC: Glioma Iniating Cell

GPCR: G-Protein Coupled Receptor

GPR56: G-Protein Coupled Receptor 56

GPS: GPCR Proteolytic Site

gRNA: Guide RNA

GSCs: Glioma Stem-Cells

GSEA : Gene Set Enrichment Analysis

HC: Hierarchical Clustering

HCC: Hepato Cellular Carcinoma

HGF: Hepatocyte Growth Factor

hnRNP-K: Heterogeneous Nuclear Ribonucleoprotein K

HOTAIR: HOX Transcript Antisense RNA

HOX: Homeobox

HR: Hazard Ratio

IDH: Isocitrate Dehydrogenase

IDH-wt: IDH-Wild Type

IkB: Inhibitor of Kappa B

IKK: Inhibitor of Kappa Kinase

IL6: Interleukin 6

IR: Infrared

KAP1: Kinesin-ii-Associated Protein1

KD: Knockdown

kDa: KiloDaltons

KM: Kaplan–Meier

KO: Knockout

lncRNA: Long-Non-Coding RNAs

MAD: Maximum Absolute Deviation

MCAM: Melanoma Cell Adhesion Molecule

MDM2: Murine Doble Minute 2

MERTK: C-Mer Proto-Oncogene Tyrosine Kinase

MES: Mesenchymal

mESCs: Mouse Embryonic Stem Cells

MET: Mesenchymal-Epithelial Transition Factor

MMP9: Matrix Metallopeptidase 9

MR: Magnetic Resonance

MREs: miRNA Response Elements

MRI: Magnetic Resonance Imaging

mRNA: Messenger RNA

mTOR: mammalian Target of Rapamycin

MW: Multi-Well

NCL: Nucleolin

ncRNAs: Noncoding Ribonucleic Acids

NES: Normalized Enrichment Scores

NF1: Neurofibromatosis Type 1

NF-κB: Nuclear Factor-kappaB

NHEJ: Non-Homologous End Joining

NKX2-2: Nk2 Homeobox 2

NMF: Non-Negative Matrix Factorization

NPC: Neural Progenitor Cells

Npsh: Neurospheres

NSC: Neural Stem Cell

OLIG: Oligodendrocyte Transcription Factor

OPC: Oligodendrocyte Precursor Cells

ORF: Open Reading Frame

Par: Parental

PAUPAR: Pax6 Upstream Antisense RNA

PBS: Phosphate-Buffered Saline

PC: Protein-Coding RNA

PCR: Polymerase Chain Reaction

PDGFR: Platelet-Derived Growth Receptor

PDLSC: Periodontal Ligament Stem Cells

PIK3CA: Phosphatidylinositol 3-Kinase, Catalytic, Alpha Polypeptide

PIK3R1: Phosphatidylinositol 3-Kinase Regulatory

PMT: Proneural to Mesenchymal Differentiation

PN: Proneural

PRC2: Polycomb Repressive Complex 2

PRKCA: Protein Kinase C Alpha

PROCAR: Proneural C/Ebpβ-Associated Lncrna

PTBP1: Polypyrimidine Tract Binding Protein 1

PTEN: Phosphatase and Tensin Homolog

PTN: Pleiotrophin

RB1: Retinoblastoma

RDT: Radiotherapy

RFP: Red Fluorescent Protein

RIN: RNA Integrity Number

RNA: Ribonucleic Acid

ROS: Reactive Oxygen Species

rRNA: Ribosomal RNA

RT-qPCR: Quantitative Real-Time PCR

scTDA: Single-Cell Topological Data Analysis

SEM: Standard Error Of The Mean.

sgRNA: Small Guide RNA

SOM: Self-Organizing Maps

SOX2: Sex Determining Region-Box 2

SOX4: SRY-Box 4

STAT3: Signal Transducer and Activator Of Transcription 3

SVM: Support Vector Machines

TALNEC2: Tumor-Associated Long Non-coding RNA Expressed on Chromosome 2

TAZ: Tafazzin

TCGA: The Cancer Genome Atlas

TEC: To be Experimentally Confirmed

TERT: Telomerase Reverse Transcriptase

TF: Transcription Factor

TGFβ: Transforming Growth Factor-Beta 1

TIMP1: Tissue Inhibitors of Metalloproteinases

TME: Tumor Microenvironment

TMZ: Temozolomide

TNFα: Tumour Necrosis Factor-alpha

TO: Topological Overlap

TP53: Tumor Protein P53

TRAMP: Transgenic Adenocarcinoma of the Mouse Prostate Model

TUG1: Taurine Upregulated Gene 1

TUNA-lncRNA: Tcl1 Upstream Neuron-Associated Lincrna

VEGF: Vascular Endothelial Growth Factor

WB: Western Blot

WGCNA: Weighted Gene Co-Expression Network Analysis

WHO: World Health Organization

Wt: Wild Type

1 INTRODUCTION

1.1 CHARACTERISTICS OF GLIOMAS

1.1.1 Definition and classification of gliomas

In 2019, the National Cancer Institute estimates that 23,820 adults were diagnosed with brain and other nervous system malignancies and that 17,760 of these diagnoses resulted in death (Bethesda, 2019). Although their incidence is not as high as with other tumours, their anatomical localization and aggressiveness makes these malignancies into a huge burden on society.

Gliomas are defined as tumours that phenotypically resemble glial cells, such as astrocytes, oligodendrocytes or ependymal cells. Accordingly, gliomas are divided into astrocytomas, oligodendrogliomas, ependymomas and mixed gliomas (oligo-astrocytomas) (Louis et al., 2016).

Astrocytomas are the most common type of gliomas in both adults and children. The World Health Organization (WHO) grades astrocytomas based on histological features according to their degree of malignancy into low-grades, including grade I (or pilocytic astrocytoma) and grade II (or diffuse astrocytoma), and high-grades, including grade III (or anaplastic astrocytoma) and grade IV (or glioblastoma multiforme, GBM) (P.Sulman, Guerrero, & Aldape, 2009) (Figure 1.1). Additionally, astrocytomas, of all histological grades, can be subdivided according to their genetic features: the deletional status of chromosomal arms 1p and 19q and the mutational status of Alpha-Thalassemia/mental Retardation syndrome X-linked (ATRX), Tumour Protein p53 (TP53) and Isocitrate Dehydrogenase 1 or 2 (IDH1 or IDH2) (Pisapia, 2017) (Figure 1.1)

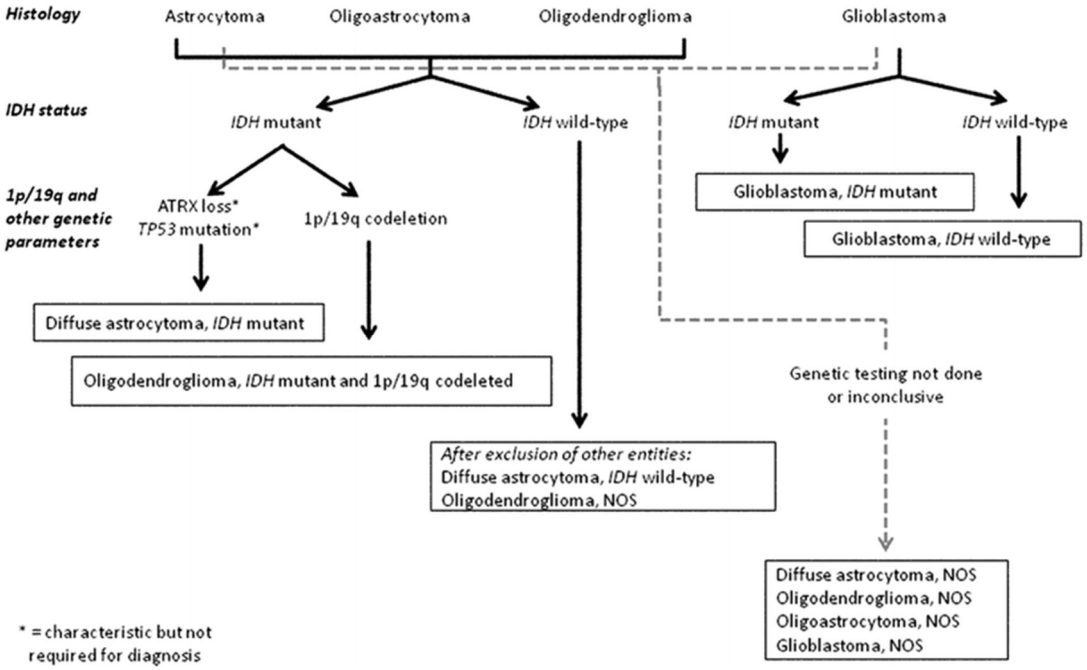

Figure 1.1: A simplified algorithm for the classification of the diffuse gliomas based on histological and genetic features. *Histologically gliomas are classified into astrocytomas, oligoastrocytomas, oligodendrogliomas and glioblastoma. Regarding to their genetic features, all gliomas might be classifiedaccording to the status of IDH (mutant or wild-type), 1p/19q (codeletion or not), ATRX (lost by mutation or wild-type) and TP53 (mutatant or wild-type). NOS (not otherwise specified). (Reprinted from Louis et al., 2016)*

This thesis is focused in glioblastoma (GBM), which is the most malignant and frequent primary brain tumour in adults. It accounts for 54% of all gliomas and 16% of all primary brain tumours (Ostrom et al., 2013).

1.2 GLIOBLASTOMA

1.2.1 GBM epidemiology and pathological features

Glioblastoma is the most frequent and aggressive primary brain tumour in the central nervous system due to its fast clinical course and uniform lethality. Despite the variety of modern therapies against GBM, it is still a deadly disease with extremely poor prognosis. Patients with GBM usually have a median of survival of approximately 15 months from diagnosis (Ohka, Natsume, & Wakabayashi, 2012; Thakkar et al., 2014).

In the 2016, Central Nervous System (CNS) WHO divided GBMs into (1) glioblastoma, IDH-wild type (IDH-wt) (about 90% of cases) (2) glioblastoma, IDH-mutant (about 10% of cases), and (3) glioblastoma NOS, tumours for which full IDH evaluation cannot be performed. The first group, the IDH-wt, corresponds most frequently with the clinically defined primary or *de novo* glioblastoma. On the other hand, the patients classified in the second group, IDH-mut, are closely to secondary glioblastoma (Louis et al., 2016; Tamimi & Juweid, 2017).

The terms “primary GBM” and “secondary GBM” were first used by the German neuropathologist Hans Joachim Scherer in Antwerp in 1940 (Scherer, 1940). Primary or *de novo* GBM accounts for more than 80% of GBM that occurs in older patients (mean age 64 years old), and typically shows Epidermal Growth Factor Receptor (EGFR) over expression, Pleiotrophin (PTN) mutation, Cyclin Dependent Kinase Inhibitor 2A (CDKN2A) deletion, and less frequently Murine Doble Minute 2 (MDM2) amplification. Secondary GBM develops from lower grade astrocytoma or oligodendrogliomas and usually occurs in younger patients (mean age 45 years old). The secondary GBM often contains TP53 mutations (Ohgaki et al., 2004) (Figure 1.2).

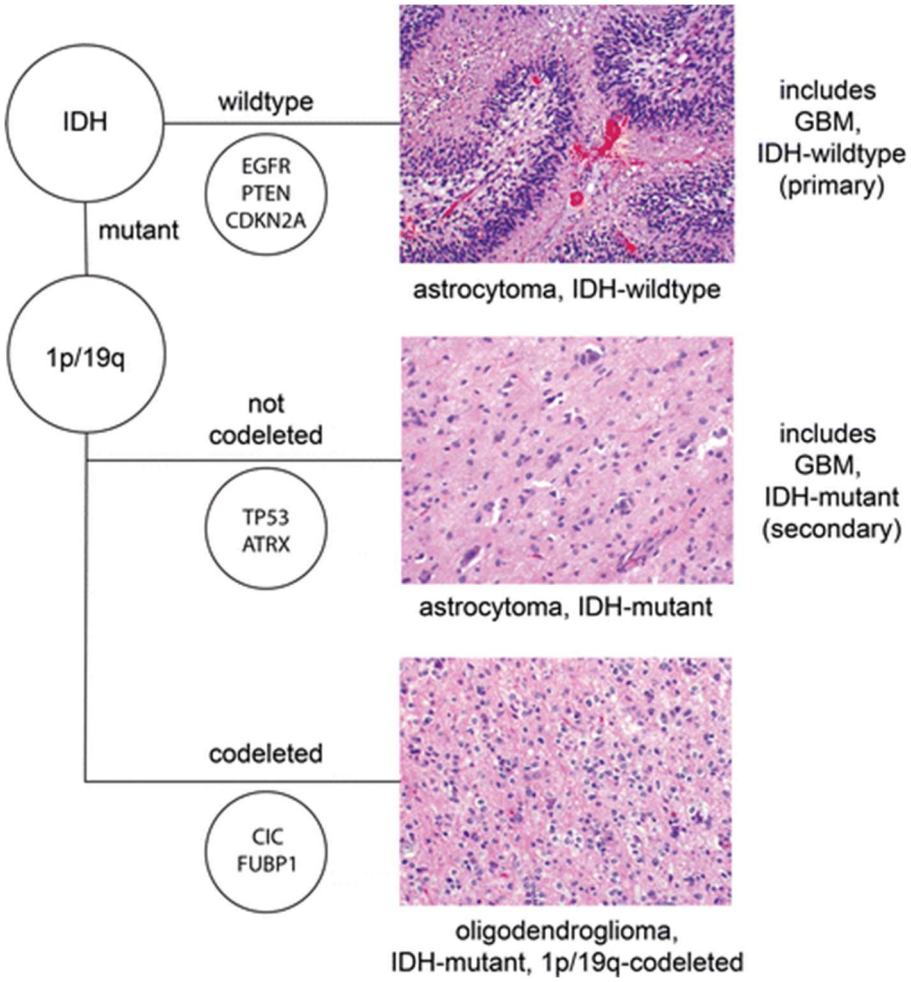

Figure 1.2: World Health Organization classification of infiltrating gliomas. *The diagram depicts the three major categories of adult diffusely infiltrating gliomas based on IDH1/2 mutational status and 1p/19q codeletional status and histologic images stained with hematoxylin-eosin. The category of "astrocytoma, IDH-wildtype" includes glioblastoma, IDH–wild type, also known as primary glioblastoma. The category of "astrocytoma, IDH-mutant" includes glioblastoma, IDH-mutant, also known as secondary glioblastoma. (Reprinted from David et al., 2017)*

Mutations in IDH1 and IDH2 are present in 70–80% of low-grade glioma and secondary GBM, and only in 5–10% of primary GBM (Appin et al., 2013; Dillman et al., 2004; Hartmann et al., 2010; H. Yan et al., 2009). IDH1 mutation is associated with a better outcome and increased overall survival (Ohgaki & Kleihues, 2013). Thus, the IDH1 mutation is a reliable molecular marker for secondary GBM over clinical and pathological criteria (Table 1.1).

Table 1.1: Key characteristics of IDH-wildtype and IDH-mutant GBMs. *In the table are the synonyms of IDH-wt GBM and IDH-mut GBM, the precursor lesion, the proportion of GBM, the median age at diagnosis, the necrosis and the main genetic features. (Modified from Louis et al., 2016)*

	IDH-wild type glioblastoma	**IDH-mutant glioblastoma**
Synonym	Primary glioblastoma, IDH-wt	Secondary glioblastoma, IDH-mut
Precursor lesion	Not identifiable, develops *de novo*	Diffuse astrocytoma, Anaplastic astrocytoma
Proportion of glioblastoma	~90%	~10%
Median age at diagnosis	62 years	44 years
Necrosis	Extensive	Limited
TERT promoter mutations	72%	26%
TP53 mutations	27%	81%
ATRX mutations	Exceptional	71%
EGFR amplification	35%	Exceptional
PTEN mutations	24%	Exceptional

Macroscopically, GBM is quite heterogeneous featuring multifocal haemorrhage, necrosis, and cystic and gelatinous areas (Agnihotri et al., 2013; Smith & Ironside, 2007). A characteristic feature of GBM is the variation in gross appearance of the tumour from one region to the other. The gold standard imaging technique used to detect glioblastoma is magnetic resonance (MR) scans (Figure 1.3A-B). According to CNS WHO classification, histologic criteria for GBM diagnosis includes nuclear atypical, cellular pleomorphism, mitotic activity, vascular thrombosis, microvascular

proliferation and the distinctive necrotic area typically specified as pseudopalisading necrosis (Louis et al., 2007) (Figure 1.3C-D).

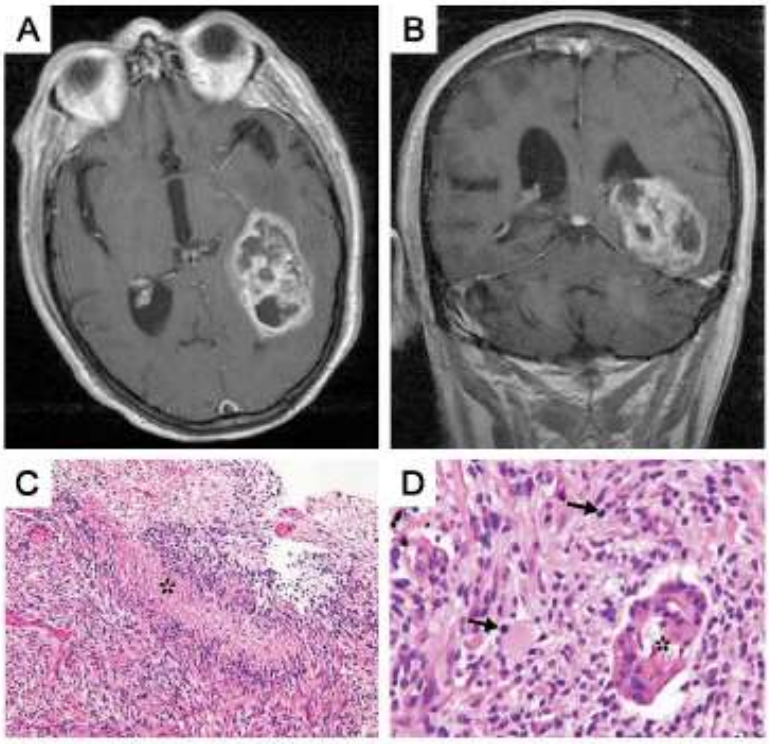

Figure 1.3: Macroscopic and microscopic features of GBM. *(A-B) Axial (A) and coronal (B) magnetic resonance images showing a heterogeneously enhancing mass with central necrosis. (C-D) Histologic appearance of GBM in hematoxylin and eosin stain. (C) Picture with recognizable nuclear pleomorphism, dense cellularity and pseudopalisading necrosis (asterisk). (D) Panel showing vascular-endothelial proliferation (asterisk) and mitotic figures (arrows). (A and B modified from Altman et al. 2007; C and D modified from Wen & Kesari, 2008)*

1.2.2 GBM heterogeneity

1.2.2.1 Inter-tumoural heterogeneity: Molecular classification

Despite all GBM have similar anatomopathologic characteristics; these tumours are very different at the molecular level from one patient to another.

Adult GBMs can be classified according to their gene expression and epigenetic profiles into four different subtypes as follows: glioma-CpG island methylator phenotype (G-CIMP^{+}), associated with IDH 1 and 2 mutation (Figure 1.4:), and three non-G-CIMP (G-CIMP^{-}) subtypes, termed proneural (PN), classical (CL), and mesenchymal (MES) (Brennan et al., 2013; Noushmehr et al., 2010; Verhaak et al., 2010; Q. Wang, Hu, Hu, Kim, et al., 2017) (Figure 1.4 and Figure 1.5).

Verhaak et al. classified GBMs in four subtypes based on transcriptional profile (classical, mesenchymal, neural and proneural). However, the transcriptional footprint left by the tumour microenvironment, which may constitute 10-80% of cells in a tumour biopsy, can obscure the true activity of the signalling network. Wang et al. performed more in silico analysis from glioma samples and glioma cell culture models to provide insights into glioma-intrinsic pathway activities and classification, and to deconvolute the glioma associated stroma into its immunological cellular components. The transcriptional glioma subtypes defined through clustering based on tumour-intrinsic genes strongly overlapped with the PN, CL, and MES subtypes, but identified the neural subtype as normal neural lineage contamination. Thus, currently, the molecular GBM subtypes are PN, CL and MES (Figure 1.5).

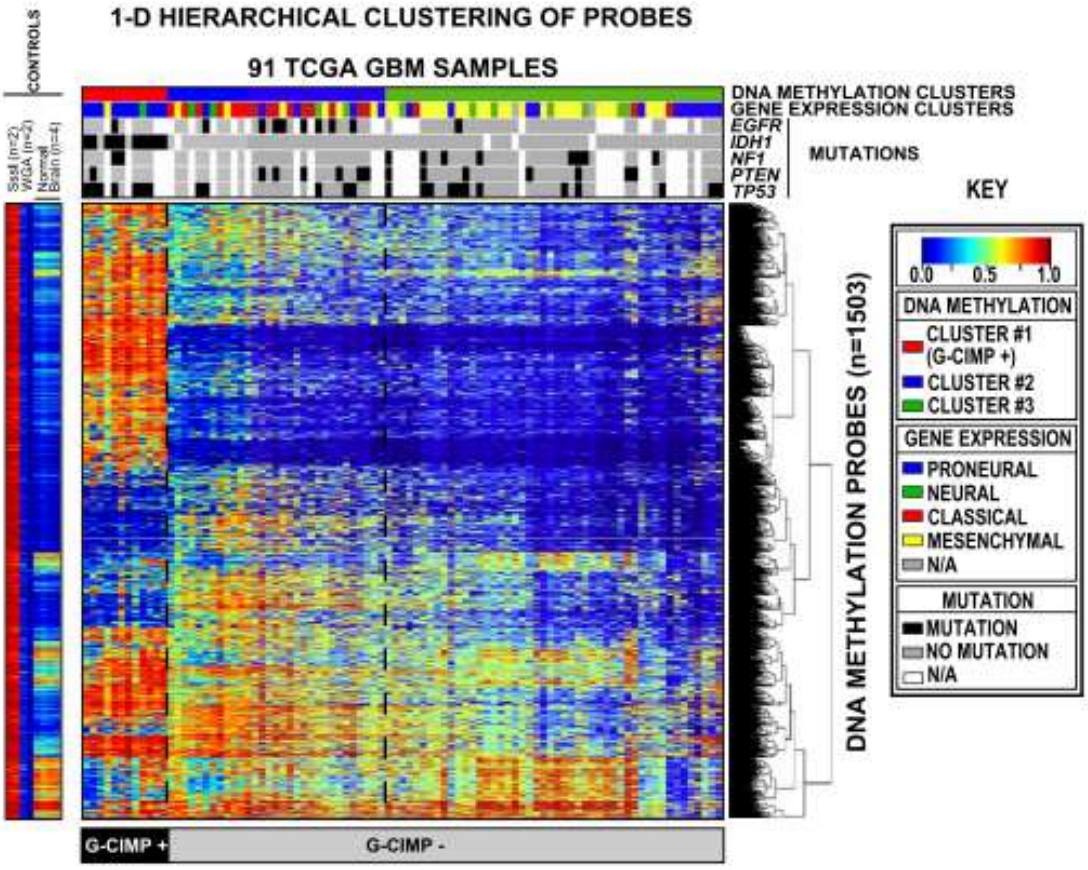

Figure 1.4: Clustering of TCGA GBM tumours and control samples identifies a CPG island methylator phenotype. *DNA methylation clusters are distinguished with a colour code at the top of the panel: red, consensus cluster 1 (n = 12 tumours); blue, consensus cluster 2 (n = 31 tumours); and green, consensus cluster 3 (n = 48 samples). Each sample within each DNA Methylation cluster are colour labelled as described in the key for its gene expression cluster membership (proneural, neural, classical, and mesenchymal from Verhaak et al., 2010 classification). The somatic mutation status of EGFR, IDH1, NF1, PTEN, and TP53) are indicated by the black squares, the grey squares indicate the absence of mutations in the sample, and the white squares indicate that the gene was not screened in the specific sample. G-CIMP-positive samples are labelled at the bottom of the matrix. (Figure reproduced from Noushmehr et al., 2010)*

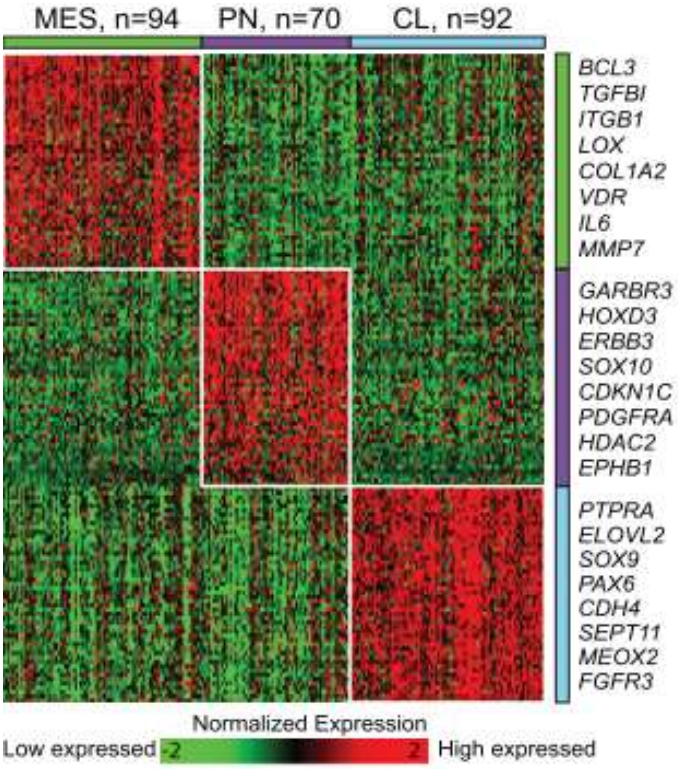

Figure 1.5: Molecular classification of non-G-CIMP GBMs. *Clustering identified three subtypes: PN, CL and MES with different signatures overexpressed. Representative genes are shown for each subtype. (Reprinted from Wang et al., 2017)*

Several studies correlated the genetic alterations with molecular subtypes (PN, MES and CL) and observed that each subtype have different features associated. The Cancer Genome Atlas (TCGA) pilot project identified genetic changes of primary DNA sequence and copy number, DNA methylation, gene expression, and patient clinical information for a set of GBM tumours (The Cancer Genome Atlas Program - National Cancer Institute, 2008).

TCGA reaffirmed genetic alterations in TP53, PTEN, EGFR, Retinoblastoma (RB1), neurofibromatosis type 1 (NF1), Erb-b2 receptor tyrosine kinase 2 (ERBB2), Phosphatidylinositol 3-kinase regulatory (PIK3R1), and a phosphatidylinositol 3-kinase catalytic alpha polypeptide (PIK3CA) mutation in GBM patients (The Cancer Genome Atlas Program - National Cancer Institute, 2008). Loss of chromosomal 10 is frequently observed in CL subtype as well as chromosome 7 amplification, EGFR amplification or mutation, mutations in TP53 and IHD1 and RB alterations. The PN

subtype is enriched in genes expressed in oligodendrocytes, platelet-derived growth factor receptor alpha polypeptide (PDGFRA), NK2 Homeobox 2 (NKX2-2) and Oligodendrocyte transcription factor (OLIG) and characterized by alterations in platelet-derived growth receptor (PDGFR) gene, IDH1/2 mutation and TP53 and CDKN2A loss (Kumabe, Sohma, Kayama, & Yoshimoto, 1992; Verhaak et al., 2010). The MES subtype is enriched in the gene expression pattern of astrocytes, such as Cluster of Differentiation 44 (CD44) and c-Mer proto-oncogene Tyrosine Kinase (MERTK), as well as microglial marker and MES markers, such as Chitinase-3-Like protein 1 (CHI3L1) and Mesenchymal-Epithelial Transition Factor (MET) (Phillips et al., 2006). Additionally, MES subtype is characterized by NF1 and PTEN alterations and hyperactivation of Nuclear Factor-κB (NF-κB) and Tumour Necrosis Factor-alpha (TNFα) signalling pathways (Bhat et al., 2013; Verhaak et al., 2010) (Table 1.2) (Figure 1.6:).

Table 1.2: Features of GBM subtypes. *Mutations and gene alterations characteristics of GBM and GBM subtypes.*

Subtypes	Features
General	Mutations of: TP53, PTEN, EGFR, RB1, NF1, ERBB2, PIK3R1 and PIK3CA
CL subtype	Loss of chromosome 10 Amplification of chromosome 7 and EGFR gene Mutation of: EGFR, TP53 and IHD1 Alterations of RB
PN subtype	Gene enrichment of oligodendrocytes genes, PDGFRA, NKX2-2 and OLIG Alterations of PDGFR Mutations of IDH1/2 and TP53 Loss of CDKN2A

MES subtype	Gene enrichment of CD44, MERTK, CHI3L1 and MET Alterations of NF1 and PTEN Hyperactivation of NF-κB and TNFα

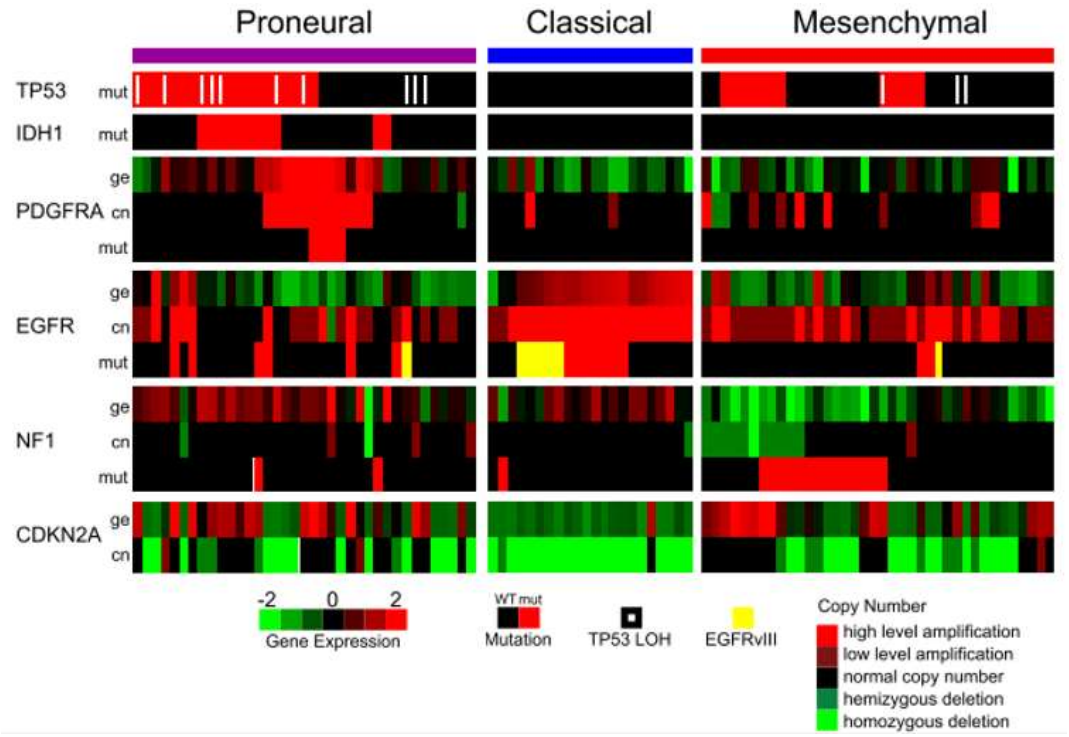

Figure 1.6: Integrated view of gene expression and genomic alterations across glioblastoma subtypes. *Mutation and copy number data from 116 GBM samples. Mutations (mut) are indicated by a red cell, a white pipe indicates loss of heterozygosity, and a yellow cell indicates the presence of an EGFRvIII mutation. Copy number events (cn) are illustrated by bright green for homozygous deletions, green for hemizygous deletions, black for copy number neutral, red for low-level amplification, and bright red for high-level amplifications. A black cell indicates no detected alteration. (Figure reproduced from Verhaak et al., 2010)*

G-CIMP^{+} GBMs show more favourable prognosis, whereas non-G-CIMP GBM patients have the poorest prognosis (Noushmehr et al., 2010) (Figure 1.7:A). Within non-G-CIMP GBMs, alterations related to PN GBM such as IDH1 mutations have been associated with an increase in the overall survival of GBM patients (Parsons et al., 2008; H. Yan et al., 2009), whereas elevated expression of MES genes, such as

CD44 or TGFβ is associated with poorer patient prognosis (Figure 1.7:B) (Bruna et al., 2007; Pietras et al., 2014).

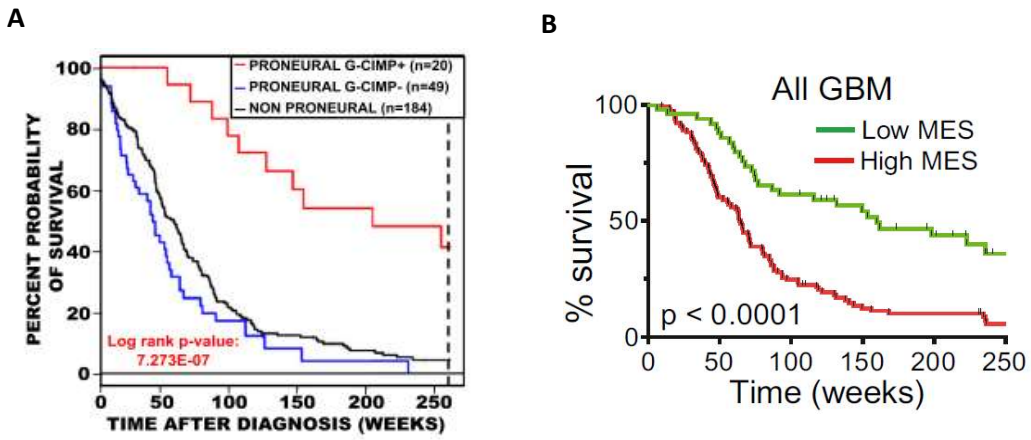

Figure 1.7: Kaplan-Meier survival curves of GBM patients. *(A) Kaplan-Meier survival curves among PN G-CIMP⁺- (red), PN non-G-CIMP-(blue), and all non-PN GBM tumours (black). PN G-CIMP⁺ had better prognosis than non-G-CIMP- and non PN GBM patients. (B) Kaplan Meier curves show survival of newly diagnosed patients based on PN/MES metagene scores. Patients with a higher MES metagene showed reduced survival respect to patients with a lower MES metagene. Log rank test was used to assess statistical significance. (Figure reproduced from (A) Noushmehr et al., 2010 and (B) Bhat et al., 2013)*

1.2.2.2 Intra-tumoural heterogeneity: Glioma Initiating Cells

In addition to the intertumoural heterogeneity, different subpopulations of cells in the tumour bulk have been described in GBM, increasing the heterogeneity that characterize GBMs. Two different hypothesis have been postulated to explain this intratumoural heterogeneity (1) the stochastic model or clonal evolution model and (2) the hierarchical model or cancer stem cell (CSC) model (Figure 1.8) (Campbell & Polyak, 2007; Plaks, Kong, & Werb, 2015; Reya, Morrison, Clarke, & Weissman, 2001; Rich, 2016). Although these models are dissimilar, they are not mutually exclusive (Cabrera, 2015; Meacham & Morrison, 2013).

In the clonal evolution model, tumours are proposed to arise from normal cells that undergo somatic mutations which make them tumourigenic. These tumour cells generate offspring that can accumulate further mutations, due to their genetic

instability, creating a tumour with phenotypically different cancer cells (Figure 1.8). Through time, these changes may increase tumour aggressiveness, invasiveness, treatment resistance and increases tumour heterogeneity (Gerdes et al., 2014; Michor & Polyak, 2010; Piccirillo et al., 2009; Reya et al., 2001). On the other hand, the cancer stem cell model hypothesizes that tumour initiation and propagation are driven by a small subpopulation of cells with stem-like properties, also known as cancer initiating cells (CIC) (Gerdes et al., 2014; Meacham & Morrison, 2013; Michor & Polyak, 2010; Plaks et al., 2015; Reya et al., 2001). In analogy to normal stem cells, these stem-like cells are able to self-renew and differentiate into a variety of cell types, generating phenotypically diverse non-tumourigenic and tumourigenic cancer cells (Figure 1.8). These CSCs are, therefore, the source of tumour initiation and heterogeneity (Michor & Polyak, 2010).

The clonal evolution and CSC models are not mutually exclusive. The plasticity model defends that cancer cells can turn between stem cell and differentiated states (Plaks et al., 2015). According to the plasticity model, intrinsic tumour cell processes and/or stimuli within the tumour microenvironment could influence differentiated tumour cells to reacquire stem cell characteristics (Andriani et al., 2016; Cabrera, 2015; Michor & Polyak, 2010; Rich, 2016). Conversely, these processes could also drive CSCs toward differentiation into non stem cancer cells (Cabrera, 2015) (Figure 1.8).

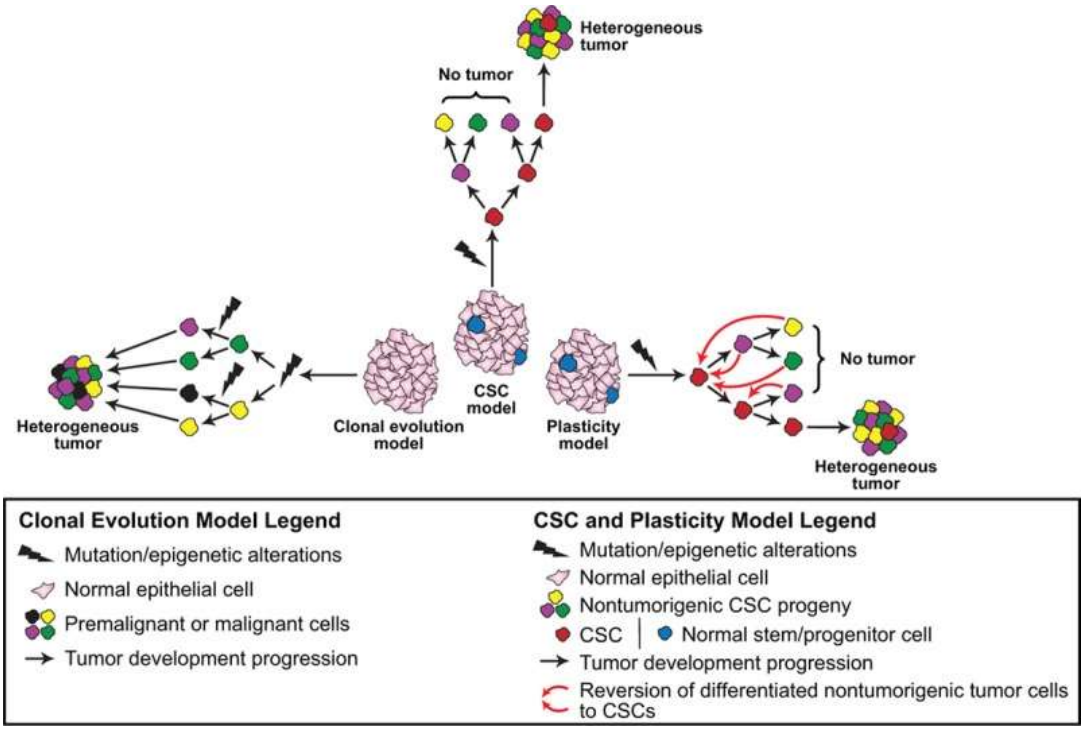

Figure 1.8: Clonal evolution vs. Cancer Stem Cells (CSC) vs. plasticity models. *The clonal evolution model (A) proposes that heterogeneity is achieved by random mutations in cells giving rise to different tumourigenic clones. Mutations can be accumulated through time and any cell may have tumourigenic potential. In the CSC model, only a small subpopulation of stem cells can proliferate extensively and sustain the growth and progression of a neoplastic clone. Thus, only the CSC possess tumourigenic potential while differentiated cells have little or none. According to the plasticity model, differentiation can be bidirectional so that differentiated non-tumourigenic cancer cells may revert back to CSCs. CSC=cancer stem cell. (Reprinted from Jeremy et al., 2016)*

In GBM, several groups have described the presence of stem-like cells known as glioma-initiating cells (GIC) or glioma stem-cells (GSCs). GIC are considered to be tumour drivers, responsible for tumour initiation and resistance to therapeutic agents (Fomchenko & Holland, 2005; Natsume et al., 2011; Piccirillo et al., 2009; Reya et al., 2001; Sanai, Alvarez-Buylla, & Berger, 2005; Sulman, Aldape, & Colman, 2008).

Analogously to whole tumours, isolated tumour cell cultures, that are also enriched in GICs, display the GBM-subtype-specific phenotypes, retaining the phenotypic and molecular profile of primary tumour (Bhat et al., 2013; Patel et al., 2014; Segerman et al., 2016). Bhat et al. isolated GICs from different patients and characterized them by gene expression. GICs were classified according to gene expression in two

different groups that correlated with genes expressed in PN subtype and MES subtype, respectively (Figure 1.9).

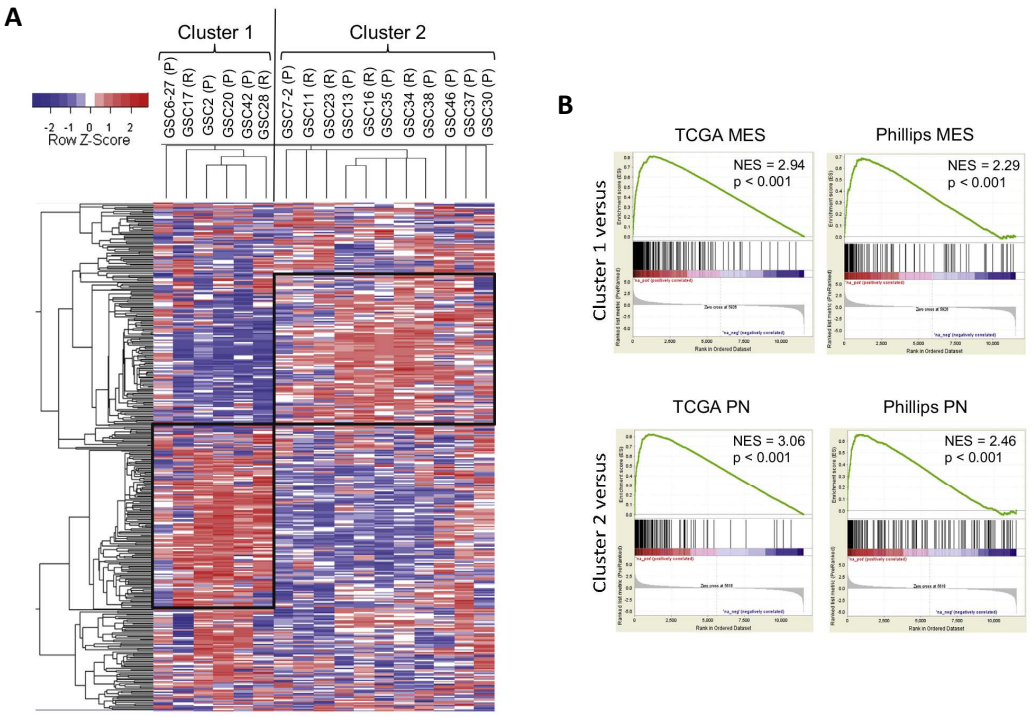

Figure 1.9: Patient-derived GSCs bear resemblance to PN and MES Signatures. *(A) Unsupervised hierarchical analysis of the top 500 highest median absolute deviation genes from expression microarray of 17 GSC get two different clusters. Relatively lower expression is shown in blue and higher expression is shown in red. The vertical black line identifies the first dendrogram splitting of the GSCs. Primary (P) or recurrent (R) status of the GSCs is indicated. (B) GSEA enrichment plots of GSC cluster 1 high and cluster 2 high gene lists versus queried gene lists using TCGA. Cluster 1 obtained in the heatmap correlated with MES signature, whereas Cluster 2 was enriched in PN signature. The normalized enrichment scores (NES) and the p values are shown for each plot. (Figure modified from Bhat et al., 2013)*

Recent studies show that tumour heterogeneity is a dynamic process that changes with time. GBM contains multiple cellular states with the transcriptional genes of the different molecular subtypes (Patel et al., 2014) (Figure 1.10A). Within the same tumour, cells with PN features coexist with MES-like cells that express different stem-like markers (Figure 1.10B). In addition, GICs are highly plastic and undergo transitions from one subtype to another, as has been observed in GBM patients,

especially in response to inflammation or after therapy. After treatment, GICs suffer a transition to MES subtype, conferring resistance to therapy (Bhat et al., 2013; Mao et al., 2013; Moreno, Pedrosa, Paré, Pineda, Bejarano, Martínez, Balasubramaniyan, Ezhilarasan, Kallarackal, Kim, Wang, Audia, Marín, et al., 2017; Segerman et al., 2016). On the other hand, Patel et al., found that increased heterogeneity in the tumour was associated with decreased survival (Figure 1.10C-D). This suggests that the clinical outcome of a PN glioblastoma is influenced by the proportion of tumour cells of alternate subtypes, and emphasizes the clinical importance of intratumoural heterogeneity.

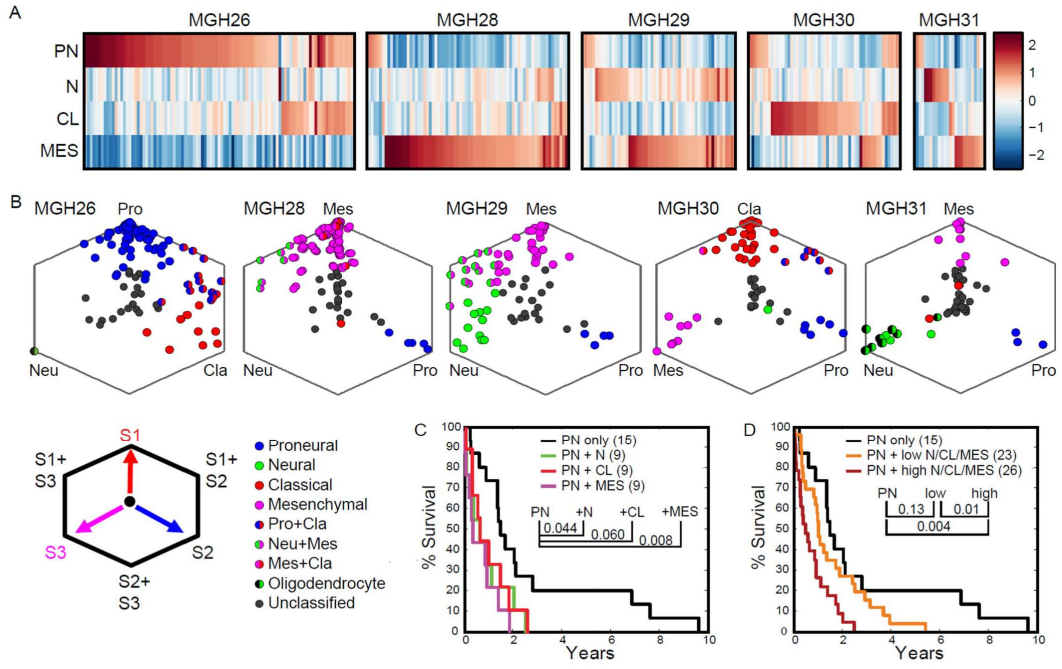

Figure 1.10: Individual tumours contain a spectrum of glioblastoma subtypes and hybrid cellular states *(A) Heatmap depicts average expression of classifier genes for each subtype (rows) across all classifiable cells grouped by tumour (columns). PN: proneural, CL: classical, MES: mesenchymal, N: neural. Each tumour contains a dominant subtype, but also has cells classified as other subtype. (B) Hexagonal plots depict bootstrapped classifier scores for all cells in each tumour. Each data point corresponds to a single cell and is positioned along three axes according to its relative scores for the indicated subtypes. Cells corresponding to each subtype are indicated by solid colour, while hybrid cells are depicted by two colours. (C) Kaplan-Meier survival curves are shown for PN tumours from the Cancer Genome Atlas. Intratumoural heterogeneity was estimated based on detected signal for alternative subtypes, and used to partition the tumours into a pure PN group and three groups with*

the indicated additional subtype. Tumours with MES signal had significantly worse outcome than pure PN ($p<0.05$). (D) Kaplan-Meier survival curves shown for PN tumours partitioned based on the relative strength of alternative subtype signatures in aggregate. Tumours with high signal for alternative subtypes had significantly worse outcome than pure PN ($p<0.05$). (Figure reprinted from Patel et al., 2014)

1.2.3 GBM therapy

GBM is a highly heterogenous tumour, either at the cytophatological or at the genomic levels. These malignant features make GBM one of the most difficult cancers to understand and treat.

The current standard therapy for newly diagnosed patients is surgical resection followed by radiotherapy with adjuvant or maintenance chemotherapy (Stupp regimen) (Stupp et al., 2005). Temozolamide (TMZ) is the oral alkylating agent, developed by Malcolm Stevens et al., wider used in GBM chemotherapy due to its effectiveness in crossing the blood-brain barrier as the first-line treatment. However, a considerable percentage of GBMs have inherent or acquired resistance to TMZ-based chemotherapy, which critically impedes the clinical outcome (Goellner et al., 2011) (Figure 1.11).

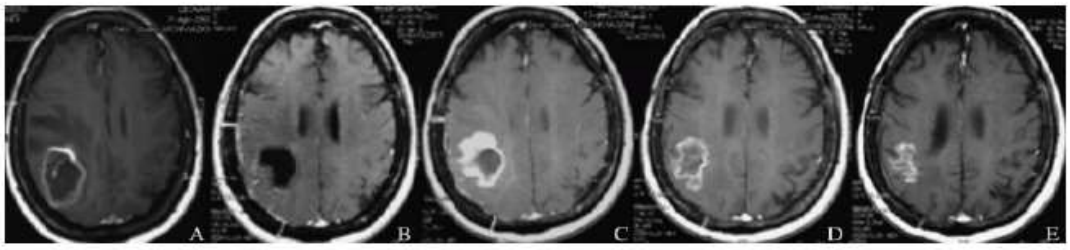

Figure 1.11: Clinical course of a 65-year-old patient with glioblastoma. *(A) presurgical MRI scan. (B) Postsurgical MRI scan. (C) MRI scan performed one month after combined temozolomide plus radiotherapy (TMZ/RDT). Treatment with adjuvant TMZ was continued. (E) MRI scan eight months later during administration of maintenance TMZ. (Figure reproduced from Stupp et al., 2008)*

Various studies have been carried out to explore how GBM cells acquire resistance to TMZ; however, the underlying mechanisms remain unknown. Thus, a deeper understanding of the molecular characteristics underlying this resistance and the identification of novel therapeutic target is imperative.

A Food Drug Administration (FDA)-approved anti-Vascular Endothelial Growth Factor (VEGF) humanized monoclonal antibody that interacts with VEGF receptor of tumour endothelial cells (Bevacizumab) has improved progression-free survival but not the overall survival. It is typical for patients to have an initial benefit lasting 3 to 4 months but, unfortunately, these tumours continue to progress (Friedman et al., 2009). Clinical observations and retrospective studies indicate that glioblastoma becomes more aggressive and treatment-resistant at the time of bevacizumab failure (Norden et al., 2008; Quant et al., 2009; Scott et al., 2010).

Despite treatment, tumour recurrence appears in almost all patients. Consequently, several new-targeted agents and novel approaches are being developed. Targeted therapies such as EGFR tyrosine kinase inhibitors (erlotinib and gefitinib), mammalian target of rapamycin (mTOR) antagonists (temsirolimus and everomilus), PDGFR inhibitors (imatinib) or inhibitors of avb3 and avb5 integrin (cilengitide) have shown minimal benefit until now (Tanaka, Louis, Curry, Batchelor, & Dietrich, 2013). On the other hand, vaccines targeting tumour-specific epitope (like EGFRvIII), radiotherapy with intraoperative injection of herpes simplex virus-thymidine kinase gene vectors (Cerepro) or radiolabeled monoclonal antibodies against tumour-specific antigens (like EGFR, tenascin or integrins) have shown some efficacy in clinical and preclinical trials (Daga, Bottino, Castriconi, Gangemi, & Ferrini, 2011; Sampson et al., 2009; Veeravagu et al., 2008) (Figure 1.12).

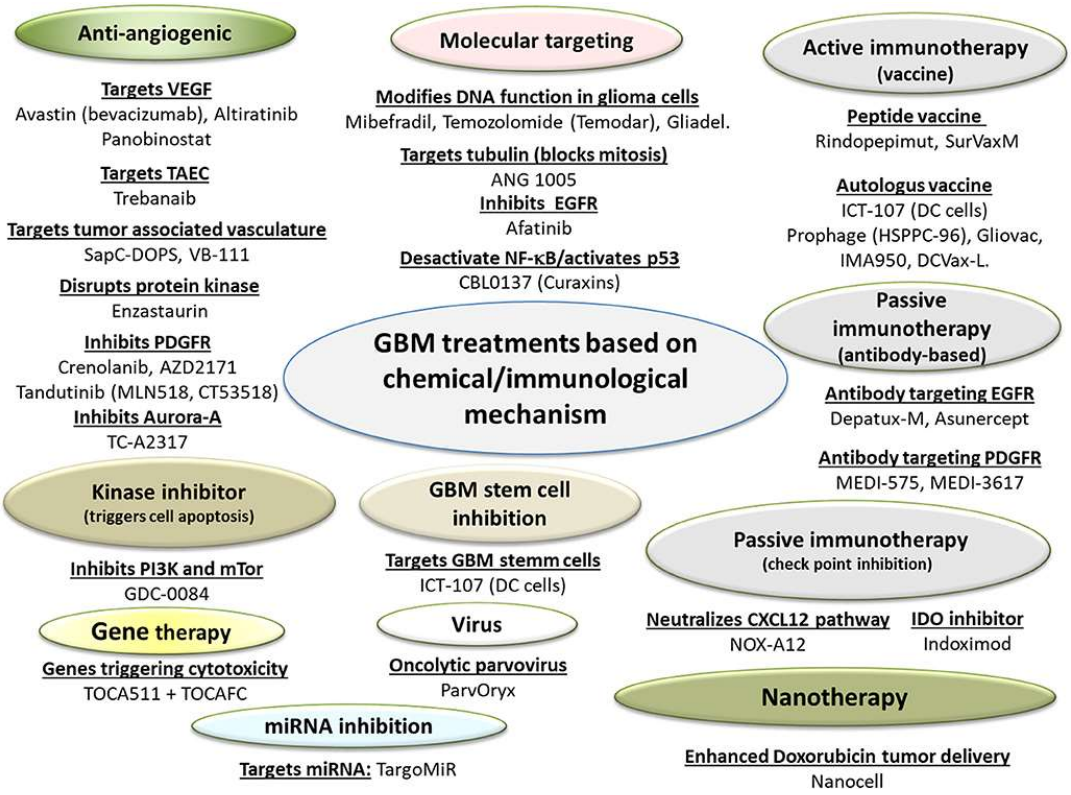

Figure 1.12: Summary of different strategies of therapy to glioblastoma based on chemical/immunological mechanism. *There are different approaches to treat glioblastoma: anti-angiogenic therapies, molecular targeting, active immunotherapy, passive immunotherapy, nanotherapy, GBM stem cell inhibition, virus, miRNA inhibition, gene therapy and kinase inhibitors. (Alphandéry Edouard 2018)*

1.2.4 GBM tumour progression

Therapeutic resistance reflects active tumour evolution, and environmental resistance shows the dynamic interplay between tumour cells and their surroundings when the selective pressure of a drug is applied. Thus, tumour cell plasticity in response to microenvironment changes has become the main hallmark for success in tumour progression. Several studies show that elevated cell plasticity is inherent in tumour cells, suggesting that cellular programs that promote cell conversion are playing a major role in tumourigenesis. One of these transitions is the PN-to-MES differentiation, which is associated with tumour recurrence (Phillips et al., 2006) and acquired resistance therapy (Moreno, Pedrosa, Paré, Pineda, Bejarano, Martínez, Balasubramaniyan, Ezhilarasan, Kallarackal, Kim, Wang, Audia, Marín, et al., 2017; Y. Piao et al., 2013).

The recurrent tumour shows a more aggressive behaviour due to a phenotypic shift toward the MES subtype (Bhat et al., 2013; Fedele, Cerchia, Pegoraro, Sgarra, & Manfioletti, 2019; Moreno, Pedrosa, Paré, Pineda, Bejarano, Martínez, Balasubramaniyan, Ezhilarasan, Kallarackal, Kim, Wang, Audia, Marín, et al., 2017). MES differentiation may represent for GBM the equivalent of epithelial–mesenchymal differentiation associated with other aggressive cancers (Alison, Lim, & Nicholson, 2011; Steinbichler et al., 2018; Thiery, Acloque, Huang, & Nieto, 2009). Patients with a MES signature belong to the poorest prognosis subclass and are resistant to standard treatments. PN tumours tend to shift to the MES phenotype upon recurrence or in response to radiation therapy. Therefore, the tumour plasticity may render GBM cells more invasive or resistant to current therapies at different stages in their development. Another explanation of the recurrence and resistance to therapy is presence of pre-existing resistant subpopulations of GICs upon treatment, due to their intra-tumoural heterogeneity.

1.2.4.1 Mesenchymal Differentiation

Some cancer cells can reversibly transition between epithelial and mesenchymal states, and some evidences show that cancer cells in the mesenchymal state are more competent at tumour formation than those in the epithelial state (Balic et al., 2006).

The transitions between these cells stages are called epithelial to mesenchymal transition (EMT) and, its reverse, mesenchymal to epithelial transition (MET) (Thiery et al., 2009). Both transitions are a common process in embryonic development, during tissue remodelling, cancer progression and metastasis (Guarino, Rubino, & Ballabio, 2007). A similar process has been described in GBMs and GICs, called mesenchymal differentiation (Bhat et al., 2013; Mikheeva et al., 2010; Moreno, Pedrosa, Paré, Pineda, Bejarano, Martínez, Balasubramaniyan, Ezhilarasan, Kallarackal, Kim, Wang, Audia, Marín, et al., 2017; Myung, Choi, Kim, Wang, & Park, 2014). However, mesenchymal differentiation in GBMs/GICs is somewhat different from the classical EMT in epithelial tumours, although they share some molecular mediators such as Transforming Growth Factor-beta 1 (TGF-β) or Signal Transducer and Activator of Transcription 3 (STAT3).

As previously mentioned, non-G-CIMP GBMs display elevated transcriptional plasticity and have an intrinsic ability to transition from one subtype to another. The best characterized of these transitions is the above-mentioned MES differentiation, which is associated with a gain of MES markers, such as CD44, and the loss of PN markers, such as Oligodendrocyte Transcription Factor 2 (OLIG2) (Bhat et al., 2013), tumour recurrence (Phillips et al., 2006) and acquired resistance to anti-angiogenic therapy (Y. Piao et al., 2013).

The acquisition of a MES phenotype in GBM has been linked to the activation of master Transcription Factors (TF) and co-factors that control an EMT, such as STAT3, CCAAT Enhancer Binding Protein Beta (C/EBPβ), and Tafazzin (TAZ) (Bhat et al., 2011; Carro et al., 2010) (Figure 1.13).

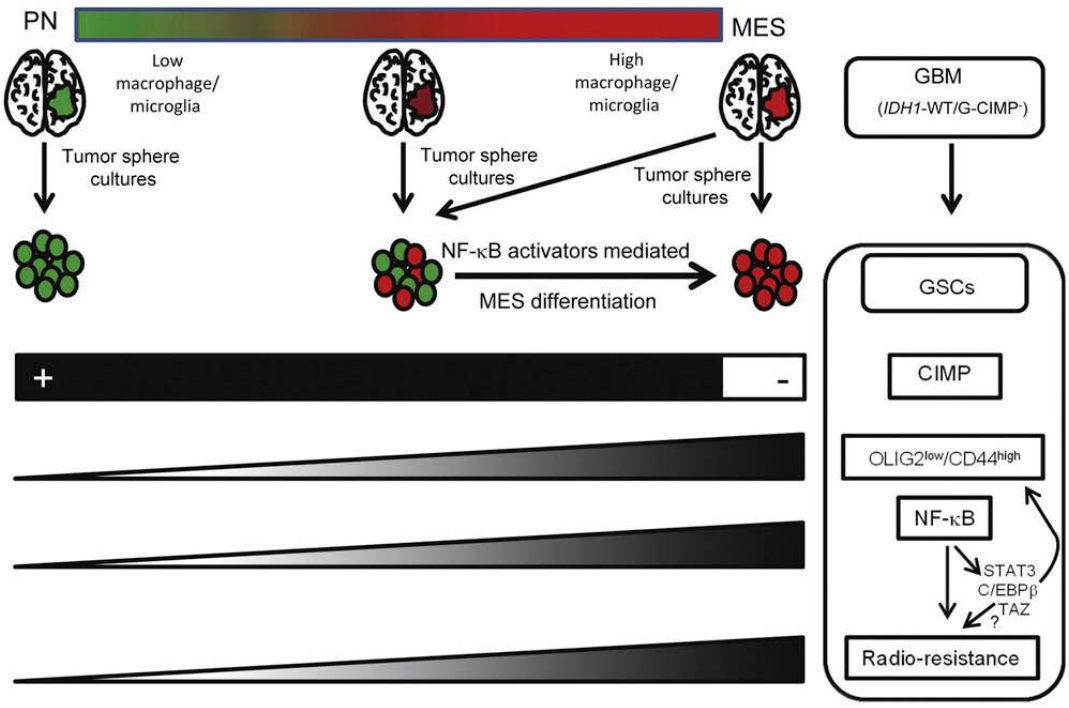

Figure 1.13: Summary of mesenchymal differentiation in GBM. *MES differentiation, induced in PN/CIMP− GSCs, is characterised by the CD44 enrichment and radioresistance by activation of NF-κB and downstream master TFs (STAT3, C/EBPβ, and TAZ). In contrast, MES GSCs are G-CIMP⁻, predominantly express CD44, are radioresistant, and exhibit constitutive activation of NF-κB and downstream master TFs. (Figure reproduced from Bhat et al., 2013)*

MES differentiation can be initiated by different extracellular signals from the tumour microenvironment. Infiltrated immune cells secrete cytokines, chemokines and Growth Factors (GF) such as TGFβ, TNFα, Interleukin 6 (IL6), Fibroblast Growth Factor (FGF), Epidermal Growth Factor (EGF) and Hepatocyte Growth Factor (HGF) (Joyce & Pollard, 2009). TNFα activates the NFκB pathway of PN-GICs promoting their MES differentiation (Bhat et al., 2013).

1.2.4.1.1 Cell adhesion

During EMT, either in embryonic development or in tumourigenesis, epithelial cells lose polarity, reduce cellular adhesion, and increase cell migration (Thiery et al., 2009). An essential step in tumour progression is the interaction of tumour cells with

ECM leading to its destruction and the tumour cells' invasive behaviour (Shashidhar et al., 2005). Loss of cell adhesion is required to initiate EMT and it is thus considered a hallmark of this process.

In a large number of systems, the loss of cell adhesion that is required to initiate EMT is achieved through the repression of the epithelial marker E-cadherin, which is responsible for cell-to-cell adhesion. However, limited expression of E-cadherin in normal brain tissue and GBMs suggests that other adhesion proteins might be playing a role in this process (Lewis-Tuffin et al., 2010).

The functional relationship between G-protein-coupled receptors (GPCR) signalling and EMT has also been extensively described. In cancer, deregulation of GPCR signalling has been implicated in cell migration, invasion and metastasis (X. Tang et al., 2013). GPCR constitutes more than the 40% of the molecular targets of drugs being developed by pharmaceutical industries (X. L. Tang, Wang, Li, Luo, & Liu, 2012). However, there are few GPCR that are cancer therapeutic targets. Therefore, studying GPCR function becomes of crucial interest to understand cancer progression and develop novel targeted therapies to treat GBM.

1.2.4.1.1.1 GPR56

GPCR, also known as seven-transmembrane receptors, are integral membrane proteins participating in the transmission of signals from the extracellular environment to the cytoplasm. GPR56 is an orphan GPCR, which is characterized by an extremely long extracellular domain with a typical GPCR proteolytic site (Ke et al., 2007) and belongs to the so-called Adhesion-GPCR family.

GPCR, also known as seven-transmembrane receptors, are characterized for large, multi-domain N terminal and a highly conserved region that can be autoproteolytically cleaved (Andre Gerhard Wolff, 2020). These allow to GPCRs be activated by a high variety of external stimuli, such as neurotransmitters, hormones, phospholipids, growth factors and proteases (Schiöth & Lagerström, 2008). Upon ligand is attached to the receptor, this change its conformation that is transmitted to the Ga subunit of the heterotrimeric GTPase protein. Ga subunit exchanges GTP in

place of GDP triggering the dissociation of Gα subunit from the Gβγ dimer and allowing them to interact with other proteins to continue the signal transduction (Digby, Lober, Sethi, & Lambert, 2006). Additionally, this receptor family exhibit discrete distribution patterns in different tissues.

Although GPCRs overall have well-established pharmacological tractability, currently no therapies that target any of the 33 members of the adhesion-GPCR family are either approved or in clinical trials. Despite, several studies have strengthened the links between adhesion-GPCRs and disease. In cancer, deregulation of GPCR signalling has been implicated in cell migration, invasion and metastasis (Sahai & Marshall, 2002; X. Tang et al., 2013; Vallon & Essler, 2006).

GPR56 is widely expressed in several tissues and organs with the highest expression in brain, thyroid gland and peripheral tissues (M. Liu et al., 1999). Neural and hematopoietic progenitors express high levels of GPR56 (X. Piao et al., 2004; Terskikh et al., 2001). In the brain, GPR56 function is indispensable for normal cortical development (McLendon et al., 2008). In addition to the cortical development, GPR56 is also involved in oligodendrocyte development and CNS myelination. GPR56 expression was highest in the oligodendrocyte precursor cells (OPC), but declined gradually during oligodendrocyte maturation and was very low in mature myelinating oligodendrocytes. Importantly, disruption of the GPR56 gene reduced the proliferation ability of OPC leading to a defect of CNS myelination (Ackerman, Garcia, Piao, Gutmann, & Monk, 2015). Furthermore, GPR56 is up-regulated in some types of cancers compared with their normal counterparts such as breast, ovarian and pancreatic cancers, suggesting that GPR56 might function as an oncogene (Ke et al., 2007; Shashidhar et al., 2005; Sud, Sharma, Ray, Chattopadhyay, & Ralhan, 2006).

In cancer, deregulation of GPCR signalling has been implicated in cell migration, invasion and metastasis (Sahai & Marshall, 2002; X. Tang et al., 2013; T. Wang et al., 2005; M. P. Wu et al., 2013). Moreover, previous results obtained from TGCA dataset analysis revealed that MES subtype express lower levels of GPR56 compared with the other GBM subtypes (Figure 1.14A). Additionally, GPR56 is co-expressed with PN markers and negatively correlated with MES markers (Figure 1.14B) and, during the MES differentiation, GPR56 is downregulated (Moreno, Pedrosa, Paré,

Pineda, Bejarano, Martínez, Balasubramaniyan, Ezhilarasan, Kallarackal, Kim, Wang, Audia, Marín, et al., 2017). Altogether, GPR56 might have a functional role PN to MES differentiation.

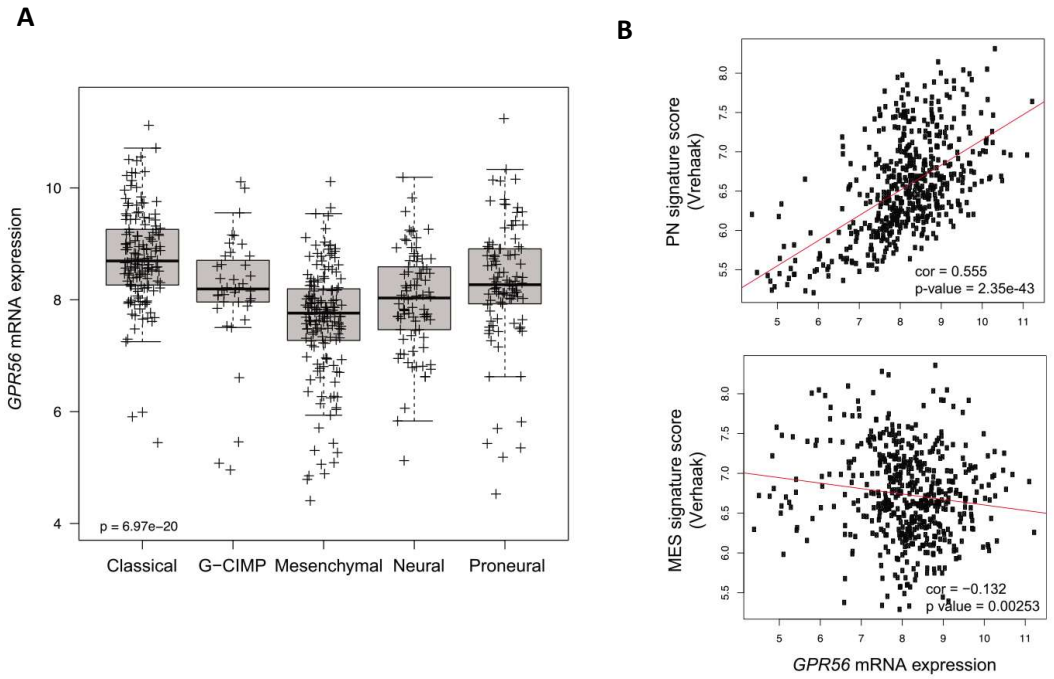

Figure 1.14: GPR56 is downregulated in MES-GBMs and inversely correlated with MES markers. *(A) GPR56 mRNA expression comparison across the five different subtypes of GBM (TCGA dataset). Gene expression data were obtained from Brennan et al., 2013. Differences in GPR56 expression among subtypes were assessed by a Kruskal-Wallis rank-sum test (Dunn's post hoc multiple comparison test: mesenchymal versus classical and proneural, $p < 0.0001$; MES versus G-CIMP, $p < 0.001$; MES versus neural, $p < 0.01$). In the box-plots, the horizontal line indicates the median, boundaries of the box indicate the first and third quartiles, and whiskers indicate confidence intervals (95%). (B) Correlation plots between GPR56 mRNA levels and PN (upper panel) or MES (lower panel) signature scores in GBM patients from the TCGA dataset. Pearson's correlation coefficients and p values are indicated in each plot. (Figure reproduced from Moreno, et al. 2017)*

1.3 LONG NON-CODING RNAS

Only 2% of human DNA sequences are protein-coding and the transcripts of the other 98% human genome are named noncoding ribonucleic acids (ncRNAs). ncRNAs are divided into small/short non-coding RNAs (miRNA, piRNA, siRNA, etc.) and long non-coding RNAs (lncRNAs) (Birney et al., 2007; Jarroux, Morillon, & Pinskaya, 2017).

Long non-coding RNAs are RNA molecules over 200 nucleotides-long that lack a complete open reading frame (ORF). Similar to mRNAs, most lncRNAs are transcribed by RNA polymerase and generated by splicing and modification in the nucleus. They can be nuclear or cytoplasmic and are generally expressed at lower levels compared with protein-coding mRNAs (Lander et al., 2001).

LncRNAs are versatile molecules that either can interact physically and functionally with DNA, other RNAs, and proteins, through nucleotide base pairing or via formation of structural domains generated by RNA folding. These properties endow lncRNAs with a versatile range of capabilities that are only beginning to be appreciated (Hu, Alvarez-Dominguez, & Lodish, 2012; Paralkar & Weiss, 2013) (Figure 1.15).

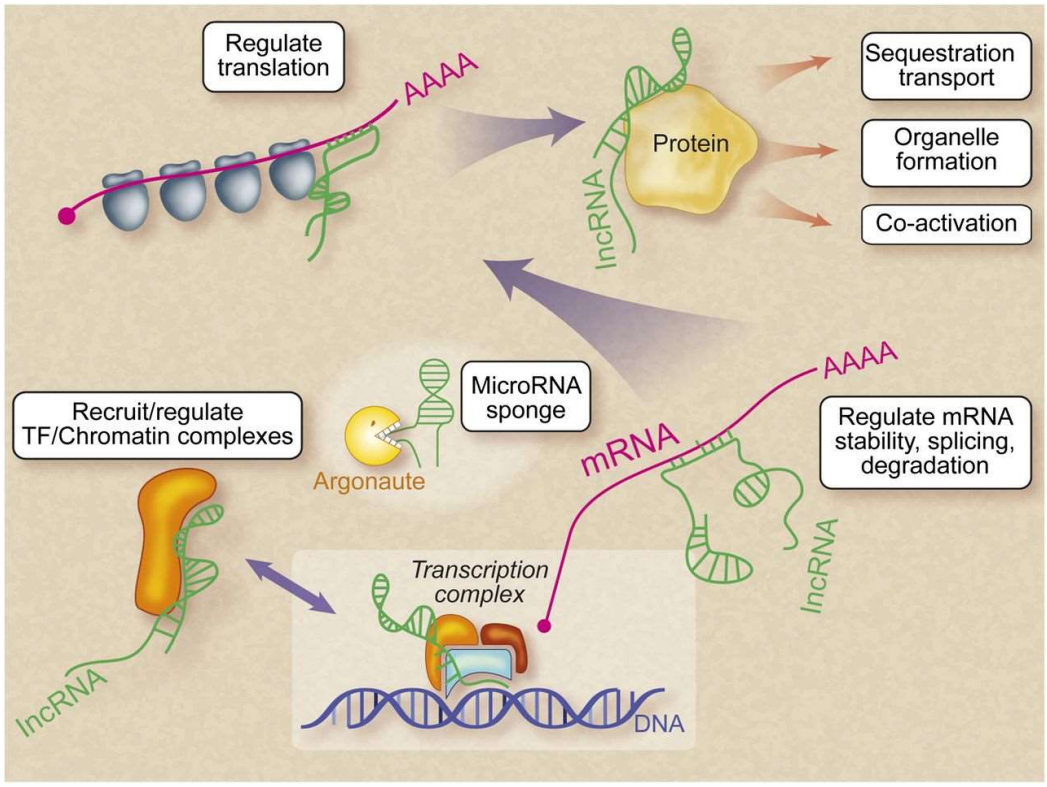

Figure 1.15: Mechanisms of LncRNA action. *lncRNAs (indicated in green) have been shown to regulate gene expression at multiple levels: chromatin, transcription, mRNA, translation, and protein. (Illustration by Debra T. Dartez. From Paralkar & Weiss, 2013)*

Although more than 3,000 human lncRNAs have been identified, less than 1% of these have been characterized. In recent years, lncRNAs have been implicated in multiple processes related to the stem cell properties such as pluripotency and differentiation (Fanale, Castiglia, Bazan, & Russo, 2016; Khalil et al., 2009; Khanduja, Calvo, Joh, Hill, & Motamedi, 2016; J. Kim et al., 2018; Sarkar, Leung, Baguley, Finlay, & Askarian-Amiri, 2014; Sheng, Wu, Tang, & Liang, 2017; Su et al., 2017).

1.3.1 lncRNAs in cell differentiation

Many of LncRNAs are expressed spatially and temporally, contributing to cell differentiation (Fatica & Bozzoni, 2014; Hong et al., 2020; Ju et al., 2019; Q. Yang et al., 2018). A subset of lncRNA loci show changes of chromatin state during lineage specification, such as in the glial-neuronal lineage specification of multipotent adult stem cells. Emerging studies suggest that lncRNAs play critical roles in central nervous system development. For instance, in embryonic stem cells (ESC), specific lncRNAs repress neuroectodermal differentiation (Guttman et al., 2011).

Rizvi et al. applied a single-cell topological data analysis (scTDA), an algorithm for topology-based computational analyses, to study temporal transcriptional regulation during the differentiation of mouse embryonic stem cells (mESCs) into neurons. Rizvi et al. characterized the dynamic appearance of mRNAs encoding signalling proteins, transcription factors, RNA splicing factors, and lncRNAs. These transcripts were dynamically regulated during the transition from pluripotent cells to neural pre-cursors, progenitors, interneurons and motor neurons. This results suggest that lncRNAs are involved in differentiation processes (Rizvi et al., 2017).

Another study identified two lncRNAs involved in neural differentiation by single-cell topological RNA-seq analysis, the LncRNA C130071C03Riken variants Riken-201 (Riken-201) and Riken-203 (Riken-203). Both lncRNAs are highly expressed in brain, and increase gradually during neural differentiation. Repression of Rik-201 and Rik-203 inhibited neural differentiation from mESC (Lei Zhang et al., 2019).

Lin et al. found that Tcl1 Upstream Neuron-Associated lincRNA (TUNA-lncRNA) regulates neuronal gene expression forming a complex with three RNA-binding proteins, nucleolin (NCL), Polypyrimidine Tract Binding Protein 1 (PTBP1), and heterogeneous Nuclear Ribonucleoprotein K (hnRNP-K). This complex localizes to neural gene promoters in differentiating mouse ESCs. Knockdown of TUNA, or anyone of the three interacting RNA-binding proteins, is sufficient to inhibit neural differentiation (Lin et al., 2014).

Chalei et al. showed that the DALI-lncRNA drives the expression of an essential neuronal differentiation gene expression program in neuroblastoma cells. Genomic target mapping by Capture Hybridization Analysis of RNA Targets (CHART)

revealed that this function is mediated through direct interactions with the transcription factor POU3F, the DNA methyltransferase DNA methyltransferase 1 (DNMT1), and thousands of target loci across the genome (Chalei et al., 2014). Similarly, the PAX6 Upstream Antisense RNA (PAUPAR)-lncRNA interacts with the PAX6 transcription factor and localizes to specific promoter loci, including SOX2, to regulate a transcriptional program that influences the cell-cycle profile and differentiation of neuroblastoma cells (Keith W. Vance et al., 2014).

1.3.2 lncRNAs in cell proliferation

Another important function of stem cell property where the lncRNAs are involved is the proliferation process, such as Linc-RoR that preserves hESC self-renewal by acting as a ceRNA (Na Xu, Papagiannakopoulos, Pan, Thomson, & Kosik, 2009) and GAS5-lncRNA that controls hESC self-renewal by maintaining NODAL signaling (C. Xu et al., 2016). LncKdm2b also positively regulates the self-renewal capacity of ESC self-renewal and early embryogenesis. LncKdm2b recruits Snf2-related CREBBP activator protein (SRCAP)-contained remodeling complex to the Zbtb3 promoter and activates Zbtb3 expression to induce Nanog expression (Ye et al., 2018). Zeqyuan et al. found that LincRAM-lncRNA may participates in proliferation process of human periodontal ligament stem cells (PDLSCs), regulating FGF2 expression (X. Wu et al., 2020).

In addition, several studies show that long non-coding RNAs impact tumour progression by affecting cancer stem cell self-renewal and differentiation capacity (Cai, Liu, & Xiao, 2018; Kim et al., 2018; Li et al., 2020; M, M, & S, 2016; Qiu, Zheng, & Huang, 2020; Xu et al., 2018; Z. Zhang et al., 2018). RHPN1-AS1-lncRNA, which also regulate FGF2 and its implication in proliferation, was upregulated in cervical cancer. In vitro functional assays demonstrated that RHPN1-AS1 overexpression promoted SiHa cell proliferation, invasion, and migration (Duan, Li, Chen, Wang, & Li, 2019).

1.3.3 lncRNAs in cancer

LncRNAs may regulate tumourigenesis by activating or suppressing oncogene or tumour-suppressor genes and regulating stem cell-like properties of CSC (Fu et al., 2016; W. Liu et al., 2017; Lynch et al., 2004). Liu et al. found that AC105461.1-lncRNA impair CSC properties. The knockdown of AC105461.1-lncRNA inhibit the proliferation, migration and self-renewal capacity of CSC (Figure 1.16) (W. Liu et al., 2017).

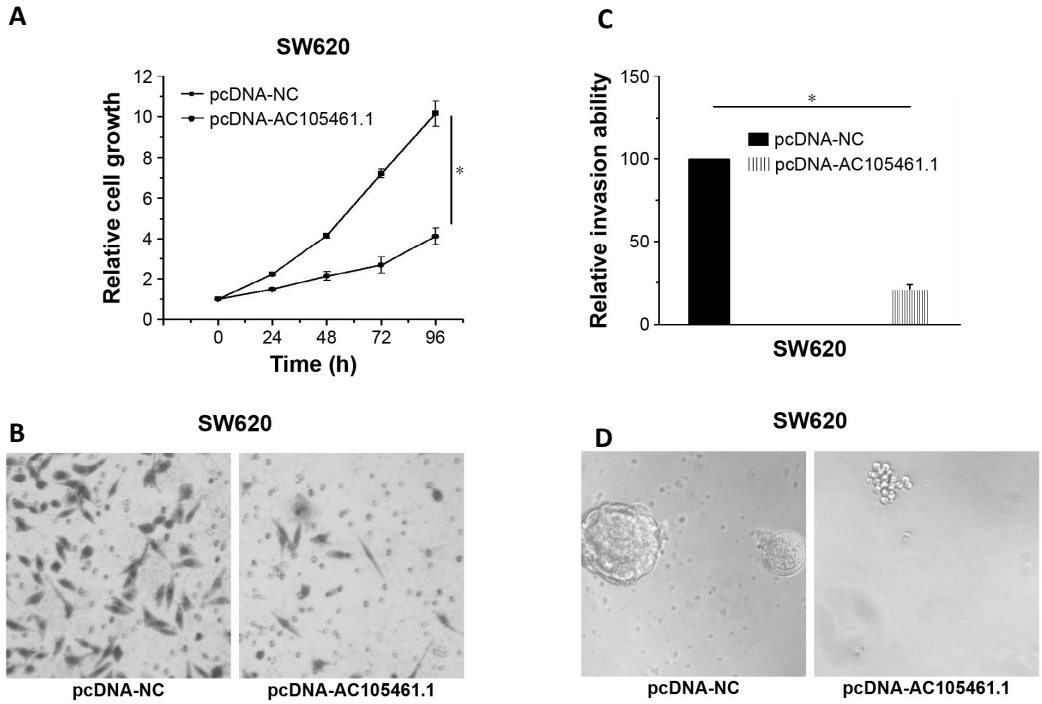

Figure 1.16: AC105461.1 overexpression impaired the CSC properties*. (A) Cell proliferation assay showed that cell growth of SW620 cells in knockdown of- AC105461.1 (pcDNA- AC105461.1) was slower than the cell growth of control cells (pcDNA-NC) (*p<0.05). (B, C) The matrigel invasion assay showed that the cell invasion was inhibited in pcDNA-AC105461.1 compared with the control (*p<0.05) (D) Spheroid formation assay revealed that the spheroid formation rate in knockdown of-AC105461.1 (pcDNA-AC105461.1) was slower compared with control. (W. Liu et al., 2017)*

Chen et al. demonstrated that lncSOX4-RNA was able to promote the self-renewal property of liver tumour-initiating cells regulating Sox4 expression (Z. Z. Chen et al., 2016). Moreover, Liu et al. observed that an increased lncSOX4 expression level was positively associated with larger tumour sizes, a decreases in apoptosis and more distant metastases, in epithelial ovarian carcinomas (Figure 1.17) (Y. Liu, Wang, Yao, & Cui, 2018).

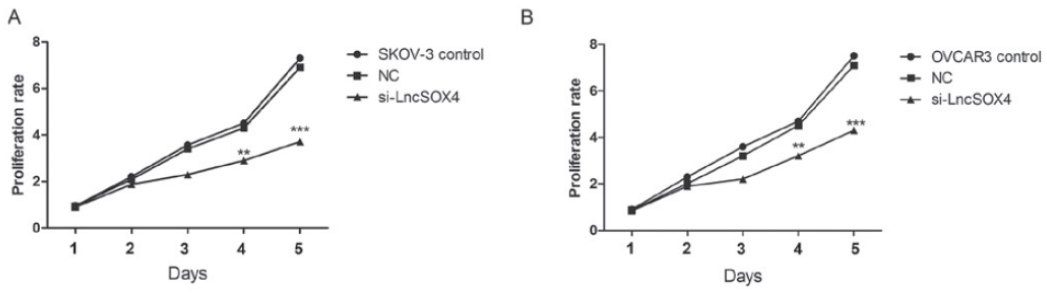

Figure 1.17: Proliferation of epithelial ovarian carcinomas cell lines following LncSOX4 silencing. *(A) SKOV-3 and (B) OVCAR-3 cell proliferation was inhibited by knockdown of LncSOX4 (si-lncSOX4) compared with their controls. (**p<0.01, ***p<0.001) (Reprinted from Y. Liu, Wang, Yao, & Cui, 2018)*

Moreover, lncRNAs influences in the radiosensitivity by regulating various mechanisms, including DNA damage repair, cell cycle arrest, apoptosis, cancer stem cell regulation, epithelial-mesenchymal differentiation, and autophagy (Zhu et al., 2019).

Radiotherapy is an effective treatment for many cancers. However, radioresistance is a primary factor that leads to poor prognosis. During radiotherapy, ionizing radiation first induces water radiolysis to produce reactive oxygen species (ROS). Oxygen then provides unpaired electrons for free radicals in DNA molecules, thereby stabilizing infrared-induced DNA damage. Damaged DNA or excessive ROS activate apoptotic-signalling pathways in cancer cells, leading to cell death (Redza-Dutordoir & Averill-Bates, 2016). Radioresistance can be overcome by reducing DNA repair through the activation of intracellular pro-survival and antiapoptotic signalling pathways. DNA damage can be repaired either by homologous recombination or through non-homologous end joining (NHEJ) (Cromie, Connelly, & Leach, 2001). The latter is a major pathway for the repair of damaged DNA and is a key determinant of infrared (IR) resistance in cancer cells (Goldstein & Kastan, 2015). Zhang et al. found that lncRNA in the NHEJ pathway 1 (LINP1) accelerated NHEJ repair and decreased the sensitivity of tumours to ionizing radiation (Y. Zhang et al., 2016). Following IR-induced DNA damage, molecules at cell cycle checkpoints begin to regulate and arrest cell cycle progression, subsequently repairing damaged DNA or initiating apoptosis if this repair is unsuccessful. Cell cycle arrest is closely related to

radiosensitivity, and when cancer cells are arrested in the G2/M phase, their radiosensitivity increases (Y. Chen et al., 2017). Further researchers have found that lncRNAs regulate radiosensitivity by affecting DNA damage repair via cell cycle arrest (Jing, Yuan, Ruofan, Jinjin, & Haifeng, 2015; Z. Li et al., 2017; H. Lu et al., 2016; M. Zhang et al., 2018).

Several lncRNAs were identified as regulators of the cell cycle that might be impaired in the tumourogenesis. Zhang et al. found that the colorectal neoplasia differentially expressed (CRNDE) gene contributed to radioresistance in lung cancer cells by affecting the G1/S transition. CRNDE was initially identified as a lncRNA whose expression is highly elevated in colorectal cancer, but it is also upregulated in many other solid tumours and leukemias and it is associated with a "stemness" signature (M. Zhang et al., 2018). Jin et al. examined the radiosensitivity of neural progenitor cells (NPC) and observed that MALAT1 decreased the sensitivity of NPC cells to IR by modulating CSC activity (Jin, Yan, Lu, Lin, & Ma, 2016) .

Another mechanism implicated in the gain of resistance to the therapy is the EMT, where lncRNA may be involved. LncRNA taurine upregulated gene 1 (TUG1) has been shown to induce radioresistance by promoting EMT (J. Tan, Qiu, Li, & Liang, 2015). Yuan et al. examined hepatocellular carcinoma cell lines, and found the lncRNA-ATB upregulates the expression of ZEB1 and ZEB2 genes inducing the EMT, and promoting invasion and resistance to therapy (Yuan et al., 2014). Similarly, (BRAF)-activated noncoding RNA (BANCR) induces the EMT via the MEK pathway in colorectal cancer cell lines (Guo et al., 2014) and long non-coding RNA expressed on chromosome 2 (TALNEC2) promotes mesenchymal transformation of GSCs increasing their resistance to radiation (Brodie et al., 2017).

Altogether, lncRNAs may play an important role in different stages in the development of cancer and during cancer progression and resistance to therapies (Figure 1.18). Thus, cancer-associated lncRNAs may provide new approaches to the diagnosis and treatment of cancer.

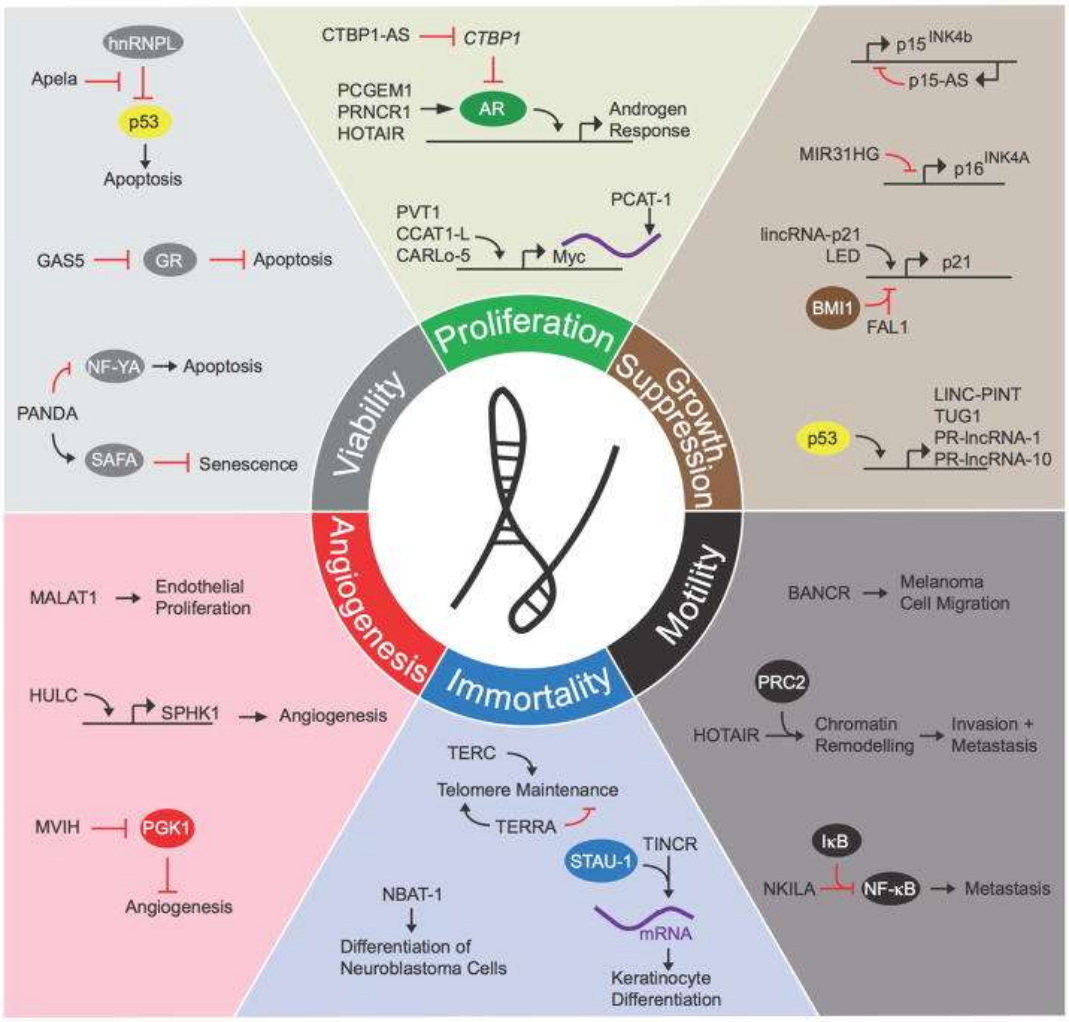

Figure 1.18: LncRNAs in cancer phenotypes. *LncRNAs contribute to each of the six hallmarks of cancer (diagram adapted from Hanahan and Weinberg, 2000). Selected examples of lncRNAs and their molecular partners or genomic targets are shown for proliferation, growth suppression, motility, immortality, angiogenesis, and viability cancer phenotypes. (Figure reproduced from Schmitt & Chang, 2016)*

1.3.3.1 lncRNAs in GBM

In gliomas, lncRNAs also serve an important role. Zhang et al. identified the ASB16-AS1-lncRNA that was significantly associated with tumour staging and grading in GBM from TCGA database. Furthermore, the proliferation, invasion, and migration of U87MG and U251 glioblastoma stem-like cells (U87GS, U251GS) were significantly inhibited upon inhibition of ASB16-AS1, and the expression of key proteins in the EMT signalling pathway was affected by knocking down ASB16-AS1

(D. Zhang, Zhou, Liu, & Mao, 2019). Kiran et al. identified 584 lncRNAs correlated with a poor prognosis and 282 lncRNAs associated with better survival outcomes in GBM patients (Kiran, Chatrath, Tang, Keenan, & Dutta, 2018).

Pastori et al. found that HOX transcript antisense RNA (HOTAIR) promotes proliferation and decreases apoptosis in GBM cells in vitro and in vivo assays (Pastori et al., 2015). Additionally, HOTAIR expression may be utilized as a peripheral biomarker for GBM. Tan et al. measured HOTAIR expression in serum from 43 GBM and 40 controls using quantitative real-time PCR (RT-qPCR). HOTAIR levels in serum samples from GBM patients were significantly higher than in the corresponding controls (S. K. Tan et al., 2018).

TMZ and RDT therapy combination for GBM patients is considered the most effective therapy after surgical procedure. However, the overall clinical prognosis remains unsatisfactory due to intrinsic or developing resistance to TMZ. Recently, increasing evidence suggested that lncRNAs play a critical role in various biological processes of tumours, that they are implicated in the resistance to various drugs. However, the role of lncRNAs in TMZ resistance is poorly understood. Ningbo et al. found that the expression of lncRNA AC003092.1 was markedly decreased in TMZ resistance of GBM cells compared with their Parental cells (Ningbo Xu et al., 2018). Similarly, Cai et al. showed that MALAT1 was significantly upregulated in TMZ-resistant GBM cells and, MALAT1 knockdown reduces TMZ resistance of GBM cells both in vitro and in vivo by inhibiting cell proliferation and promoting apoptosis (Cai et al., 2018).

Brodie et al. found that TALNEC2-lncRNA is involved in resistance to therapy in GBMs. TALNEC2 was highly expressed in GBM with poor prognosis, in GBM specimens derived from short-term survivors and in glioma cells and glioma stem cells (GSCs). Silencing of TALNEC2 inhibited cell proliferation and arrested the cells in the G1\S phase of the cell cycle in various cancer cell lines (Brodie et al., 2017).

In conclusion, under the growing evidences that implicate lncRNAs in the pathology of GBM, they might be a potential new target to treat this disease. lncRNAs might be a potential new target to treat GBM, since several studies have found various

lncRNAs implicated in this pathology. However, further investigation about which lncRNAs are implicated in GBM, as well as their regulation mechanisms, is necessary.

2 AIMS

The main objective of this Ph.D. thesis is to identify molecular mechanisms involved in GBM pathogenesis, more specifically in resistance to therapy, in order to find actionable targets for a more effective anti-GBM therapy.

- Aim 1: Identification and characterization of single lncRNAs or lncRNA signatures that have an impact on the pathogenesis, diagnosis and prognosis of glioblastoma patients
    - Identification of lncRNAs associated to each subtype of glioblastoma
    - Validation of the short-hairpin-RNA (shRNAs) technic to generate lncRNA knockdowns in GICs
    - Functional characterization of lncRNAs identified above:
        - Study their role in self-renewal property of GICs
        - Study their role in regulating gene expression, analysing their possible role in the transition between GBM subtypes
- Aim 2: Corroboration of the role of GPR56 in glioblastoma, especially in the mesenchymal differentiation of GICs
    - Generation of GPR56 knockouts in GICs using CRISPR/Cas9 gene editing and knockdowns of GPR56 using shRNAs
    - Characterization of modified-GICs analysing the MES differentiation by western blotting, RT-qPCR, microarrays and flow cytometry

3 METHODOLOGY

3.1 PATIENTS AND SAMPLES

Our studies, related to lncRNA project, are part of a coordinated project funded by "La Marató de TV3" named "Gene expression profiling (GEP) of glioblastoma, including long intergenic non-coding RNA (lincRNA), in a homogeneous population: correlation with immunophenotype, radiology, clinical outcome and response to therapy.

This study was approved by the Institutional Review Board of the Hospital Germans Trias I Pujol (PI-14-016) and by the Ethics Committees of all the participating institutions and conducted in accordance with the Declaration of Helsinki. Six tertiary hospitals in Catalonia are sharing GBM tissue specimens and clinical data of more than 200 GBM patients treated homogeneously with radiotherapy and temozolomide after surgery. RNA has been extracted from 236 formalin-fixed, paraffin-embedded (FFPE) GBM samples, which has been submitted to RNA-sequencing. RNA-sequencing allow for identification of both mRNA and lncRNA expression in these samples.

3.2 BIOINFORMATICS

3.2.1 RNA library construction and sequencing

Samples were sequenced at Centro Nacional de Análisis Genómico (CNAG-CRG, Barcelona, Spain). A modified TruSeq™ Stranded Total RNA kit protocol (Illumina Inc.) was used to prepare the RNA-Seq libraries from FFPE samples. Ribosomal RNA (rRNA) was depleted from 0.5–1.0 μg of total RNA using the RiboZero Magnetic Gold Kit (Human/Mouse/Rat, Epicentre). rRNA-depleted RNA samples were purified using Agencourt RNA Clean XP beads (Beckman Coulter Genomics) and RNA was eluted with the Elute, Prime, Fragment Mix from the TruSeq Stranded Total RNA kit. The RNA fragmentation time was shortened to 2.5 minutes due to the low quality of the initial total RNA (assessed by Eukaryote Total RNA Nano Bioanalyzer assay, Agilent). Following the fragmentation, first and second strand

synthesis, the Illumina barcoded adapters were ligated at 1/10 dilution of the recommended concentration. Libraries were enriched with 15 cycles of PCR. The size and quality of the libraries were assessed in a High Sensitivity DNA Bioanalyzer assay (Agilent).

3.2.2 Alignment and quantification

RNA-Seq reads were aligned to the human reference genome (GRCh38) using STAR (version 2.5.1b) with ENCODE parameters for long RNA. The Y chromosome was removed from the reference genome to map the female samples. Genes were quantified using RSEM (version 1.2.28) with default parameters. Human gene annotation file was downloaded from gencode release 24.

3.2.3 Sample quality metrics

PCR duplicates were calculated with sambamba. The number of detected genes was calculated taking into account genes with at least one paired- end read mapped. The number of genes consuming 25% of the reads was calculated by ranking the genes according to expression values (read counts) and then computing the cumulative sum until the number of reads was equal to 25% of the total sum. Mapping statistics were calculated with the tool 'gtfcounts' using GEMtools (http://gemtools.github.io/). Gene body coverage, GC content, paired-end inner distances, median transcript integrity number (TIN) across all the transcripts and distribution of mismatches across reads were computed with RSeQC. The percent spliced index (PSI) values were calculated with Spladder.

3.2.4 Differential gene expression analysis

RSEM read counts were used as input for DESeq2 (version 1.10.1). The cut-off for considering a gene significantly up-sampled or down-sampled in the FFPE-derived samples was FDR<5%. Gene ontology enrichment analysis of the down- sampled FFPE genes was performed with DAVID database beta version 6.8.

3.2.5 Prediction of GBM molecular subtype

The glmnet R package was used to fit a multinomial logistic regression model with alpha = 1 lasso penalty. The cross-validation RNA-seq dataset was downloaded from the The Cancer Genome Atlas (TCGA) repository using the RTCGAToolbox R package (http://mksamur.github.io/RTCGAToolbox/). The core function 'getFirehoseData' with 'dataset = GBM' and 'runDate = 20151101" was used to access and download the data. The associated clinical annotation for each sample was downloaded using the cgdsr R package (https://github.com/cBioPortal/cgdsr). Read counts were transformed with the variance stabilizing transformation using DESeq2. Batch effect correction between the RNA-seq datasets was carried out with the sva R package. Genes with non-zero coefficient estimates were selected as best predictors.

3.2.6 Weighted Gene Co-Expression Network Analysis (WGCNA)

The WGCNA package was run on R to construct a gene co-expression network and identify modules. Briefly, a weighted correlation network was created by calculating the correlation coefficients. The weighted network was transformed into a network of topological overlap (TO), an advanced co-expression measurement that considers not only the correlation of two genes with each other but also the extent of their shared correlations across the weighted network. The TO matrix was then used to group highly co-expressed genes by hierarchical clustering. Finally, a dynamic tree cut algorithm was used to cut the hierarchical clustering tree, and modules were defined as the branches resulting from this tree cutting.

3.2.7 Non-negative Matrix Factorization (NMF)

We performed non-negative matrix factorization (NMF) clustering method to identify distinct subtypes among the 118 G-CIMP-negative GBMs based on lncRNA expression. NMF analysis was performed in R using ''NMF'' package (https://cran.r-project.org/package=NMF). Genes were ranked k=2-7 according to their maximum absolute deviation (MAD) values from high to low in the expression matrix. When

the 118 GBMs were clustered into two subtypes according to expression of 400 lncRNAs, we received the highest average clustering cophenetic scores.

3.2.8 Statistical Analysis

Experimental data were represented as mean ± SEM (Standard Error of the Mean). Data represented with the help of the statistics software GraphPad Prism (GraphPad Prism v5.0a – GraphPad Software). To compare two different groups, we used a Student's T test (paired or unpaired) for parametric variables. To compare different groups of samples, we used One-Way ANOVA (ANalysis of VAriance) test coupled to a Bonferroni post-test. Statistical significance for each analysis is shown in the corresponding figure. Kaplan–Meier (KM) estimate was used for comparing survival differences between the low-risk group and the high-risk group. Hazard ratio (HR) with a 95% confidence interval (CI) was used in Cox regression analysis, and a p-value<0.05 was considered significant. KM data were analysed by R program.

3.2.9 Microarray data analysis

Microarray data were extracted with Agilent Feature Extraction Software version 10.7 and data analysis was carried out using GeneSpring GX version 11.5 (Agilent Technologies). In the hypoxic versus normoxic NSC study, normalized data was analysed using paired t-test Limma (Morrissey & N Diaz-Uriarte, 2009) to detect differentially expressed transcripts (multiple test correction: Benjamini & Hochberg). Microarray data was also examined by Gene Set Enrichment Analysis (GSEA) using the KEGG pathway gene sets (for pathway enrichment) or the TF gene sets (for TF binding site enrichment) (Subramanian et al., 2005). To correct for multiple hypothesis testing, GSEA uses FDR to focus on controlling the probability that each reported result is a false positive. Since the primary goal of GSEA is to generate hypothesis, an FDR <0.25 is considered significant.

3.3 CELL CULTURES

3.3.1 Cell lines

Glioma initiating cells (GIC) are glioblastoma patient-derived stem-like cells lines obtained from different collaborators (Table 3.1). GIC were cultured in laminin-coated cell plates (0.75 mg/mL; Invitrogen) and maintained in Dulbecco's Modified Eagle Medium: Nutrient Mixture F-12 (DMEM/F12; Invitrogen) supplemented with 4.5% glucose (Sigma), 5 mM Hepes (Invitrogen), 100 U/mL penicillin, 100 mg/mL streptomycin (Invitrogen), 4 µg/mL heparin (Sigma Chemical), N-2 Supplement (Life Technologies), bFGF (20 ng/mL; Life Technologies) and EGF (20 ng/mL; Life Technologies). GIC were cultured at 37 °C, 5% CO2 and 5% oxygen.

293T-HEK were cultured using Dulbecco's Modified Eagle Medium (DMEM; Life Technologies) supplemented with 10% Fetal Bovine Serum (FBS, Invitrogen). Cells were kept at 37 °C in a humidified atmosphere containing 5% CO2 and 20% O2.

The cells were passaged when they reached 70-80% confluence in a new 100 mm plate. Cells were washed once with phosphate-buffered saline (PBS) without calcium and magnesium (Life Technologies) and incubated at 37 °C/5% CO2 for 10 minutes with Trypsin-like Enzyme (TripLE; Life Technologies). Cells were recollected with PBS and centrifuged during 5 minutes at 900 rpm or 1500 rpm for GICs and 293T-HEK respectively. The supernatant was aspirated and the cell pellet was re-suspended in 4 mL of complete fresh medium. Cell suspension was transferred to a new plate already containing 3-4 mL of complete fresh medium.

Table 3.1: Cells used to experimental procedures

Cell line	Cell type	Origin	Medium
GIC2	Human (glioblastoma, proneural subtype)	Dr. Alonso (CIMA, Pamplona)	DMEM/F12
GIC7	Human (glioblastoma, proneural subtype)	Dr. Gómez-Manzano/ Dr Juan Fueyo (MD Anderson Cancer Center, Houston)	DMEM/F12

PG88	Human (glioblastoma, mesenchymal subtype)	Dr. Tortosa I Moreno (IDIBELL)	DMEM/F12
PG90	Human (glioblastoma, mesenchymal subtype)	Dr. Tortosa I Moreno (IDIBELL)	DMEM/F12
GSC268	Human (glioblastoma, classical subtype)	Dr. Krishna P.L. Bhat (MD Anderson Cancer Center)	DMEM/F12
GSC6-27	Human (glioblastoma, classical subtype)	Dr. Krishna P.L. Bhat (MD Anderson Cancer Center)	DMEM/F12
293T-HEK	Human (Kidney)	Clontech	DMEM

3.4 DNA TECHNIQUES

3.4.1 Transformation into competent cells (DH5a)

Plasmid DNA amplifications were carried out after their introduction in chemically competent E. coli cells. Transformation of competent E. coli cells was carried out following the manufacturer's instructions (Subcloning Efficiency DH5 Competent Cells; Invitrogen). Briefly, cells were incubated with the DNA on ice for 30 minutes. Then, cells were placed at 45ºC for 90 seconds. 500 mL of XY Medium (2xYT Medium; Sigma) were added and incubated at 37ºC for 1 hour. After a briefly centrifugation, transformed cells were spread on pre-warmed selective plates during an overnight at 37ºC. For large-scale isolation of plasmid DNA, commercial maxipreparations were used following the manufacturer's instructions (NucleoBond Xtra Maxi; Macherey-Nagel). DNA determinations were made using a spectrophotometer (Nanodrop; Thermo Scientific).

3.5 CELL TRANSDUCTION

3.5.1 DNA electroporation

We used CRISPR/Cas 9 system to get GPR56 knock out in $CD44^{low}$ GIC7s. To do that, cells were washed once with PBS without calcium and magnesium and get off

plate with Trype. Then, the GICs were recollected with 5 mL of PBS and were counted by Countess® Automated Cell Counter/invitrogen ($10 \cdot 10^{-6}$ L of cells + $10 \cdot 10^{-6}$ L trypan blue). The volume necessary to obtain $3 \cdot 10^{6}$ of cells/well was calculated and put it in a new tube. Then, the tube was centrifuged during 5 min at 900 rpm. After pour off the supernatant, the pellet was resuspended in $100 \cdot 10^{-6}$ L of electroporation buffer. Next, $3 \cdot 10^{-6}$ g of plasmids were added, homogenised and placed in a electroporation cuvette. Finally, the cells were electroporated using the Nucleofector II device (Lonza) at A-033 and seeded in 6MW plate with $2 \cdot 10^{-3}$ L of complete NSC medium to the maintenance.

To obtain GPR56 knockout GICs, we used a pool of three GPR56 KO plasmids (sc-406370; Santa Cruz Biotechnology), each of which encode for a GPR56-specific 20 nt guide RNA (gRNA) together with the Cas9 ribonuclease. These plasmids were co-electroporated along with a GPR56-HDR plasmid, which enables the insertion of specific selection markers by homologous recombination where Cas9-induced DNA cleavage has occurred. We used an HDR plasmid that incorporates Red Fluorescent Protein (RFP) anda gene to puromycin resistance (sc-406370-HDR; Santa Cruz Biotechnology).

3.5.2 Lentiviral and retroviral infection

Lentiviral vectors were generated by co-transfection of the plasmids of interest plus viral packaging vectors. 293T-HEK were cultured in 100 mm cell plates (70% confluence). 293T-HEK were transfected with the three-lentiviral packaging plasmids (VSVG, RSV-REV and pMDL g/p RRE) using the GeneJet Plus DNA transfection Reagent (SignaGen Laboratories). At 24 and 48 hours post-transfection, culture supernatants were collected and purified by centrifugation at 18,000 g for 2 hours at 4ºC. Pellets were resuspended in PBS and used it or stored at -80ºC until use.

For infection, cells were treated with 100 µL of viral suspension for overnight (O/N). Cells were then washed and fresh medium was added. 48h later, infected cells were selected with the appropriate drug selection.

The sequences of plasmids used to lentiviral infection was a custom design of vector PLKO.1-PURO to target three different sequence of same gene:

- ENST00000608502.1 (PROCAR.1): TCGGCTTTGGAAATAGAATTT
- ENST00000608502.2 (PROCAR.2): ATCTCCTCGGCTTTGGAAATA
- ENST00000608502.3 (PROCAR.3): TTCGCAGTTGTTCTAACTTAT

- ENST00000547804.1 (LINC00941.1); ATGGACCAACTATGCTTATAA
- ENST00000547804.2 (LINC00941.2); TGGGCTCTTGATTTGAATTGA
- ENST00000547804.3 (LINC00941.3); TGGAGCATGTATCCATCTTAT

- ENST00000630360.1 (PAUPAR.1): TGCCCTAGTGATTGTCGAATT
- ENST00000630360.2 (PAUPAR.2): TCCAGGCTTACCTCTTCTTAA
- ENST00000630360.3 (PAUPAR.3): TCTGCCCAATTCACCTATAGT

3.6 SELF-RENEWAL ASSAY

We performed neurosphere formation assays to analyze the self-renewal capacity of GICs. 50 cells/well were seeded in a 96MW plate. The total number of newly formed neurospheres was counted, under a microscope, after 7 days in culture. The secondary neurospheres formation assay was performed to validate GIC's capacity to form a new neurosphere and their self-renewal capacity. The neurospheres formed in each well were re-collected, separately, and 50cells/well were re-seeded, after disaggregate them. Then, the newly neurospheres were manually counted under microscopy on day 7.

All experiments were done in sextuplicate. For primary neurosphere formation assay 48 wells were seeded for each condition. For the secondary neurosphere formation assay 12 wells were used for each condition.

3.7 RNA MANIPULATION

3.7.1 RNA extraction

The RNA extraction of FFPE tumour specimens was performed on five 15µm-deep tissue cuts using the RNeasy Mini Kit (Qiagen), according to the manufacturer's recommendations. RNA quantity and purity were measured with the NanoDrop ND-1000 spectrophotometer (Thermo Scientific). RNA integrity, determined by the RNA integrity number (RIN), was deter- mined with the 2100 Bioanalyzer (Agilent).

For RNA extraction of GICs, approximately, 10^6 cells were rinsed with PBS and lysed in RLT buffer (RNasy Mini Kit; Qiagen). Total RNA was immediately extracted according the manufacture's instructions (RNasy Mini Kit; Qiagen). RNA concentration and quality was assessed with a Nanodrop (Thermo Scientific).

3.7.2 RT-qPCR

A reverse transcription was performed using 500ng of the total RNA by using the High Capacity cDNA Reverse Transcription Kit according to the manufacture's recommendations (Applied Biosystems).

mRNA Reverse Transcription Conditions:

1. 25ºC for 10'
2. 37ºC for 2h
3. 4ºC

The real time quantitative PCR (RT-qPCR) was performed in the StepOnePlus Real-time PCR Systems (Applied Biosystems) using TaqMan Fast Universal. For human samples the following TaqMan probes (Life Technoligies) were used:

- CTGF. Ref:Hs01026927_g1
- TGFb1. Ref: Hs00998133_m1
- TGFbI. Ref: Hs00932747_m1
- FN1. Ref: Hs00365052_m1
- ZEB1. Ref: Hs00232783_m1

- CHI3L. Ref: Hs00609691_m1
- MCAM. Ref: Hs00174838_m1
- SNAI1. Ref: Hs00195591_m1
- SNAI2. Ref: Hs00950344_m1
- TAZ. Ref: Hs00794094_m1
- TIMP1. Ref: Hs00171558_m1
- CD44. Ref: Hs01075861_m1
- PAX6. Ref: Hs0108814_m1
- SERPINE1. Ref: Hs01126606_m1
- OLIG2. Ref: Hs00377820_m1
- SOX2. Ref: Hs01053049_s1
- SOX9. Ref: Hs0000165814_m1
- PAUPAR. Ref: Hs04405704_s1
- LINC00941. Ref: Hs05002771_g1
- PROCAR. Ref: Hs04231540_s1
- GPR56. Ref: Hs00938469_m1
- GAPDH. Ref: Hs99999905_m1

mRNA qPCR conditions:

1. 95ºC for 20’
2. 95ºC for 1’
3. 60ºC for 20’
4. Go to 2 x 39 cycles

The DCT value was obtained by subtracting the CT value of housekeeping genes to the CT value of the targeted genes. The relative mRNA expression level of the target genes was obtained by the formula 2-DCT.

3.7.3 Microarray analysis

Total RNA was extracted using the RNeasy Mini Kit (Qiagen). RNA quality control was performed in a 2100 Bioanalyzer (Agilent Technologies). In all samples, the RNA integrity number was >7. Complementary RNAs were prepared for hybridization in a G3 Human GE 8x60k array (Agilent Technologies), using the One-Colour Low Input Quick Amp labelling protocol according to the manufacturer's instructions (Agilent Technologies). Microarray data were extracted with Agilent Feature Extraction Software version 10.7 and data normalization was carried out using GeneSpring GX version 11.5 (Agilent Technologies). To identify genes differentially expressed across groups, normalized microarray data were analysed using a multiclass significance analysis of microarrays (SAM) with a false discovery rate (FDR) <5%.

3.8 PROTEIN MANIPULATION

3.8.1 Flow cytometry

Approximately 10^6 cells per each condition were collected, rinsed with PBS and blocked with PBS-BSA 1% for 20 minutes at 4 °C. Then, cells were stained with a APC-conjugated anti-CD44 (1/50; BD Pharmingen. Ref: 559250) for 1 hour at 4 °C. After three washes, cells were resuspended with PBS-BSA 1% and immediately assessed by flow cytometry using FACSCanto (Becton Dickinson). Analysis was performed using FlowJo software (Miltenyi Biotec).

3.8.2 Western blot

Cells were lysed by lyses buffer (50% of Buffer NP40 2x, 29,8% H_2O milliQ, 5% NaCl 5M, 5% NaF 1 M, 0,1% DTT 1M, 10% cocktail of proteases inhibitor, 0,1% Na_3VO_4 100·10- 3 M) at 4ºC for 20 minutes. Protein extract was quantified using Bradford due-binding method (Protein Assay; Bio-Rad Laboratories). The samples with the Bradford were incubate at room temperature for 5-15 minutes and the absorbance at 595 nm was analysed by SynergyTM HT (from BioTek).

The protein lysates were mixed up with LB 2x (Laemmli samle buffer from Bio-rad), previously diluted with DTT (4 part LB2x with 1 part DTT). Then, the lysates were boiled for 5 minutes at 95 ºC in Corning® LSETM digital dry bath.

Cells extracts were separated on a 10% polyacrylamide gel, at 200V for 45 minutes, and transferred to Nitrocellulose membrane (from GE Healthcare Life Science), at 100V for 1 hour. The membrane was incubated with a specific blocking buffer (Odyssey blocking Buffer; LI-COR Biosciences) for 1 hour at room temperature. Primary antibody (Table 3.2**: Antibodies to Western blot**) was incubated during an O/N at 4ºC in constant agitation. The primary antibody was washed 3 times for 5 minutes. Secondary fluorescent antibody was incubated for 1 hour at room temperature, as follows: donkey anti-goat and donkey anti-mouse IRDye 680CW or IRDye 800LT (LI-COR Biosciences). Membrane was washed again and target proteins were detected using the ODYSSEY Infrared Imaging System (LI-COR Biosciences) following the manufacturer's instructions. Analysis was performed using Image Studio Software (LI-COR Biosciences).

Table 3.2: Antibodies to Western blot

Antigen	**Host**	**Manufacturer**	**Dilution**
GRP56	Goat	R&D Systems	1/500
GAPDH	Mouse	Ambion	1/40000

4 RESULTS

4.1 IDENTIFICATION OF LONG NON-CODING RNAs INVOLVED IN RESISTANCE TO THERAPY IN GBM

Long non-coding RNAs (lncRNAs) have been implicated in the regulation of stem cell properties, such as self-renewal and differentiation (Feng et al., 2015; Pu et al., 2015; Wei et al., 2017), as well as the control of gene expression (D. Li, Lu, Li, Qi, & Yu, 2019a; Rizvi et al., 2017; Lei Zhang et al., 2019; T. Zhang et al., 2019). Changes in gene expression are observed during transitions between glioblastoma (GBM) subtypes, such as MES differentiation, which confers resistance to therapy to glioblastoma (Bhat et al., 2013; Mao et al., 2013; Moreno, et al., 2017; Y. Piao et al., 2013). Therefore, we hypothesized that lncRNAs might be regulating transitions between different GBM subtypes and, subsequently, be involved in resistance to therapy.

On the other hand, the self-renewal capacity of cancer stem-cells (CSCs) also might be responsible for drug resistance and cancer relapse due in part to their ability to self-renew and differentiate into heterogeneous cancer cells (J. Chen et al., 2012; Dean, Fojo, & Bates, 2005; A. Singh & Settleman, 2010). Some lncRNAs regulate the self-renewal capacity of stem cells (W. Liu et al., 2017). Because of that, we also hypothesized that lncRNAs might be regulating the self-renewal property of GICs, which may be another mechanism of resistance to therapy and relapse of GBMs.

To test our hypothesis, we selected several candidate lncRNAs after various in silico analyses of RNA-sequencing data from 36 of 124 GBM samples (GLIOCAT dataset). Then, we performed cellular assays to assess the function of the selected lncRNAs. To study the implication of candidate lncRNAs in the biology of GICs, a loss-of-function approach was performed using shRNA-mediated knockdown of these lncRNAs. Next, we analysed the gene expression of different GBM subtype markers to study whether knockdown of candidate lncRNAs would promote GBM subtype transitions. Furthermore, we analysed the self-renewal capacity of lncRNA

knockdown-GICs, using the neurosphere formation assay, to study the implication of our candidate lncRNAs in self-renewal of GICs.

4.1.1 Network analysis using weighted gene co-expression network analysis of RNAseq data from GBM specimens

To identify candidate lncRNAs involved in GBM pathogenesis, we performed various in silico analyses of an unpublished RNAseq dataset of GBM specimens homogeneously treated by the Stupp Regimen (GLIOCAT dataset). First, 36 GBM specimens from our dataset were classified, according to their mRNA expression, into molecular subtypes (PN, CL and MES) by using the Support Vector Machines (SVM) algorithm. Next, we performed a network analysis to study the co-expression of genes (both protein-coding mRNAs and lncRNAs) in each subtype by using weighted gene co-expression network analysis (WGCNA). WGCNA allows the identification of different gene networks based on co-expression relationships between all expressed genes across all samples in the dataset (Langfelder & Horvath, 2007, 2008; B. Zhang & Horvath, 2005). The co-expression network is based on topological overlap (TO) between genes, which simultaneously considers not only the correlation of two genes with each other but also the degree of their shared correlations within the network (Ravasz, Somera, Mongru, Oltvai, & Barabási, 2002; B. Zhang & Horvath, 2005), providing a more robust measure of relatedness than correlations alone (Yip & Horvath, 2007).

WGNA constructed gene co-expression modules that assign the genes to different modules by cluster dendrogram trees (Figure 4.1, Figure 4.2 and Figure 4.3). Using this approach, we obtained different modules for each GBM subtype with each module corresponding to a group of co-expressed genes: 51 modules characteristic for the PN subtype, 51 modules characteristic for the CL subtype and 42 modules characteristic for the MES subtype (Figure 4.1, Figure 4.2, Figure 4.3 and Figure 4.4) (Table 4.1).

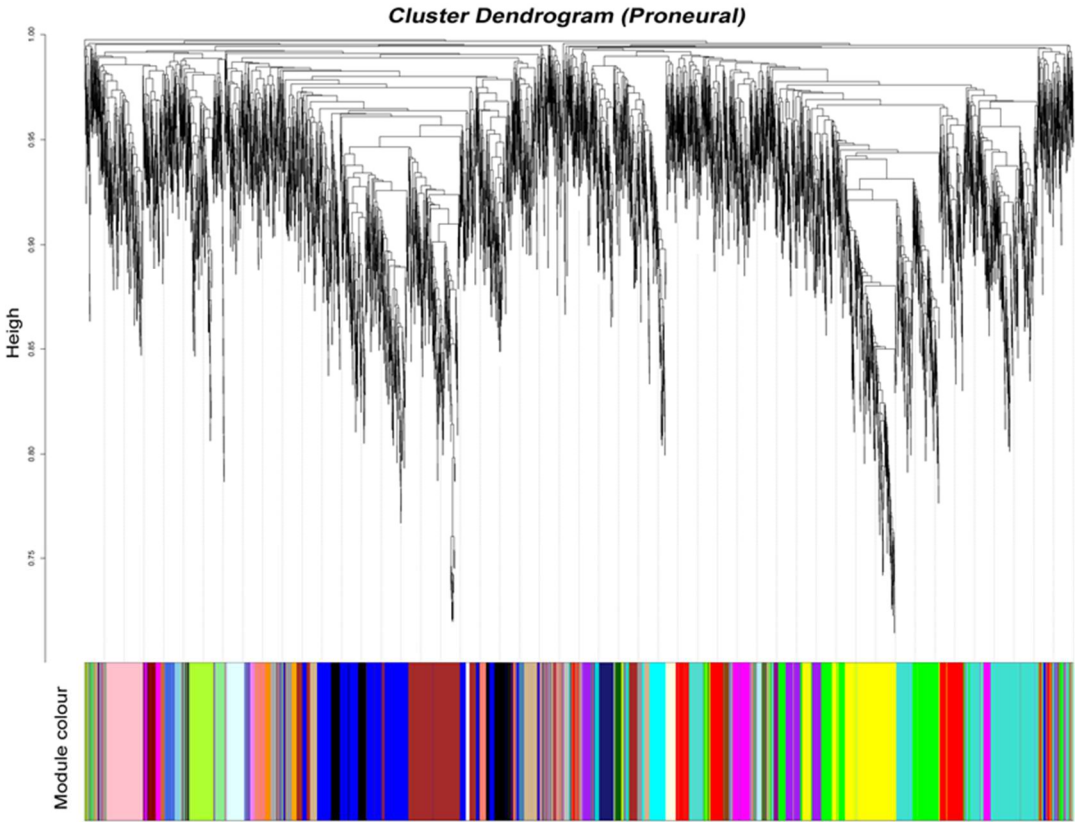

Figure 4.1: Clustering dendrogram of genome-wide genes in PN GBM obtained by Weighted Gene Co-expression Network Analysis (WGCNA). *Gene dendrogram obtained by clustering the dissimilarity based on consensus Topological Overlap with the corresponding module colours indicated by the colour row. Each coloured row represents a colour-coded module that contains a group of highly connected genes co-expressed in PN subtype. A total of 51 modules were identified.*

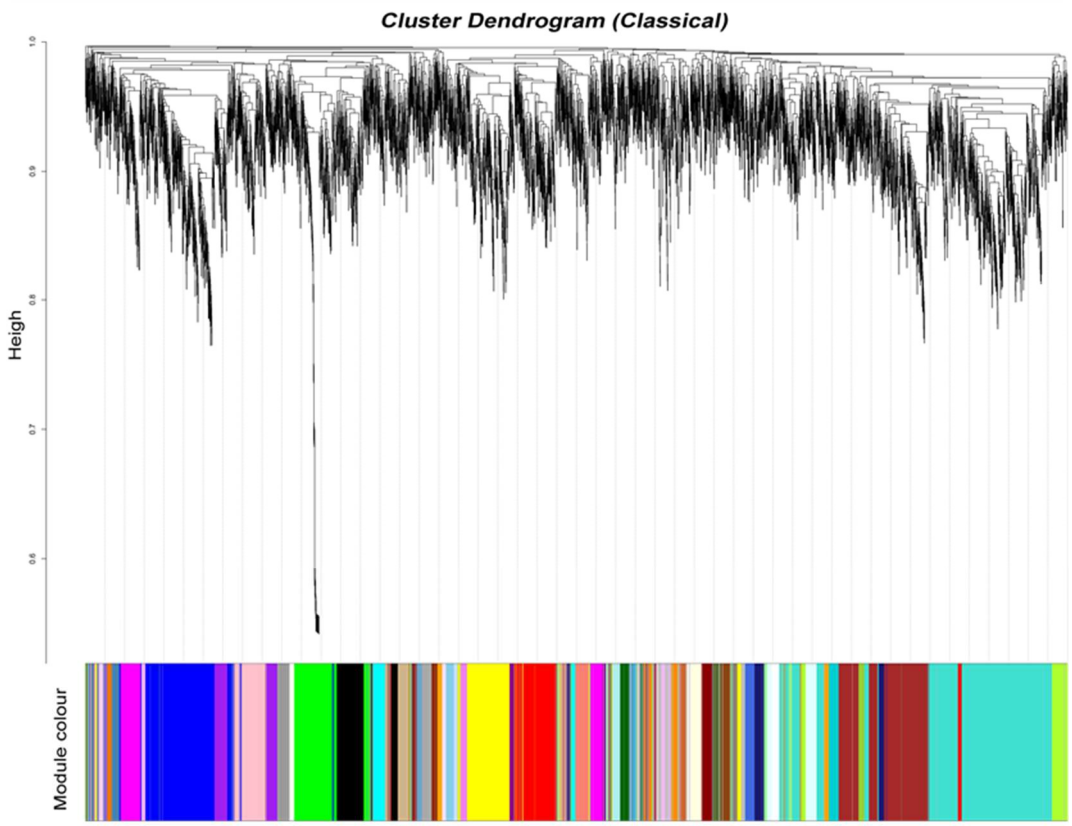

Figure 4.2: Clustering dendrogram of genome-wide genes in CL GBM obtained by Weighted gene co-expression network analysis (WGCNA). *Gene dendrogram obtained by clustering the dissimilarity based on consensus Topological Overlap with the corresponding module colours indicated by the colour row. Each coloured row represents a colour-coded module that contains a group of highly connected genes co-expressed in CL subtype. A total of 51 modules were identified.*

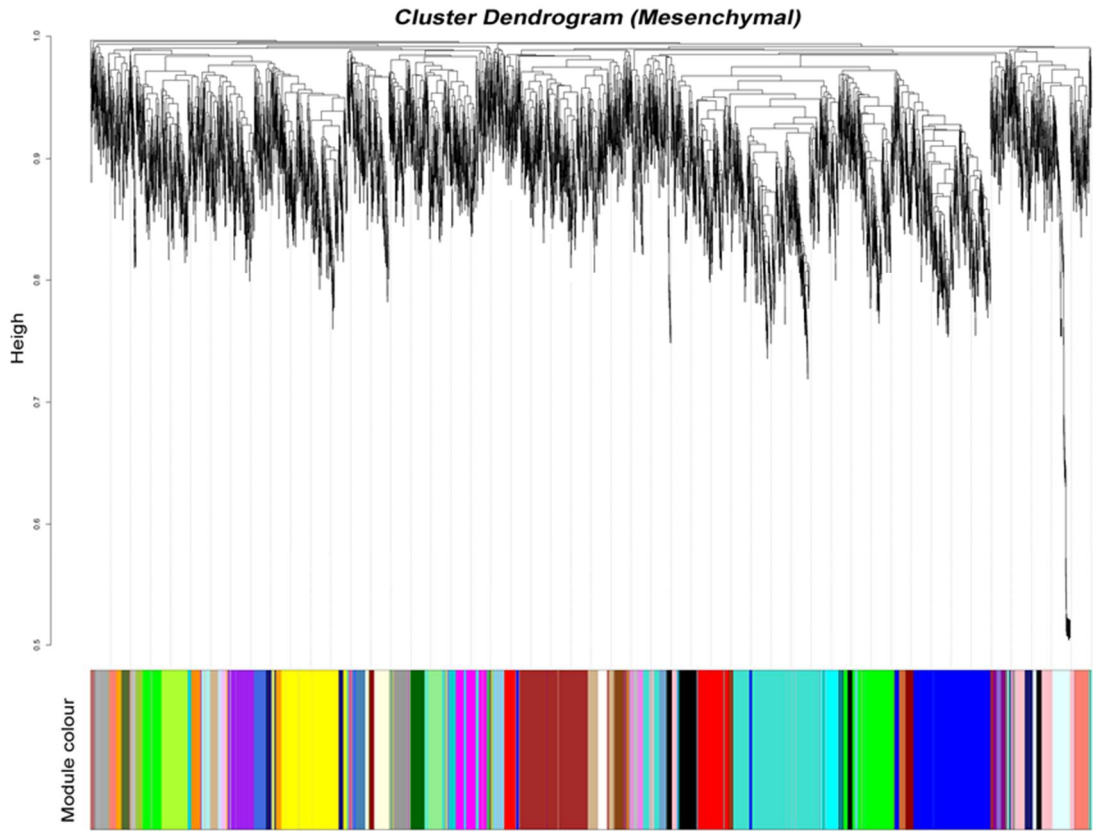

Figure 4.3: Clustering dendrogram of genome-wide genes in MES GBM identified by Weighted gene co-expression network analysis (WGCNA). *Gene dendrogram obtained by clustering the dissimilarity based on consensus Topological Overlap with the corresponding module colours indicated by the colour row. Each coloured row represents a colour-coded module that contains a group of highly connected genes co-expressed in MES subtype. A total of 42 modules were identified.*

Yellow module

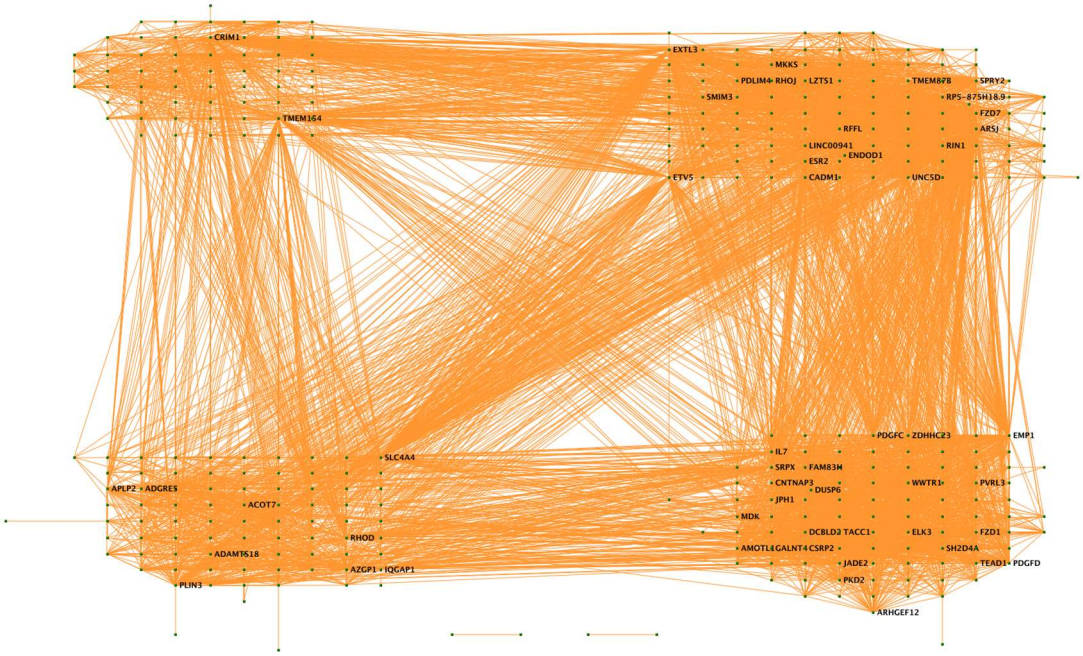

Turquoise module

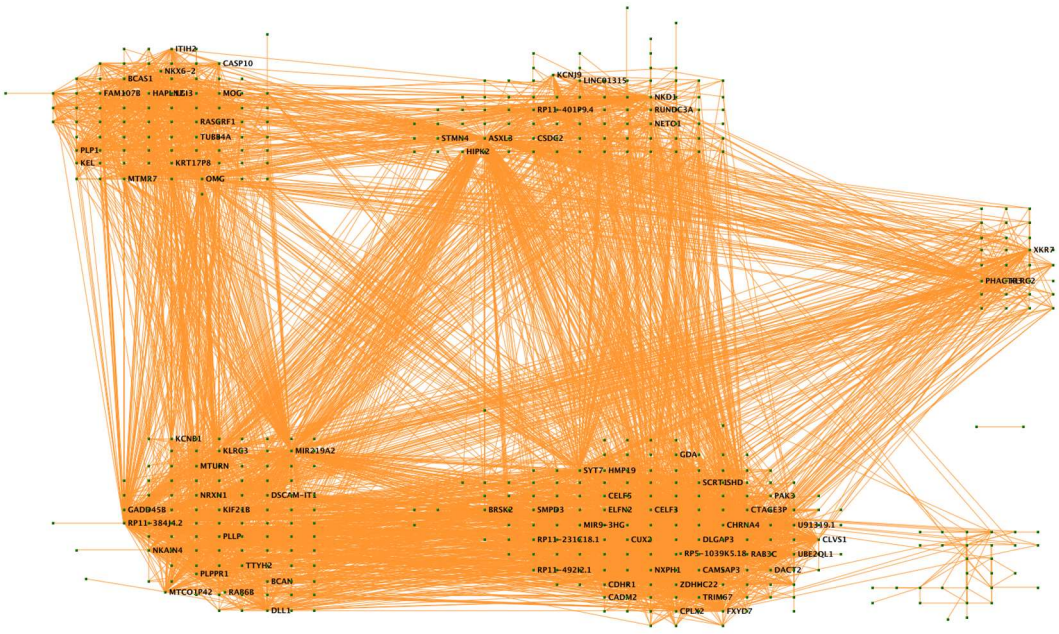

Figure 4.4: Visualization of yellow (top) and turquoise (bottom) modules in MES subtype*. The green square nodes represent specific nodes and linkage in the module network of MES GBMs. For clarify, only the top-ranked genes were represented. Some lncRNAs are in the top-ranked genes in the network, such as LINC00941 in the yellow module network and MIR219A2 in the turquoise module network.*

4.1.2 Identification of candidate lncRNAs for functional studies

To identify lncRNAs that might be involved in the regulation of the stem-like properties of GICs, we explored our WGCNA results and sought for candidate lncRNAs according to the following criteria: (1) their co-expression along with genes characterized to have a prominent role in GBM subtype pathogenesis, such as STAT3 and C/EBPβ (Bhat et al., 2013) or PDGFRA (Rand et al., 2005) (2) their specific (or at least enriched) expression in one of the molecular subtypes, (3) the kin value within a given network, which indicates the predicted prominence of the gene in the network (kin value ranges from 0 to 1, with 1 indicating the most important) (Table 4.1), and (4) their level of gene expression with a preference for those with the greatest expression. Four different lncRNAs were selected from these analyses (Table 4.2).

Table 4.1: Subtype modules from Weighted Gene Co-expression Network Analysis. *Shown the modules with the selected candidate lncRNAs (green), with the name of the gene, in which module is present, the kind of transcript (protein-coding RNA (PC), long non-coding RNA (lncRNA), antisense RNA (antisense), sense intronic (sense_intronic) and transcribed pseudogene (Pseudogene), To be Experimentally Confirmed (TEC)), the mean expression (meanExpr) along with all samples and the*

kin value. Only are represented the top 30 genes, according to their kin value, and the molecular subtype related genes (blue).

30 Top Genes in Tan Module (CL)	meanExpr	kin
ENSG00000233858.4,AC026904.1,lncRNA	4,254	1,000
ENSG00000125347.13,IRF1,PC	8,889	0,893
ENSG00000182141.9,ZNF708,PC	11,148	0,787
ENSG00000281880.1,PAUPAR,lncRNA	**5,730**	**0,758**
ENSG00000237101.1,RP11-365O16.6,antisense	3,073	0,750
ENSG00000186532.11,SMYD4,PC	9,140	0,708
ENSG00000119638.12,NEK9,PC	10,937	0,707
ENSG00000259448.2,RP11-16E12.1,lncRNA	5,403	0,683
ENSG00000115507.9,OTX1,PC	7,267	0,674
ENSG00000234617.1,SNRK-AS1,antisense	4,401	0,662
ENSG00000198920.9,KIAA0753,PC	9,301	0,658
ENSG00000108786.10,HSD17B1,PC	6,975	0,651
ENSG00000280248.1,CTD-2047H16.3,TEC	6,103	0,641
ENSG00000248221.1,STX18-IT1,sense_intronic	2,307	0,637
ENSG00000272542.1,RP11-255P5.2,lncRNA	3,730	0,607
ENSG00000185946.15,RNPC3,PC	10,291	0,596
ENSG00000264176.1,MAGOH2P,Pseudogene	2,945	0,592
ENSG00000240038.6,AMY2B,PC	9,384	0,592
ENSG00000231609.5,AC009501.4,antisense	4,632	0,582
ENSG00000186399.10,GOLGA8R,PC	7,320	0,580
ENSG00000229495.1,RP11-173D14.3,lncRNA	3,513	0,578
ENSG00000239783.1,RP5-1050K3.3,Pseudogene	2,508	0,565
ENSG00000143315.6,PIGM,PC	8,743	0,563
ENSG00000128829.11,EIF2AK4,PC	9,848	0,561
ENSG00000272405.1,RP11-284F21.10,antisense	6,450	0,528
ENSG00000274797.1,RP11-407N8.5,antisense	2,766	0,528
ENSG00000085465.12,OVGP1,PC	6,764	0,527
ENSG00000278611.1,CTC-543D15.8,lncRNA	4,474	0,522
ENSG00000127511.9,SIN3B,PC	11,222	0,520

30 Top Genes in Yellow Module (MES)	meanExpr	kin
ENSG00000180801.12,ARSJ,PC	8,846	1,000
ENSG00000155760.2,FZD7,PC	9,353	0,956
ENSG00000012232.8,EXTL3,PC	11,126	0,940
ENSG00000150938.9,CRIM1,PC	10,572	0,929
ENSG00000170006.11,TMEM154,PC	8,244	0,921
ENSG00000244405.7,ETV5,PC	10,388	0,897
ENSG00000134531.9,EMP1,PC	12,045	0,882
ENSG00000080493.13,SLC4A4,PC	11,942	0,878
ENSG00000235884.3,LINC00941,lncRNA	**6,073**	**0,843**
ENSG00000104432.12,IL7,PC	4,408	0,838
ENSG00000276851.1,RP5-875H18.9,lncRNA	0,814	0,833
ENSG00000174791.10,RIN1,PC	8,190	0,819
ENSG00000101955.14,SRPX,PC	8,822	0,815
ENSG00000136158.10,SPRY2,PC	10,649	0,812
ENSG00000105355.8,PLIN3,PC	9,091	0,790
ENSG00000173156.6,RHOD,PC	3,661	0,789
ENSG00000160862.12,AZGP1,PC	6,577	0,783
ENSG00000156687.10,UNC5D,PC	8,146	0,777
ENSG00000145431.10,PDGFC,PC	9,501	0,773
ENSG00000182985.16,CADM1,PC	11,699	0,772
ENSG00000104611.11,SH2D4A,PC	7,338	0,754
ENSG00000170962.12,PDGFD,PC	7,702	0,743
ENSG00000257594.3,GALNT4,PC	8,274	0,735
ENSG00000092871.16,RFFL,PC	10,792	0,734
ENSG00000256235.1,SMIM3,PC	8,994	0,717
ENSG00000177707.10,PVRL3,PC	9,324	0,714
ENSG00000140575.12,IQGAP1,PC	12,197	0,709
ENSG00000061337.15,LZTS1,PC	10,723	0,706
ENSG00000139318.7,DUSP6,PC	11,026	0,702
ENSG00000168610.14,STAT3,protein_coding	**11,907**	**0,271**

30 Top Genes in Turquoise Module (MES)	meanExpr	kin
ENSG00000141431.9,ASXL3,PC	7,156	1,000
ENSG00000258081.3,RP11-384J4.2,lncRNA	1,421	0,993
ENSG00000207955.3,MIR219A2,lncRNA	**3,904**	**0,982**
ENSG00000152932.7,RAB3C,PC	5,769	0,959
ENSG00000159409.14,CELF3,PC	5,691	0,947
ENSG00000126861.4,OMG,PC	5,799	0,936
ENSG00000011347.9,SYT7,PC	6,880	0,930
ENSG00000232872.2,CTAGE3P,Pseudogene	2,121	0,917
ENSG00000119283.15,TRIM67,PC	4,033	0,917
ENSG00000140807.5,NKD1,PC	9,224	0,901
ENSG00000221946.7,FXYD7,PC	3,734	0,895
ENSG00000076826.9,CAMSAP3,PC	4,521	0,894
ENSG00000101204.15,CHRNA4,PC	3,691	0,892
ENSG00000261685.2,RP11-401P9.4,lncRNA	7,599	0,885
ENSG00000087495.16,PHACTR3,PC	6,176	0,882
ENSG00000003987.13,MTMR7,PC	4,177	0,876
ENSG00000205810.8,KLRC3,PC	2,739	0,876
ENSG00000148123.14,PLPPR1,PC	5,942	0,867
ENSG00000177182.10,CLVS1,PC	4,559	0,862
ENSG00000132702.12,HAPLN2,PC	5,071	0,857
ENSG00000101198.14,NKAIN4,PC	6,482	0,853
ENSG00000174672.15,BRSK2,PC	6,812	0,851
ENSG00000162728.4,KCNJ9,PC	5,579	0,847
ENSG00000262801.5,U91319.1,lncRNA	1,655	0,846
ENSG00000122584.12,NXPH1,PC	6,005	0,840
ENSG00000273214.1,RP5-1039K5.18,lncRNA	2,163	0,829
ENSG00000230327.1,MTCO1P42,Pseudogene	3,799	0,818
ENSG00000102934.9,PLLP,PC	6,672	0,815
ENSG00000260903.2,XKR7,PC	3,513	0,808
ENSG00000172216.5,CEBPB,protein_coding	**8,826**	**0,368**

30 Top Genes in Salmon Module (PN)	meanExpr	kin
ENSG00000226840.1,PAICSP3,Pseudogene	1,564	1,000
ENSG00000242061.1,CTD-2555K7.1,Pseudogene	0,293	0,980
ENSG00000279600.1,RP11-637C24.5,TEC	4,475	0,955
ENSG00000126970.15,ZC4H2,PC	8,089	0,935
ENSG00000247199.3,RP11-373N22.3,antisense	5,817	0,906
ENSG00000272769.1,RP11-725P16.2,lncRNA	3,793	0,899
ENSG00000257703.5,RP11-328J6.1,lncRNA	1,027	0,868
ENSG00000261478.1,RP11-429B14.4,lncRNA	**7,767**	**0,864**
ENSG00000176294.4,OR4N2,PC	3,421	0,858
ENSG00000228304.1,OR4K6P,Pseudogene	3,097	0,832
ENSG00000183891.5,TTC32,PC	6,915	0,823
ENSG00000256937.1,KRT17P8,Pseudogene	3,115	0,820
ENSG00000204956.5,PCDHGA1,PC	8,883	0,812
ENSG00000198153.8,ZNF849P,Pseudogene	1,816	0,807
ENSG00000259780.3,RP11-304L19.12,lncRNA	4,243	0,791
ENSG00000139971.15,C14orf37,PC	9,795	0,789
ENSG00000256463.8,SALL3,PC	10,807	0,774
ENSG00000213131.3,YWHAZP4,Pseudogene	3,513	0,768
ENSG00000240527.1,RP11-429G19.3,sense_intronic	3,178	0,767
ENSG00000263146.2,RP11-849I19.1,lncRNA	7,144	0,761
ENSG00000272070.1,AC005618.6,lncRNA	8,764	0,757
ENSG00000183513.8,COA5,PC	9,230	0,744
ENSG00000165762.2,OR4K2,PC	0,102	0,732
ENSG00000249413.2,RP11-25H12.1,lncRNA	-0,417	0,730
ENSG00000163568.13,AIM2,PC	4,318	0,728
ENSG00000227518.3,XXyac-YRM2039.3,antisense	3,047	0,725
ENSG00000079482.12,OPHN1,PC	11,012	0,721
ENSG00000198028.3,ZNF560,PC	4,136	0,711
ENSG00000248546.3,ANP32C,Pseudogene	3,476	0,707
ENSG00000134853.11,PDGFRA,protein_coding	**11,954**	**0,445**

Table 4.2: Summary of relevant information on candidate lncRNAs. *This table shows the ID (ENSG, alternative name) of lncRNAs, the majority transcript (ENST), the lncRNA expression levels in each subtype, their kin value and the prominent genes co-expressed in the same module as per WGCNA. Differences in gene expression between subtypes were significant for all lncRNAs selected ($p<0.05$).*

ENSG ID (ALTERNATIVE NAME)	ENST ID	PN	CL	MES	RELATED GENES	KIN
ENSG00000207955.3 (MIR219A2, PROCAR)	ENST00000608502.2	**214.82**	55.54	23.72	C/EBPβ	0.98
ENSG00000261478.1 (RP11-429B14.4, LNC-TICRR-2)	ENST00000567484.1	**376.27**	151.60	78.78	PDGFRA	0.86
ENSG00000281880.1 (PAUPAR)	ENST00000630360.1	19.40	**80.57**	51.45	PAX6	0.76
ENSG00000235884.3 (LINC00941)	ENST00000547804.1	32.96	44.30	**161.44**	STAT3	0.84

ENSG00000207955.3 (MIR219A2) and ENSG00000261478.1 (RP11-429B14.4) were lncRNAs enriched in the PN subtype. ENSG00000207955.3 was expressed in the network where C/EBPβ, a master transcription factor involved in MES-GBM differentiation, was present, whereas ENSG00000261478.1 was co-expressed in the same network as PDGFRA, a PN-signature gene, which is involved in neuron and oligodendrocyte differentiation (Jackson et al., 2006).

ENSG00000207955.3, which we re-named as PROneural C/EBPβ-Associated lncRNA (PROCAR), might be correlated with microRNA 219. PROCAR and microRNA 219 are co-localized in chromosome 9 (Chromosome 9: 128,392,007-128,393,510 and Chromosome 9: 128,392,618-128,392,714, respectively), suggesting their mutual regulation. MicroRNA-219-5p inhibits the proliferation, migration, and invasion of epithelial ovarian cancer cells by targeting the Twist/Wnt/β-catenin signalling pathway (Wei et al., 2017) and inhibits breast cancer cell migration and epithelial-mesenchymal transition (Zhuang et al., 2017). Thus,

PROCAR might be involved in proliferation or mesenchymal differentiation in GBM regulating microRNA219.

Through the mutually targeted miRNA response elements (MREs) enrichment (MuTaME) method, described by Tay et al., ENSG00000261478.1 was predicted to be competing for endogenous RNA (ceRNA) of IL1R2 mRNA. MuTaME method is mainly based on the number of miRNAs with which ceRNAs and target transcripts shared, as well as the distribution of MREs in both ceRNAs and target transcripts (Tay et al., 2011). Changes in MREs of ceRNAs affect the capacity of a proper mRNA transcript to attach miRNAs (Salmena, Poliseno, Tay, Kats, & Pandolfi, 2011; Tay et al., 2011). Therefore, ENSG00000261478.1 might be regulating IL1R2 mRNA, which has been involved in tumourogenesis, such as promoting breast cancer proliferation (Lixing Zhang et al., 2020).

ENSG00000281880.1 or PAX6 Upstream Antisense RNA (PAUPAR) was enriched in the CL subtype and has been involved in the regulation of the transcription factor PAX6 (Singer et al., 2019; K. W. Vance et al., 2014). Since PAX6 is part of the metagene signature of the CL subtype (Q. Wang, Hu, Hu, Sulman, et al., 2017), we identified PAUPAR as an interesting candidate to validate functionally in GICs. PAUPAR has been found to regulate the expression of multiple genes related to cell cycle and maintains a dedifferentiated state in neuroblastoma (K. W. Vance et al., 2014). Additionally, PAUPAR has been involved in tumourigenesis in uveal melanoma (Ding et al., 2016) and can interact with the chromatin regulatory protein Kinesin-ii-Associated Protein 1 (KAP1) that regulates a set of target genes involved in neural cell differentiation (Pavlaki et al., 2018).

Finally, ENSG00000235884.3 (also known as LINC00941) is enriched in the MES subtype, compared with the CL and PN subtype, and is co-expressed in the same network module as STAT3. LINC00941 is enriched in hepatocellular carcinoma (HCC) patients (X. Yan et al., 2017) and it correlates with poor survival in HCC and LUAD patients (L. Wang et al., 2019). Using GO functional enrichment analysis, LINC00941 was found to be involved in cell adhesion (H. Liu et al., 2019). Additionally, LINC00941 has been correlated with cell migration, cell proliferation, as well as processes associated with the immune system (Luo et al., 2018). Interestingly, Yang et al. showed that knockdown of LINC00941 significantly

inhibited the expression of MES-related genes, whereas LINC00941 overexpression had the opposite effect (X. Yan et al., 2017).

Among all four lncRNAs, we selected one lncRNA for each subtype. We chose LINC00941 and PROCAR because they were in the same network as STAT3 and C/EBPβ, respectively, two transcription factors that are linked to the acquisition of a MES phenotype in GBM. Notably, both selected lncRNAs had a kin value close to 1, even higher than STAT3 (kin value = 0.27) or C/EBPβ's (kin value = 0.37). Although LINC00941 and PROCAR were related to genes associated to MES subtype, LINC00941 was enriched in the MES subtype, whereas PROCAR was enriched in the PN subtype, suggesting that these lncRNAs might be meaningful in the MES and the PN subtype, respectively. We also selected PAUPAR, based on its enrichment in the CL subtype and its high kin value within its network. Importantly, PAUPAR has been involved in PAX6 regulation (K. W. Vance et al., 2014), a transcription factor that is a core gene signature in the CL subtype and suppressor of growth in GBM (Mayes et al., 2006; Zhou et al., 2005).

4.1.2.1 Expression of candidate lncRNAs in two independent datasets

We studied the expression of our candidate lncRNAs among GBM subtypes using two different datasets (GLIOCAT and TCGA dataset). The TCGA dataset was used as an independent dataset to corroborate the expression of our candidate lncRNAs observed in our GLIOCAT dataset. As we expected, the same distribution of lncRNAs was observed in the TCGA dataset as in the GLIOCAT dataset (Figure 4.5). In both datasets, ENSG00000207955 (PROCAR) lncRNA was enriched in PN and G-CIMP^{+} subtypes, whereas ENSG00000261478.1 (RP11-429B14.4) was enriched specifically in G-CIMP^{+} subtype. ENSG00000235884 (LINC00941) was enriched in MES subtype. In the GLIOCAT dataset, ENSG00000281880 (PAUPAR) was enriched in both CL and MES subtypes, although more prominently in the CL subtype. In the TCGA dataset, ENSG00000281880 (PAUPAR) was specifically enriched in CL-GBMs (Figure 4.5).

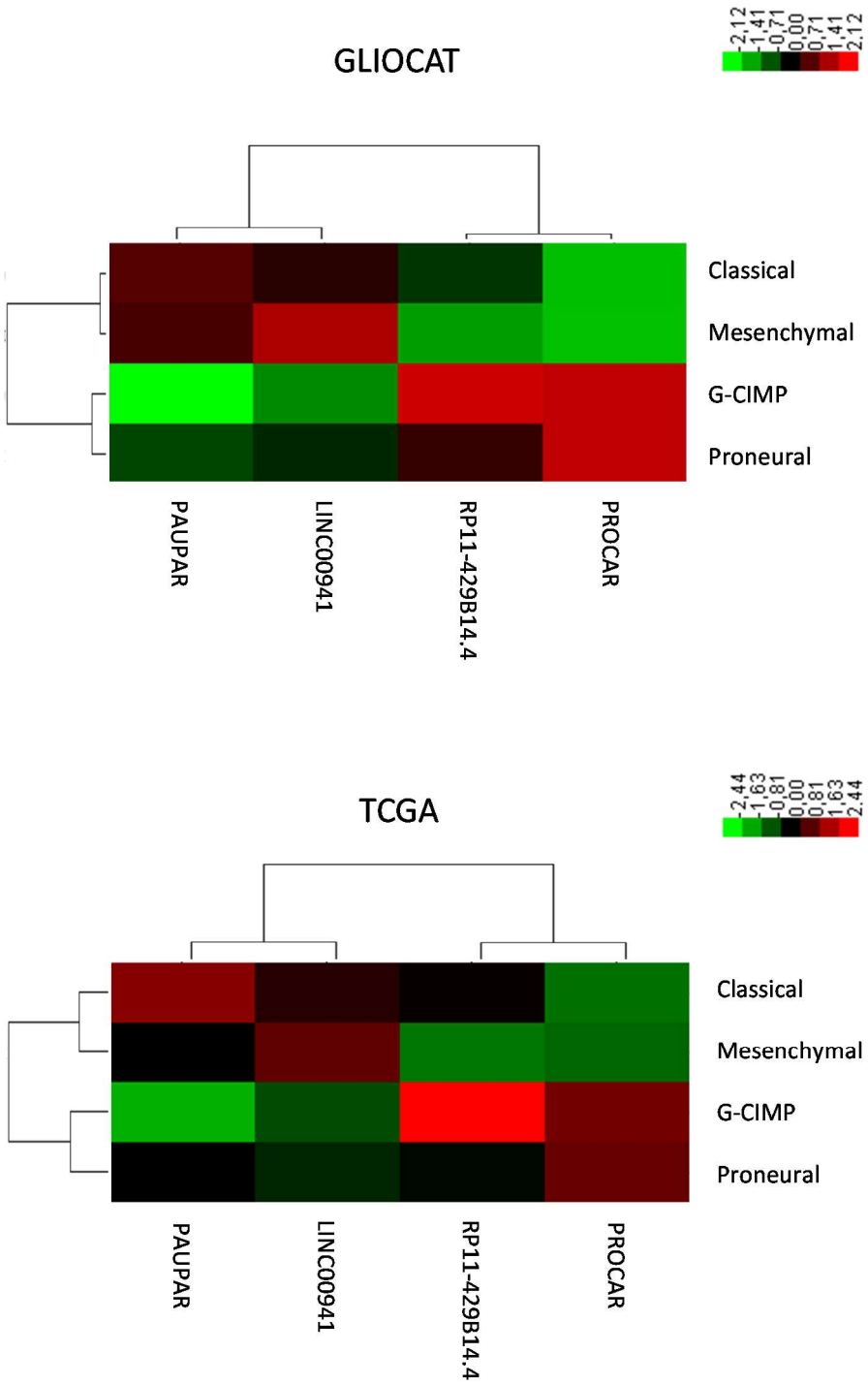

Figure 4.5: Heatmap of expression of the four candidate lncRNAs in the GLIOCAT (top) and the TCGA dataset (bottom). *"SamR" analysis was been performed (FDR<5%) by R Studio Software. Clustering 3.0 was used to perform the clusters and JavaTreeView was used to visualize the heatmap. We observed the same distribution of lncRNA expression in the TCGA dataset as in the GLIOCAT dataset. PROCAR (ENSG00000207955) was enriched in PN and G-CIMP subtypes, whereas ENSG00000261478.1 (RP11-429B14.4) was enriched especially in G-CIMP^{+}. LINC00941 (ENSG00000235884) and PAUPAR (ENSG00000281880) were enriched in the MES and in the CL subtype, respectively.*

These results validate our identified candidate lncRNAs in a larger collection of samples corroborating that they are specifically enriched in a certain GBM molecular subtype. These evidences suggest that these lncRNAs might have a role in the regulation of gene expression of GBM subtypes and might thus be involved in the transitions between subtypes.

To carry out the functional analyses in GICs (next section), we finally selected three of the four candidate lncRNAs. We did not pursue the functional characterization of ENSG00000261478.1 (RP11-429B14.4), which is enriched in GCIMP$^+$ GBMs, because we did not have any GIC cell line belonging to this subtype. This G-CIMP$^+$-enriched lncRNA merits a full functional characterization in the future.

4.1.3 Functional analyses of the candidate lncRNAs in GICs

To test the role of the candidate lncRNAs in the biology of GICs, we performed loss-of-function studies by inducing shRNA-mediated knockdown of our candidate lncRNAs in different GIC cell lines. Then, we performed cell-based assays to compare cell function and phenotypes between lncRNA knockdown-GICs versus control cells and thereby identify the function of the candidate lncRNAs. We focused our loss-of-function studies on two different cell-based assays: analysis of transitions between GBM subtypes and self-renewal assays, since both cellular processes are involved in resistance to therapy.

One of the mechanisms that confers resistance to therapy in GBM is the transition between subtypes, specifically MES differentiation (Bhat et al., 2013; Mao et al., 2013; Moreno et al., 2017; Y. Piao et al., 2013). Many lncRNAs control gene expression and some of them are involved in the differentiation process of stem cells (Rizvi et al., 2017; Lei Zhang et al., 2019) Therefore, we hypothesized that lncRNAs may have a role in the transition between GBM subtypes. Therefore, a possible transition between subtypes was studied by analysing the expression of subtype-specific markers in lncRNA knockdown-GICs by RT-qPCR (OLIG2 and SOX2 as PN markers, SOX9 and PAX6 as CL markers, SERPINE and CTGF as MES markers). Expression of the MES marker CD44 was also analysed by flow cytometry.

Another mechanism of resistance to therapy in GBM is the self-renewal capacity of GICs (Bao et al., 2006; J. Chen et al., 2012; Dean et al., 2005; G. Liu et al., 2006; A. Singh & Settleman, 2010; S. K. Singh et al., 2003). Self-renewal signature is associated with resistance to chemoradiotherapy in glioblastoma (Murat et al., 2008). Even if most of the cells in a tumour are destroyed, GICs may survive and regenerate the tumour by their self-renewal capacity (Bao et al., 2006). GICs might be in quiescent status during therapy and then, activate the proliferation and self-renewal process allowing growth glioblastoma (Steinbichler et al., 2018). Recent studies have observed that lncRNAs regulate gene expression during the differentiation and self-renewal process (Pu et al., 2015; Feng et al., 2015; Liu et al., 2017; Wang X et al., 2016). Therefore, we hypothesized that the candidate lncRNAs might regulate the self-renewal capacity of GICs, which might be a mechanism that confers resistance to therapy or allows the progression of GBMs (J. Chen et al., 2012; Dean et al., 2005; S. K. Singh et al., 2003). To test whether the self-renewal capacity of GICs was regulated by some of the candidate lncRNA, we analysed the self-renewal capacity of the lncRNA knockdown-GICs using the neurosphere formation assay.

4.1.3.1 Generation of lncRNA knockdown-GICs

First of all, we generated knockdown-GICs for each candidate lncRNA using short-hairpin RNA (shRNA)-encoding lentiviruses, which allow stable integration into the host genome and long-term knockdown of the targeted gene (Figure 4.6). We purchased lentiviral plasmids encoding shRNAs against our candidate shRNAs (Table 4.2) from Sigma. Sigma shRNA plasmids contain bacterial (ampicillin) and mammalian (puromycin) antibiotic resistance genes for selection in either bacterial or mammalian cell lines (Figure 4.7). Then, these shRNA plasmids plus packaging plasmids were transfected to 293 cell lines to generate the lentiviral particles. Finally, the GICs were infected with the lentiviral particles to down-regulate the expression of candidate lncRNAs.

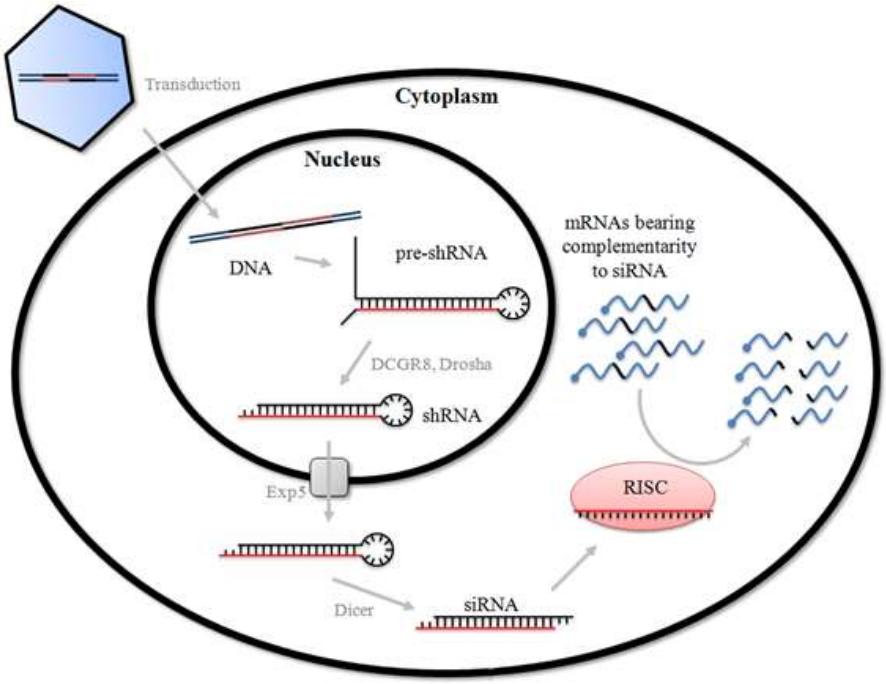

Figure 4.6: Mechanism of shRNA induced gene silencing. *Lentiviruses infect the GICs integrating the plasmid into DNA. After expression viral RNA in the nucleus, shRNAs are processed by Drosha and then exported by Exportin-5 (Exp5) to the cytoplasm, where they associate with Dicer, which removes the loop sequence, resulting into small RNA duplexes (siRNAs). SiRNAs are loaded into the RNA-induced silencing complex (RISC), which facilitates binding between one of the siRNA strands and protein-coding mRNAs that have nucleotide sequence complementary to the siRNA. Once siRNA/mRNA binding has occurred, and thus the target mRNA has been recognized, a nuclease in RISC degrades the mRNA, reducing the amount of mRNA that is available for translation and protein production. (Lord CJ, et al., 2009) (Adapted from O'Keefe, 2013)*

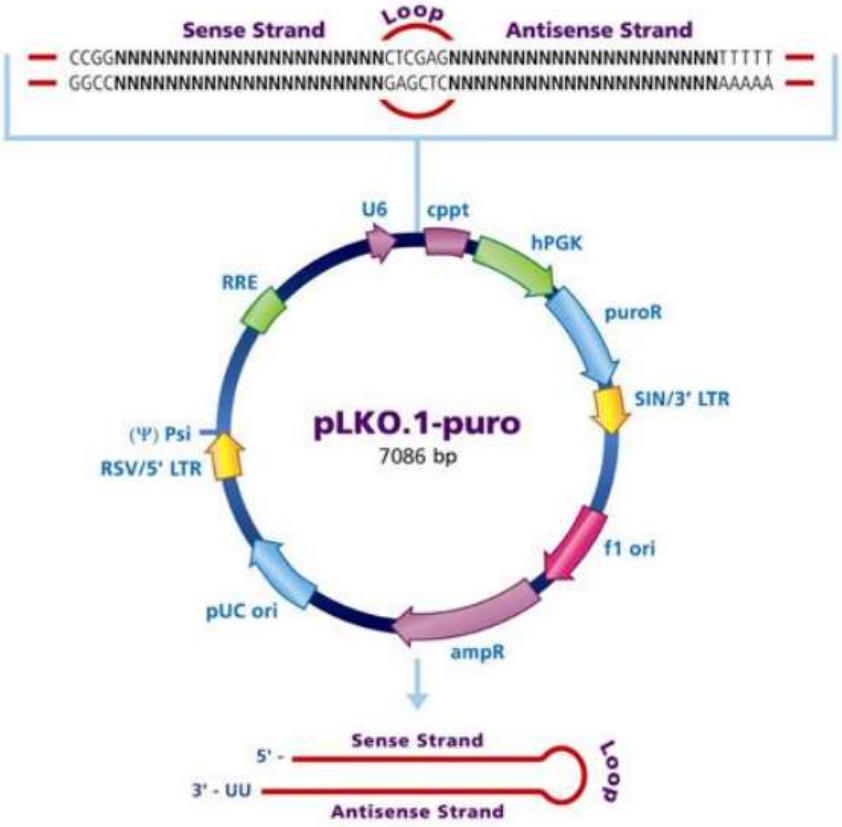

Figure 4.7: MISSION shRNA pLKO.1-puro construct. *PLKO.1-puro construct contains the shRNA sequence and ampicillin (ampR) and puromycin (puroR) antibiotic resistance genes for selection of inserts in either bacterial or mammalian cell lines.*

The shRNAs used to mediate the knockdown of our candidate lncRNAs were designed to target the most abundant transcript for each gene (Table 4.2). Additionally, we used three different shRNA constructs for each transcript to rule out possible off-target effects. To obtain knockdown of each of the following lncRNAs: LINC00941 in MES-GICs, PROCAR in PN-GICs and PAUPAR in CL-GICs (Table 4.3). We used three different plasmids with different shRNA sequences for each lncRNA, and two cell lines of each subtype, to avoid the off-target effects and to increase the specificity of the results.

After lentiviral infection, GICs were selected by 2·10-6 g/mL of puromycin for 5 days to select for GICs that had integrated the viral constructs. However, not all of the cells survived to lentivirus infection and puromycin selection. When shRNAs-GICs died, a second infection was performed to get the cell line, but in some case, it

was not possible. ShPAUPAR- GSC268 did not survive to the second lentivirus infection, the same as shPROCAR.2-PN-GICs. In summary, we finally obtained two MES-GIC lines with three different shlncRNA plasmids, one CL-GIC line with three shlncRNA plasmids and two PN-GICs with two different shlncRNA plasmids (Table 4.3).

Table 4.3: GICs and shRNAs used to generate the lncRNA knockdown-GICs. *The first column of the table shows the infected GICs and the subtype to which they belong. The second column indicates the shRNA used. The third column shows the cells that survived (✓) or did not survive (✕) to the lentiviral infection and the name that was given (sh-lncRNA.version of plasmid used-GIC).*

GIC (Subtype)	shRNA	Modified GIC → ✓/ ✕
GIC2 (PN)	shPROCAR	shPROCAR.1-GIC2 → ✓ shPROCAR.2-GIC2 → ✕ shPROCAR.3-GIC2 → ✓
GIC7 (PN)	shPROCAR	shPROCAR.1-GIC7 → ✓ shPROCAR.2-GIC7 → ✕ shPROCAR.3-GIC7 → ✓
GSC6-27 (CL)	shPAUPAR	shPAUPAR.1-GSC6-27 → ✓ shPAUPAR.2-GSC6-27 → ✓ shPAUPAR.3-GSC6-27 → ✓
GSC268 (CL)	shPAUPAR	shPAUPAR.1-GSC268 → ✕ shPAUPAR.2-GSC268 → ✕ shPAUPAR.3-GSC268 → ✕
PG88 (MES)	shLINC00941	shLINC00941.1-PG88 → ✓ shLINC00941.2-PG88 → ✓ shLINC00941.3-PG88 → ✓
PG90S (MES)	shLINC00941	shLINC00941.1-PG90S → ✓ shLINC00941.2-PG90S → ✓ shLINC00941.3-PG90S → ✓

To confirm knockdown of lncRNAs in GICs, RT-qPCR of the targeted lncRNA was performed after puromycin selection of infected GICs.

The effective knockdown of LINC00941 was achieved by the three shRNA plasmids in PG88 (Figure 4.8A, left panel), with a significant expression decreased. In contrast, in the case of PG90S, we did not observe a statistically significant knockdown of LINC00941 with respect to control cells (Figure 4.8A, right panel).

On the same way, the RNA levels of PAUPAR were significantly decreased in shPAUPAR-GSC6-27 (CL-GICs) obtained by the three shRNA plasmids compared with control GSC6-27 (Figure 4.8B). Unfortunately, the second CL-GIC cell line (GSC268) did not survive any of the lentiviral infections and we were not able to obtain PAUPAR knockdown-GICs for this cell line.

Finally, we analysed the levels of PROCAR lncRNA in shPROCAR-PN-GICs. Surprisingly, even though the transduced GICs were resistant to puromycin, the expected decrease in PROCAR lncRNA expression was observed neither in GIC2 nor in GIC7 (Figure 4.8C). We did not observe significant differences between the infected shPROCAR-PN-GICs compared to its controls. Therefore, we didn't proceed to perform the functional analyses with these cells.

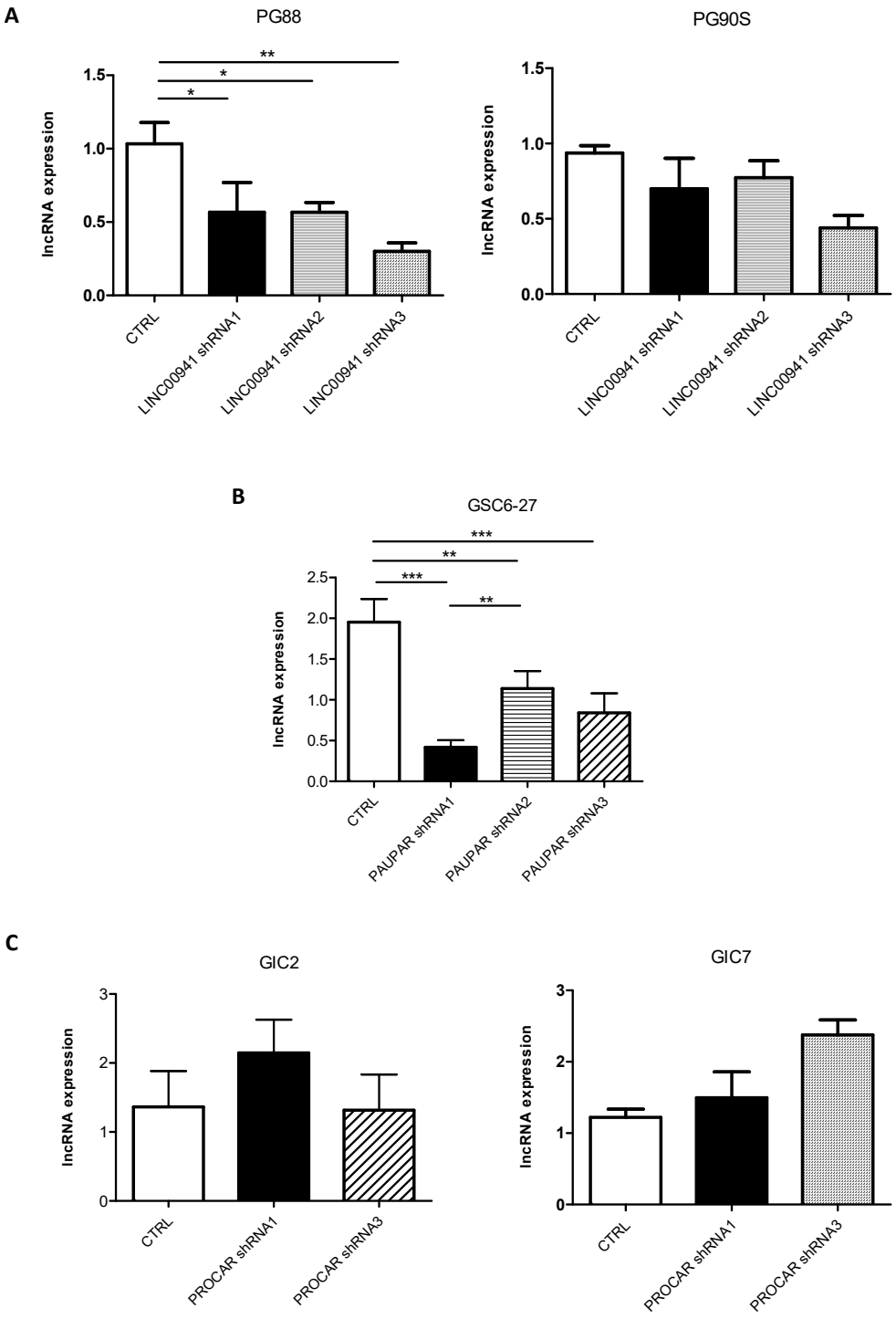

Figure 4.8: lncRNA expression levels analysed by RT-qPCR*. (A) LINC00941 lncRNA expression was analysed in PG88 (left panel) and in PG90S (right panel). Only PG88-MES-GICs infected with shLINC00941 had a significant expression of LINC00941 lncRNA decreased than the control. (B) PAUPAR lncRNA expression analysed in CL-GICs. Loss of PAUPAR RNA expression was observed in all shPAUPAR-GSC6-27 compared with the control. (C) PROCAR lncRNA expression was determined in PN-GICs, GIC2 and GIC7. Neither shPROCAR-GIC2 (left panel) nor shPROCAR-GIC7 (right panel) had lower expression of PROCAR than its controls. Data are represented as mean ± SEM of at least three independent experiments (ANOVA, *p<0.05, **p<0.01).*

In summary, we succeeded at generating MES-GICs with knockdown of the MES candidate lncRNA and CL-GICs with knockdown of the CL candidate lncRNA. We had never before tried shRNA-mediated knockdown of lncRNAs in our hands. Our results indicate that it is possible to efficiently generate a knockdown of lncRNAs by short-hairpin RNAs in GICs. Some lncRNAs are difficult to knockdown due to their localization (nuclear or cytoplasmic or dual), lncRNA transcript (in)accessibility to enzymes and their transcriptional landscape, among others (Vickers & Crooke, 2015; Zeng & Cullen, 2002). This might have been the case with PROCAR.

4.1.3.2 Role of LINC00941 in GICs

LINC00941, which we found enriched in MES-GBMs, correlates with MES-related genes (X. Yan et al., 2017) and has been involved in cell adhesion (H. Liu et al., 2019). Therefore, LINC00941 might be involved in maintaining a MES phenotype in GICs. To test this hypothesis, we studied the expression of different GBM subtype markers in LINC00941 knockdown-GICs by RT-qPCR (OLIG2 and SOX2 as PN markers, SOX9 and PAX6 as CL markers, SERPINE and CTGF as MES markers) or flow cytometry (CD44 as MES marker).

The flow cytometry analysis showed that the percentage of $CD44^+$ cells was not altered in shLINC00941-MES-GICs compared with control cells (Figure 4.9), neither in PG88 nor in PG90S GIC cell lines. These results suggest that knockdown of LINC00941 doesn't promote loss of a MES phenotype in these GICs.

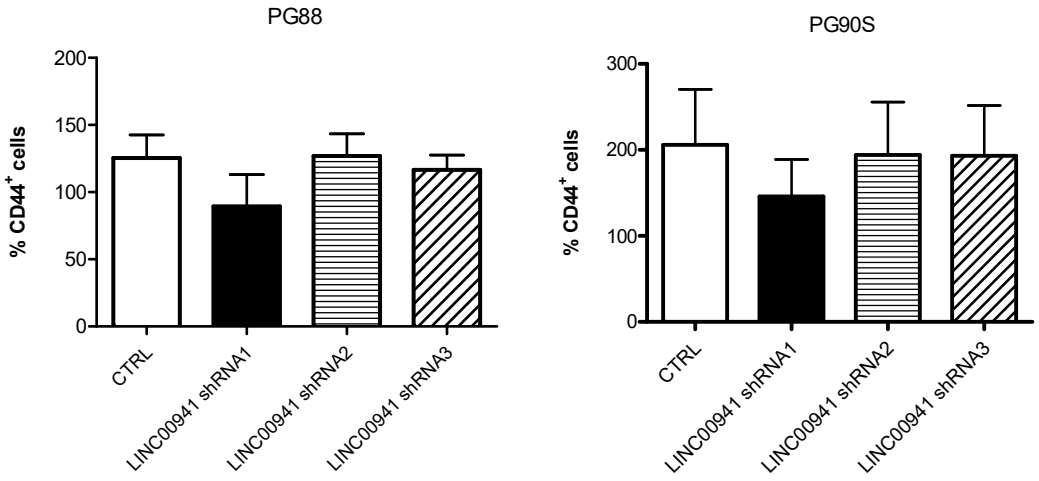

Figure 4.9: Flow cytometry performed to study the possible transition between GBM subtypes losing LINC00941 lncRNA expression in MES-GICs. *Histogram with the results of the CD44 protein expression analysed by flow cytometry in PG88 (left panel) and PG90S (right panel). No significant difference was observed between the percentage of CD44$^+$cells in shLINC00941-MES-GICs versus control-MES-GICs. Data are represented as mean ± SEM of at least three independent experiments (ANOVA, *p<0.05, **p<0.01, ***p<0.001).*

Regarding the subtype marker analysis by RT-qPCR, we observed slightly different tendencies between shLINC00941.1-PG88 and shLINC00941.3-PG88. shLINC00941.1-PG88 displayed increased CTGF expression with respect to control cells. In contrast, shLINC00941.3-PG88 showed a significant increase in the mRNA expression of SOX2, whereas they displayed a significant decrease in the expression of PAX6 and SERPINE compared with control and shLINC00941.1-PG88. Overall, from these results, we cannot conclude that there is a significant change in any subtype marker expression upon knockdown of LINC00941 (Figure 4.10). Taken together, our results suggest that LINC00941 knockdown-MES-GICs maintain their MES phenotype and that there are no GBM subtype transitions upon knockdown of LINC00941.

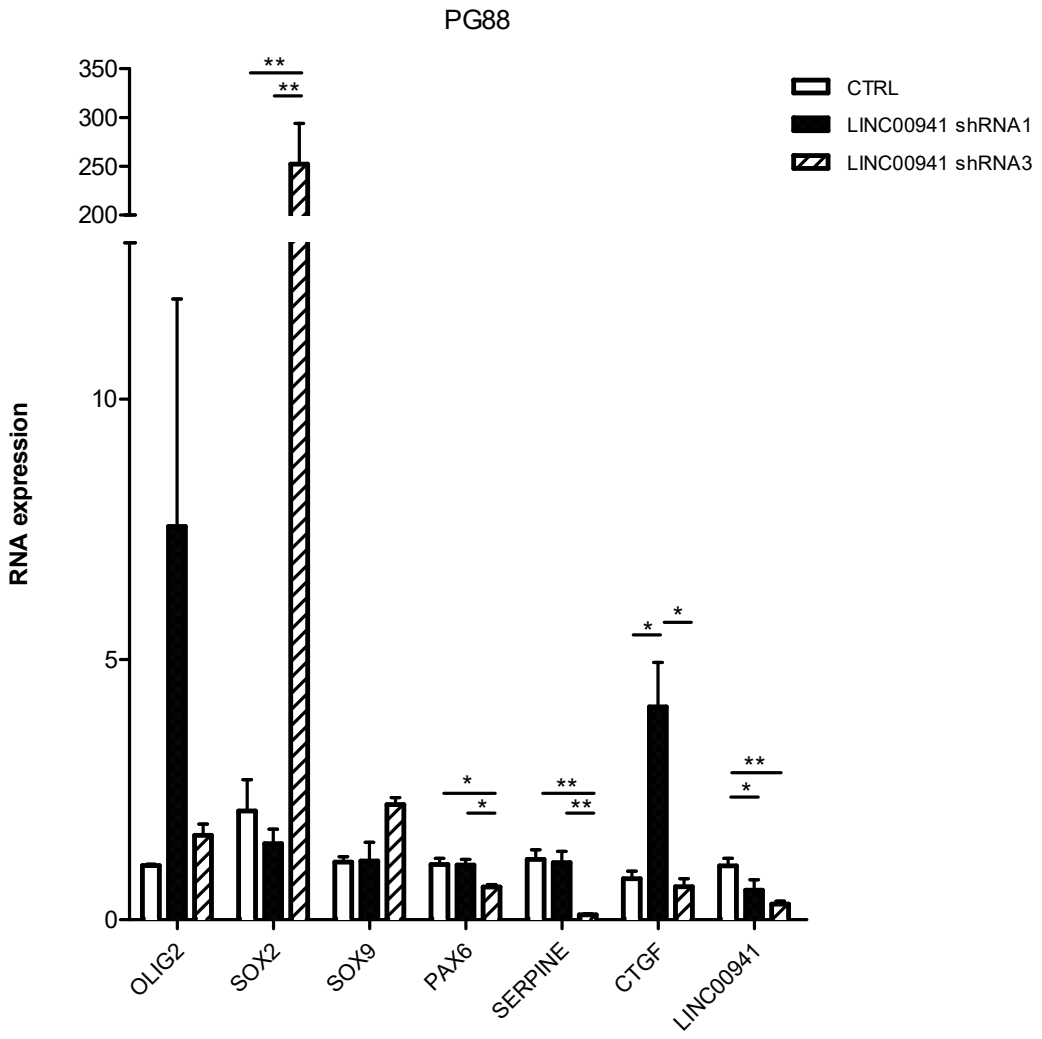

Figure 4.10: RT-qPCR performed to study the possible transition between GBM subtypes upon knockdown of LINC00941. *mRNA expression of different GBM subtype markers were analysed in shLINC00941.1-PG88 (shRNA1), shLINC00941.3-PG88 (shRNA3) and the control-GICs (CTRL). PN markers: OLIG2 and SOX2; CL markers: SOX9 and PAX6; MES markers: SERPINE and CTGF. Expression levels of LINC00941 lncRNA are also shown. Data are represented as mean ± SEM of at least three independent experiments (ANOVA, *p<0.05, **p<0.01, ***p<0.001).*

Next, to test whether the self-renewal capacity of GICs was regulated by LINC00941, we performed a neurosphere formation assay in LINC00941 knockdown-MES-GICs vs control cells. To do so, 50 cells/per well were seeded in a 96MW plate (48 wells/per condition). The number of primary neurospheres for each well was obtained by counting under the microscope the total number of newly formed neurospheres after 7 days in culture (Figure 4.11).

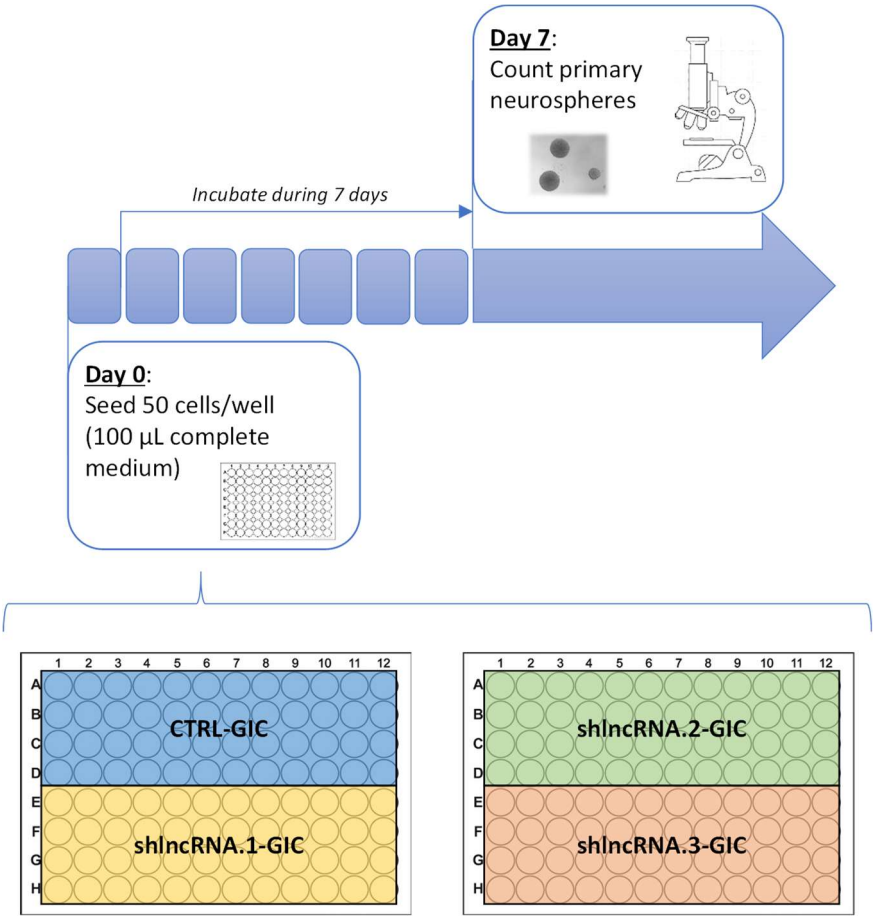

Figure 4.11: Experimental design for the neurosphere formation assay. *50 cells were seed in each well, in a 96-multiwell plate, and incubated for 7 days. After 7 days, the newly formed neurospheres were counted under the microscope to obtain the number of primary neurospheres in each condition.*

We observed fewer neurospheres in LINC00941 knockdown-MES-GICs than in control-MES-GICs, in both MES-GIC cell lines (PG88 and PG90S). The number of primary neurospheres was significantly decreased in the three LINC00941 knockdown-GICs in the PG90S GIC cell line compared to control cells (Figure 4.12, right panel). In the case of PG88, there was a significant reduction in the number of neurospheres in two of the LINC00941 knockdown-GICs, while shLINC00941.2-PG88 showed a decreasing tendency albeit without statistical significance (Figure 4.12, left panel).

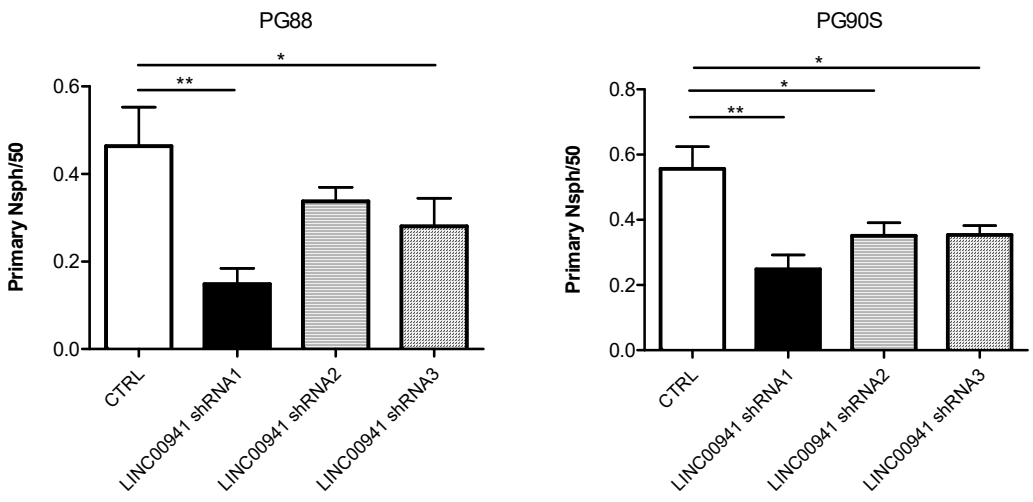

Figure 4.12: Self-renewal assay of LINC00941 knockdown-MES-GICs. *The number of primary neurospheres (Nsph) in shLINC00941-PG88 (left panel) and shLINC00941-PG90S (right panel). Knockdown of LINC00941triggers a decrease in the number of primary neurospheres in both MES-GICs. The neurospheres were counted and normalized to the number of cells seeded. Data are represented as mean ± SEM of four independent experiments (ANOVA, *p<0.05, **p<0.01).*

Taken together, our results show that LINC00941 knockdown in MES-GICs reduces their capacity to form neurospheres, without affecting their MES phenotype. Therefore, LINC00941 might promote the self-renewal capacity of MES-GICs.

4.1.3.3 Role of PAUPAR lncRNA in GICs

PAUPAR is a lncRNA that we found enriched in the CL-GBM subtype and that regulates the expression of the transcription factor PAX6 (Singer et al., 2019; K. W. Vance et al., 2014). PAX6 belongs to the core gene signature of the CL-GBM subtype (Q. Wang, Hu, Hu, Sulman, et al., 2017), and has been shown to suppress tumour growth in GBM (Mayes et al., 2006; Zhou et al., 2005). PAX6 has a pivotal role in forebrain development, where it is critical for the establishment of the pallial–subpallial boundary and it controls brain progenitor proliferation. Furthermore, PAUPAR has been involved in the regulation of cell cycle-related genes (Pavlaki et al., 2018), suppression of tumourigenesis (Ding et al., 2016) and neural cell differentiation (Pavlaki et al., 2018). Therefore, we hypothesized that PAUPAR might be regulating the expression of classical-subtype genes and/or regulating the

self-renewal capacity of GICs.

To study whether PAUPAR is involved in the establishment of the CL-subtype and whether its knockdown in GICs promotes any subtype shift, we analysed CD44 protein expression by flow cytometry in shPAUPAR-CL-GICs (Figure 4.13A). CD44 levels were not significantly altered upon PAUPAR knockdown. We also analysed by RT-qPCR the expression of several GBM subtype markers: OLIG2 and SOX2 as PN markers, SOX9 and PAX6 as CL markers and SERPINE and CTGF as MES markers (Figure 4.13B). The expression of OLIG2, SOX2 and PAX6 was increased by the three different PAUPAR shRNAs tested with respect to the control. However, only two shPAUPAR-GICs increased significantly the expression of OLIG2 and PAX6 mRNA. The rest of subtype markers analysed were not consistently altered. Taken together, these results show that knockdown of PAUPAR is not promoting any GBM subtype shift.

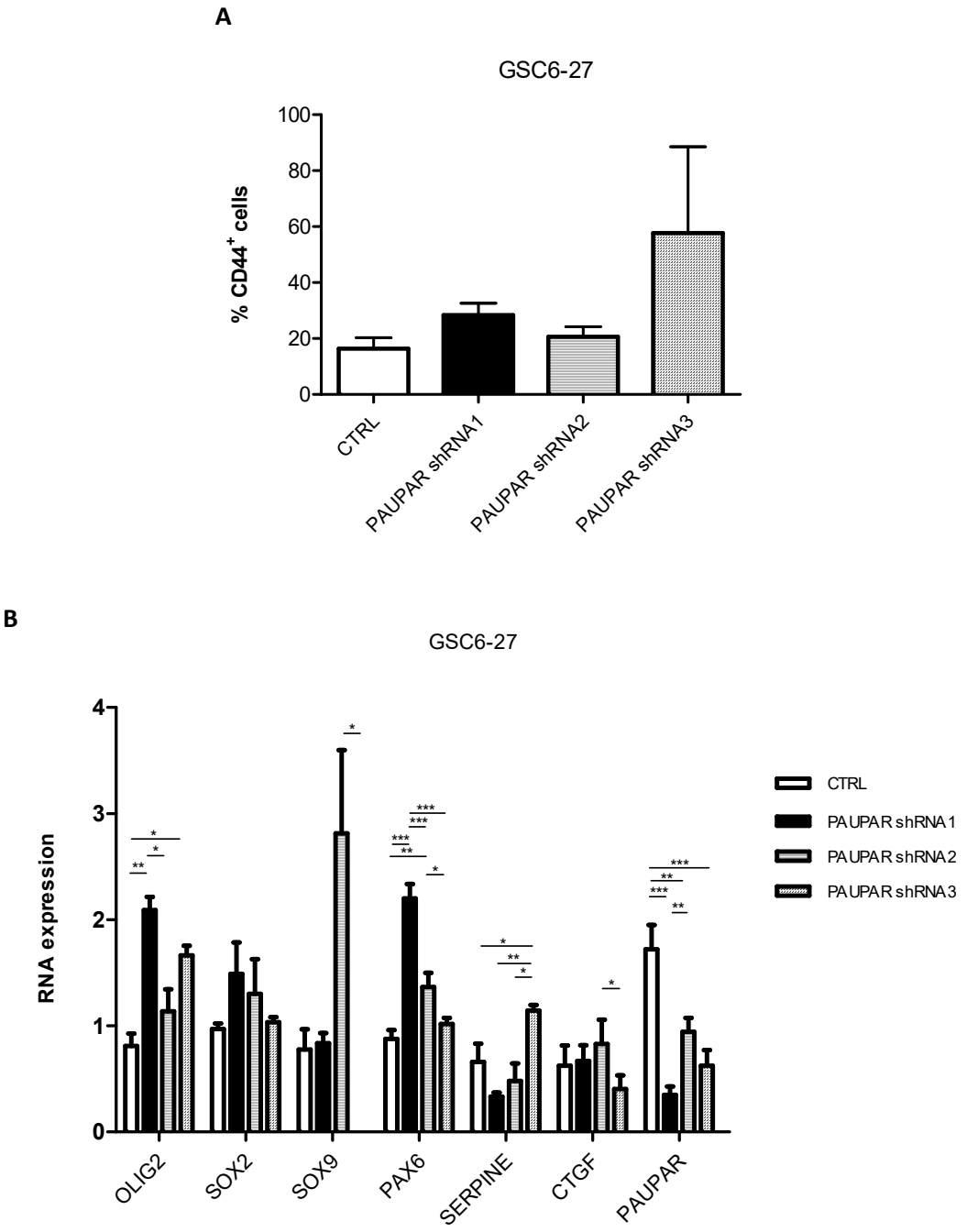

Figure 4.13: Study the expression of GBM subtype markers in shPAUPAR-GSC6-27. *A) Percentage of the CD44 positive cells based on protein expression analysed by flow cytometry of GSC6-27 control and shPAUPAR-GSC6-27. There were no significant differences in the percentage of CD44+ cells between any shPAUPAR-GSC6-27 and the control-GSC6-27. B) RT-qPCR was performed to study the mRNA expression of different GBM subtype's markers and PAUPAR. OLIG2 and SOX2 were the PN markers, SOX9 and PAX6 were the CL markers and SERPINE and CTGF were the MES markers used in the RT-qPCR. Data are represented as mean ± SEM of at least three independent experiments (ANOVA, *p<0.05, **p<0.01, ***p<0.001).*

Next, we set out to test whether PAUPAR regulates the self-renewal capacity of CL-GICs. To that end, we performed a neurosphere formation assay in shPAUPAR-GSC6-27 versus CTRL-GSC6-27. Briefly, 50 cells/per well were seeded in a 96MW plate (12 wells/per condition) and the total number of primary neurospheres for each well was counted under the microscope after 7 days in culture. Additionally, secondary neurospheres were also analysed. The secondary neurospheres validate the capacity of GICs within a primary neurosphere to form a new neurosphere, which is an indirect measure of their self-renewal capacity. To do that, the primary neurospheres formed in each well were collected, disaggregated mechanically into single cells and 50 cells/per well were re-seeded into another plate. Then, secondary neurospheres were manually counted under the microscope after 7 more days in culture (Figure 4.14).

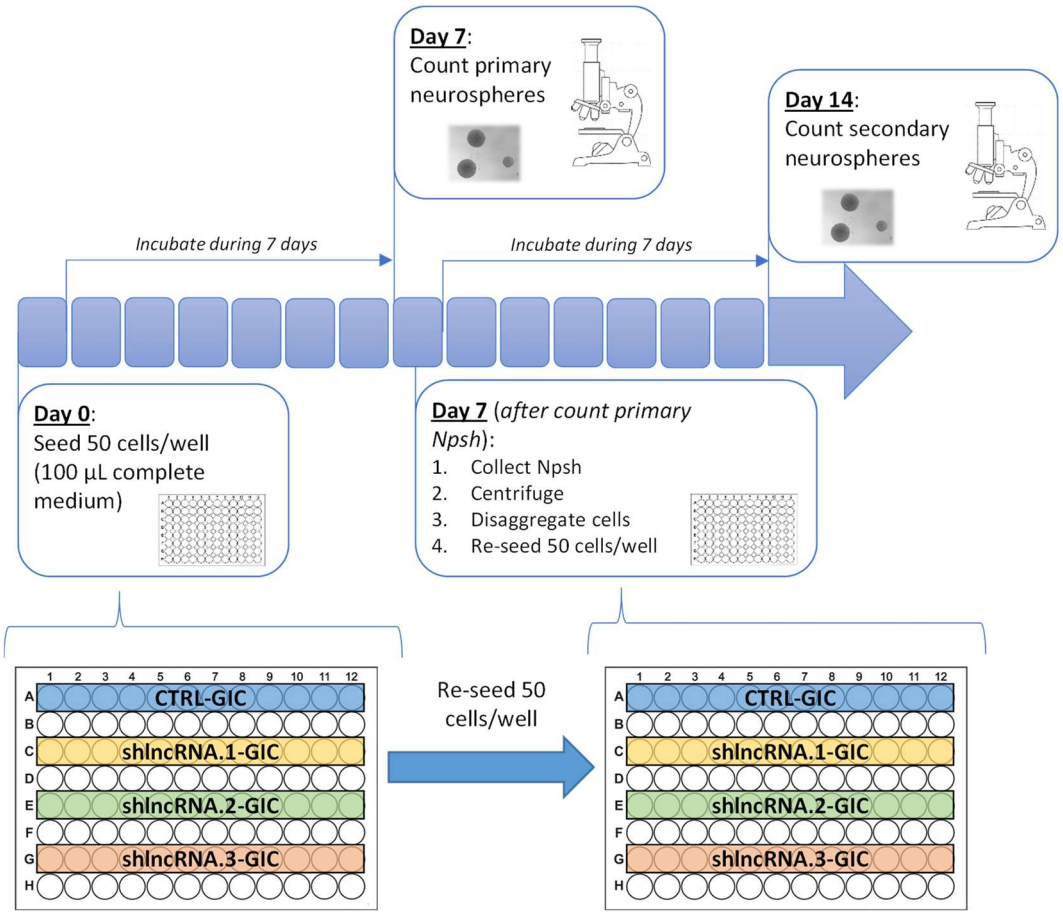

Figure 4.14: Experimental design for the neurosphere formation assay in shPAUPAR-CL-GICs. *50 cells were seed in each well, in a 96-multiwell plate, and incubate for 7 days in the incubator. After 7 days, the neurospheres (Npsh) were counted under the microscope to obtain the number of primary*

neurospheres in each condition. Next, the GICs were collected, disaggregated and re-seed in a new 96-multiwell plate (50 cells/per well). After 7 days in the incubator, the new neurospheres were counted to obtain the number of secondary neurospheres.

A significant decrease in the number of primary and secondary neurospheres was observed with the three shRNA constructs against PAUPAR in GSC6-27 (shPAUPAR.1-GSC6-27, shPAUPAR.2-GSC6-27 and shPAUPAR.3-GSC6-27) with respect to control cells (Figure 4.15). We initially observed a statistically significant decrease in the number of primary neurospheres formed in the three PAUPAR knockdown-CL-GICs with respect to the control. The secondary neurospheres were analysed to corroborate the difference in self-renewal capacity of PAUPAR knockdown-CL-GICs obtained. The effect of PAUPAR knockdown on secondary neurospheres was even more significant (p-values <0.01) in all three shPAUPAR-GSC6-27. Our results suggest that PAUPAR promotes the self-renewal capacity of CL-GICs.

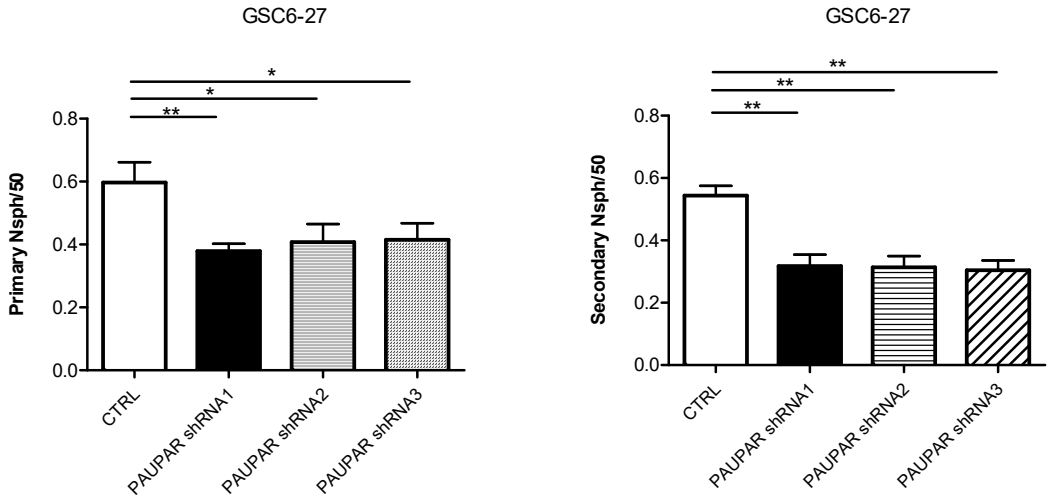

Figure 4.15: Self-renewal assay of shPAUPAR-GSC6-27*. Neurosphere formation assay (primary neurospheres (Nsph) (left panel) and secondary neurospheres (Nsph) (right panel)). CL-GICs decrease the number of primary and secondary neurospheres upon knockdown of PAUPAR lncRNA. The neurospheres were counted and normalized to the number of cells seeded. Data are represented as mean ± SEM of five independent experiments (ANOVA, *p<0.05, **p<0.01, ***p<0.001).*

Taken together, our results suggest that LINC00941 and PAUPAR lncRNA might be promoting the self-renewal capacity of GICs, but might not regulate the transition between GBM subtypes. The self-renewal capacity of GICs is prominent to initiate and propagate the tumour. Therefore, these lncRNAs might be involved in the relapse of GBM by maintaining the self-renewal capacity of GICs within tumour allowing the progression or the acquisition of resistance to therapy in GBMs. These lncRNAs may be a new target to develop new treatments to inhibit the self-renewal capacity of GICs and avoid the relapse and progression of GBM. More importantly, this inhibition would not promote any transition of GBM, avoiding the resistance to therapy acquired by mesenchymal differentiation.

4.1.4 Clustering analysis of GBM specimens according to lncRNA expression

Our WGCNA analyses of the RNAseq dataset gave us insights about novel regulators of self-renewal in different molecular subtype GICs. However, these analyses were based on the previous molecular classification according to protein-coding gene expression. Next, we set out to analyze in an unsupervised manner, whether lncRNA expression patterns would be able to sub-classify GBM tumour specimens into novel molecular subtypes, which might hopefully better correlate with clinical data, such as patient survival.

To this end, we performed gene clustering of 118 G-CIMP-negative GBM specimens of the GLIOCAT dataset according to solely to the expression of lncRNAs instead of protein-coding genes. From the 124 specimens of the dataset for which we had good quality RNAseq data, we excluded the 6 G-CIMP+ samples, which are known to have a better prognosis and might introduce a bias in our survival correlation assays. To cluster the samples, we used non-negative matrix factorization (NMF) to cluster the samples (introduced by Paatero and Tapper in 1994 (Paatero & Tapper, 1994) , and popularized by Lee and Seung in 1999 (Daniel D. Lee & H. Sebastian Seung, 1999)). NMF allows the analysis of high dimensional data and automatically extracts sparse and meaningful features from a set of nonnegative data vectors. NMF has been successfully applied for clustering gene expression and DNA methylation data and finding the genes most representative of the clusters (Devarajan, 2008; Hyunsoo Kim,

2007; Taslaman & Nilsson, 2012). NMF techniques can identify sources of variation such as cell types, disease subtypes, population stratification, tissue composition, and tumour clonality (Stein-O'Brien et al., 2017).

Brunet et al. showed that NMF classifies tumours (e.g. central nervous system (CNS) tumours) better than hierarchical clustering (HC) and self-organizing maps (SOM) method (Brunet, Tamayo, Golub, & Mesirov, 2004). Regarding results in CNS tumours clustering, HC does not give a clear four-class of the data (medulloblastomas, gliomas, rhabdoid, and normal), as it was expected. HC split samples into two or three classes, where the normal and gliomas samples are on the same branch in both rankings. NMF, together with consensus clustering, gave strong evidence for four classes in CNS tumours data. Thus, the NMF algorithm gives a more accurate clustering of this data set and appears to be more stable than the HC. Although NMF is not hierarchical per se, Brunet et al. showed that as the rank k increases the method uncovers substructures, whose robustness can be evaluated by a correlation coefficient. Thus, NMF can reveal hierarchical structure when it exists but does not force such structure on the data as HC does (Brunet et al., 2004).

In order to know how many groups of GBM are found according to the expression of lncRNAs, we forced the algorithm to cluster the samples from 2 to 7 groups (rank=2, rank=3, rank=4, rank=5, rank=6, rank=7) (Figure 4.16 and Figure 4.17). Genes were ranked according to their maximum absolute deviation (MAD) values from high to low in the expression matrix and the cophenetic correlation was calculated. Cophenetic correlation is a measure of how faithfully a dendrogram preserves the pairwise distances between the original unmodeled data points (Sokal et al., 1962). When the GBMs were clustered into two subtypes, we received the highest average clustering cophenetic scores resulting in the identification of two distinct lncRNA-based GBM subtypes amongst the 118 G-CIMP-negative specimens (Figure 4.16).

	K=2	K=3	K=4	K=5	K=6	K=7
MAD200	0,983	0,970	0,912	0,979	0,925	0,938
MAD400	**0,996**	0,972	0,943	0,895	0,937	0,943
MAD600	0,986	0,964	0,971	0,950	0,908	0,887
MAD800	0,993	0,956	0,954	0,940	0,927	0,849
MAD1000	0,992	0,933	0,983	0,952	0,938	0,870
MAD1200	0,981	0,883	0,958	0,955	0,931	0,916
MAD1400	0,987	0,924	0,959	0,951	0,958	0,949
MAD1600	0,994	0,928	0,939	0,940	0,947	0,943
MAD1800	0,976	0,935	0,943	0,953	0,943	0,952
MAD2000	0,982	0,905	0,881	0,932	0,955	0,940

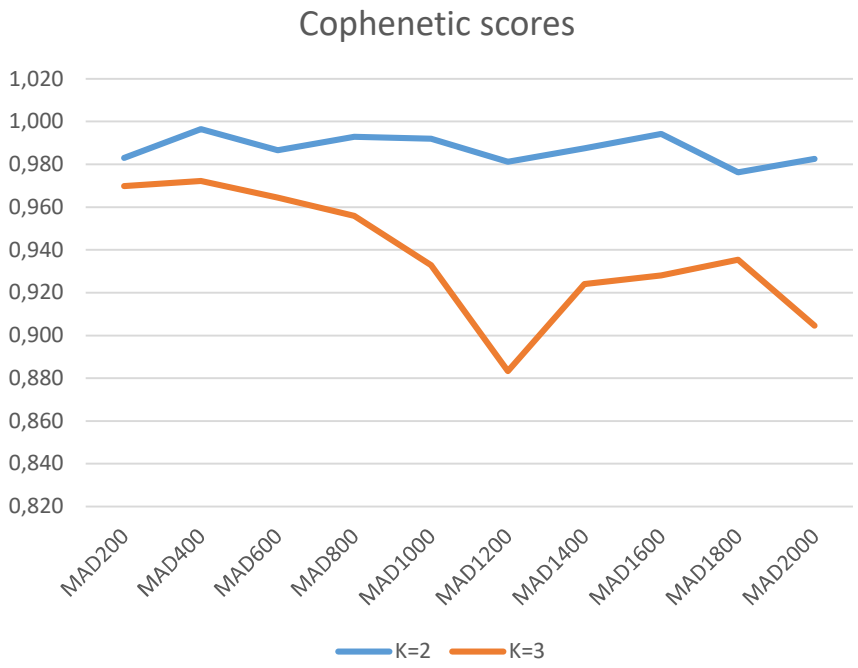

Figure 4.16: Cophenetic correlation coefficient for clusters k = 2 to k = 7. *The matrix (top) indicates the cophenetic scores of genes ranked from 2 to 7 and MAD of 200, 400, 600, 800, 1000, 1200, 1400, 1600, 1800 and 2000. The plot (bottom) demonstrates that maximum cophenetic correlation coefficient occurred for cluster k = 2 and MAD 400.*

In addition, the silhouette value was obtained to measure how similar an object is to its cluster (cohesion), compared to other clusters (separation). Silhouette values range from −1 to +1, where a high value indicates that the object is well matched to its cluster and poorly matched to neighboring clusters. The samples were ranked n times

to get the maximum number of groups without losing statistical value (silhouette value) (Figure 4.17).

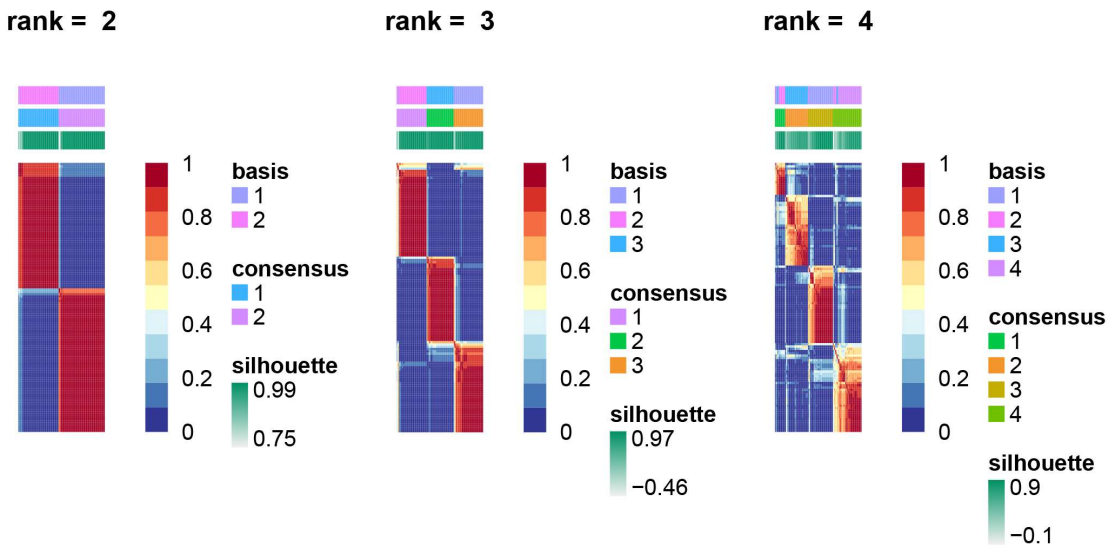

Figure 4.17: Clusters achieved by NMF clustering using lncRNA expression data from 118 G-CIMP-negative GBM specimens (GLIOCAT dataset). *Heatmaps obtained by NMF clustering of GBM samples, according to the expression of 400 most variable lncRNAs and ranked from 2 to 4. At the top of the heatmaps, the basis and consensus methods that were used to classify the patients into molecular subtypes and the silhouette values are shown.*

Among the 400 lncRNAs that separate the GBM patients into two subtypes, we found two of three candidate lncRNAs (PROCAR, aka MIR219A2, and LINC00941). This indicates that PROCAR and LINC00941 might be important for cluster 1 and cluster 2, respectively (Figure 4.18), and might be involved in the regulation of gene expression of each cluster. Interestingly, PROCAR is present in the signature of cluster 1 that correlates with the PN subtype and LINC00941 is found in the signature of cluster 2 that is enriched in MES subtype (Figure 4.5).

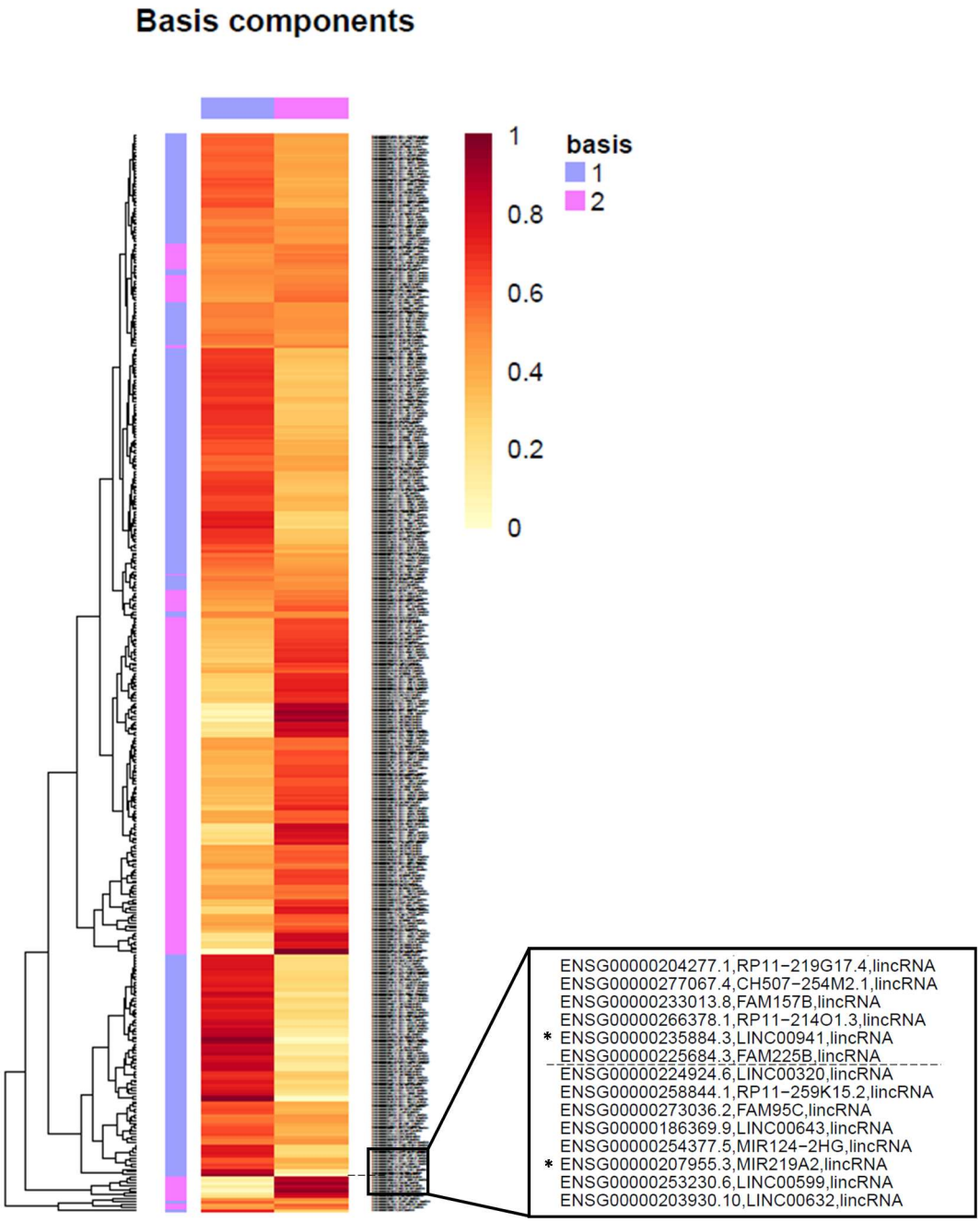

Figure 4.18: Clusters of patients and lncRNA of the basis matrix obtained by NMF. *GBM patients are separated into cluster 1 (light lilac) and cluster 2 (pink) according to the 400 lncRNAs expression. Each cluster has associated specifics lncRNAs, among them we found two of three candidate lncRNAs (LINC00941 and PROCAR (MIR219A2), indicated with *).*

According to the SVM classification, patients classified as PN subtype are mainly present in lncRNA-based cluster 1 (96,67%), whereas MES subtype is principally in cluster 2 (80.65%). CL subtype specimens are found interspersed between the two

clusters (35.09% in cluster 1 and 64.91% in cluster 2), although slightly enriched in cluster 2. This suggests that the lncRNA-based clustering is able to separate notably the PN subtype from the MES subtype, whereas CL subtype is in both clusters (Figure 4.19). Taken together, our results show that lncRNA expression clearly discriminates between two different groups of GBMs and that this new classification might have some correlation with the PN and MES molecular subtypes.

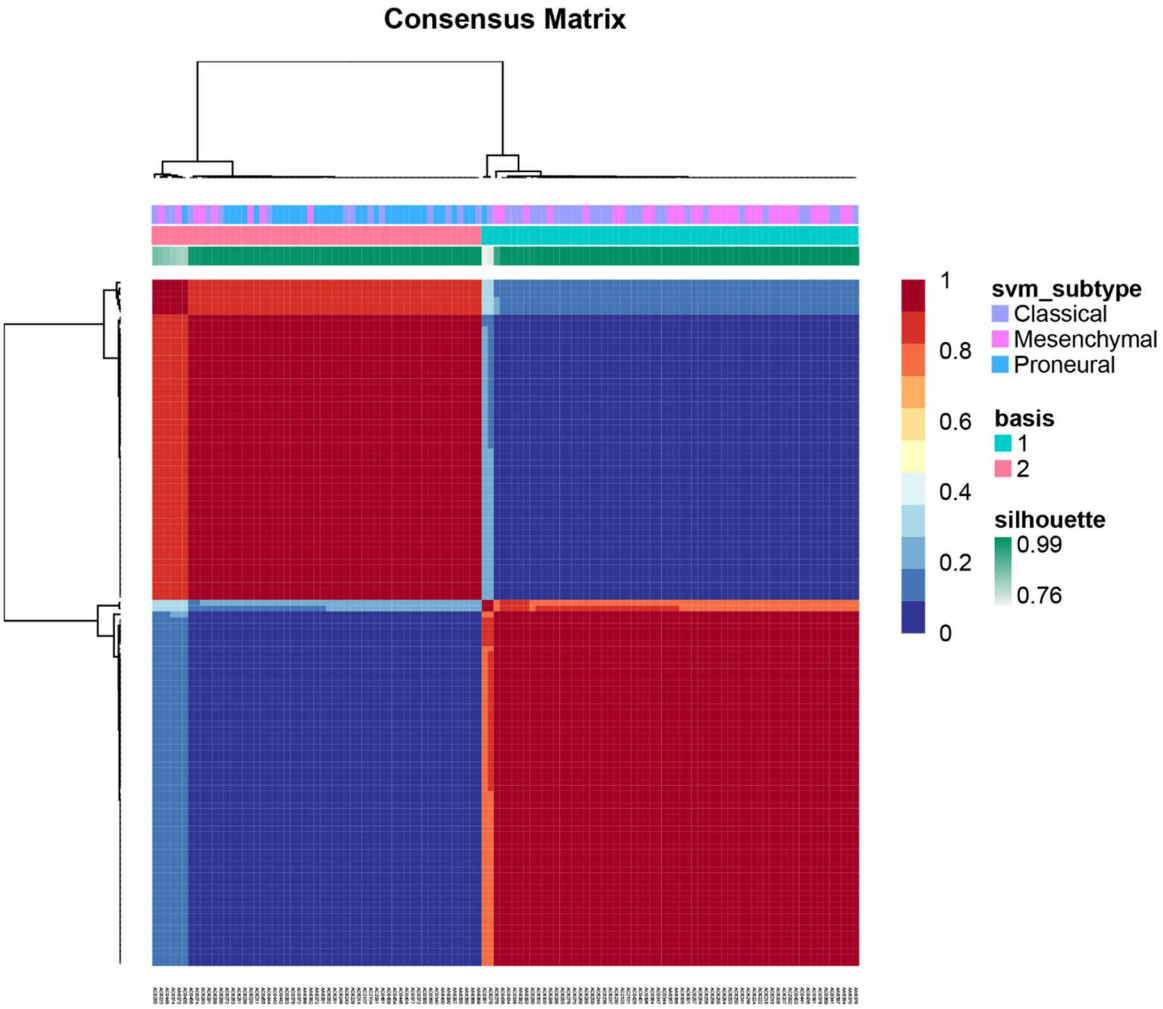

Figure 4.19: Heatmap of 118 G-CIMP-negative GBM according to the expression of 400 lncRNA by NMF clustering analysis. *At the top of the heatmap, it is shown GBM specimen classification into PN, CL and MES subtypes using SVM algorithm. LncRNA-based Clusters 1 is enriched in PN GBMs, whereas LncRNA-based Cluster 2 is enriched in MES GBMs. CL GBMs are found in both clusters. Below the molecular subtype classification, it is shown the basis method that ranks the samples into the two clusters, as well as the silhouette value of each sample in this clustering analysis (rank=2)*

Next, we studied if these two lncRNA-based signatures might be able to separate the patients according to survival. To this end, Kaplan-Meier survival curves were constructed to evaluate the differences in the overall survival time of lncRNA-based clusters 1 and 2. Unfortunately, we did not observe differences in the survival probability between cluster 1 versus cluster 2 (Figure 4.20).

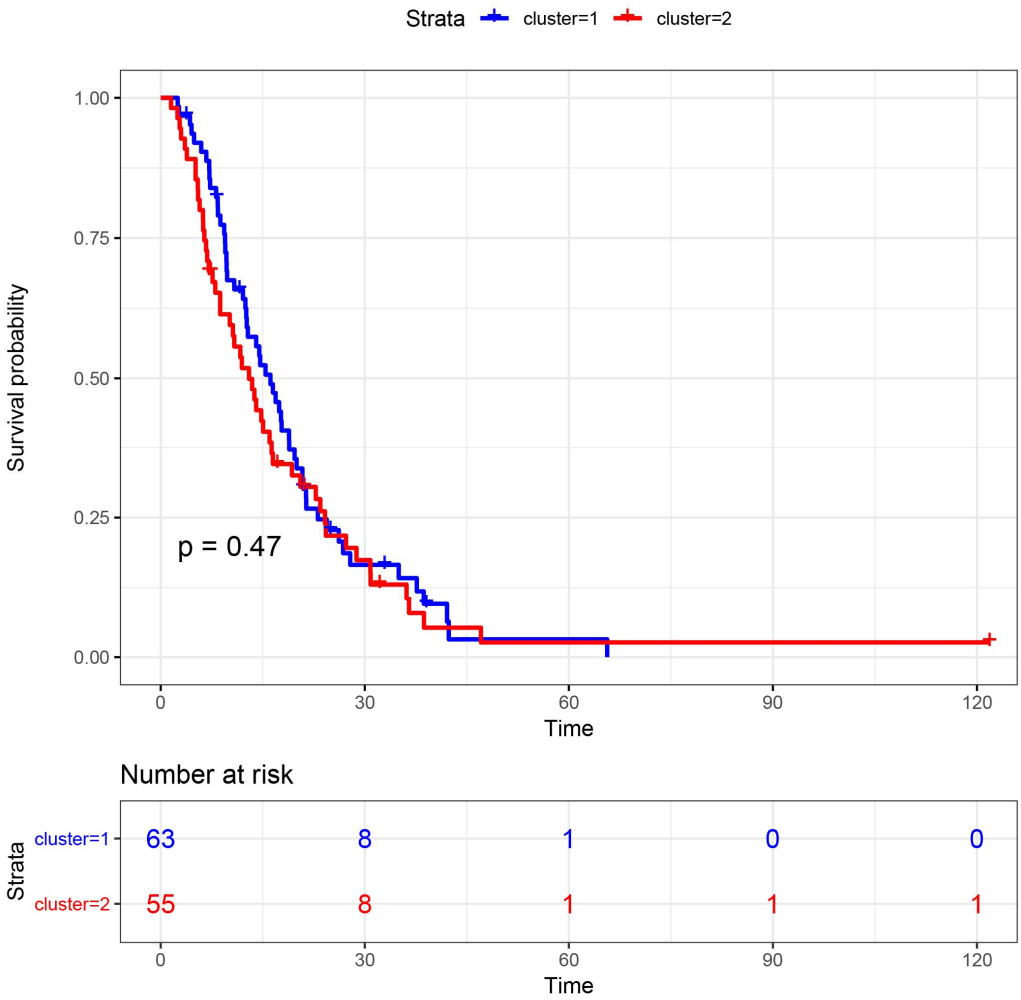

Figure 4.20: Kaplan-Meier estimates of the survival probability of GBM patients using the two-lncRNA signature. *The Kaplan-Meier plots were used to visualize the survival probabilities comparing cluster 1 versus cluster 2, obtained by lncRNA expression. There are no differences between cluster 1 and cluster 2 regarding survival probability. The differences between the two curves were determined by the two-side log-rank test.*

In conclusion, GBM patients may be classified based on lncRNA expression into two groups, suggesting that there are other methods to classify GBMs apart from the mRNA-based classification into PN, CL and MES subtypes. New classifications might better correlate with clinical features, although our classification based on lncRNAs does not separate the patients regarding survival probability. However, we cannot discard that our lncRNAs signatures may not correlate with other clinical features. Further analysis should be done to study if the new classification by lncRNAs correlates with progression-free survival or resistance to therapy.

4.2 GPR56 IS INVOLVED IN THE MESENCHYMAL DIFFERENTIATION OF GICS

Previous results obtained in our laboratory suggested that GPR56 regulates both MES differentiation and radioresistance of GICs. Loss-of-function studies using shRNA-mediated knockdown of GPR56 showed that MES differentiation is stimulated upon downregulation of the receptor in PN-GICs. However, we only had obtained results from one single GPR56 shRNA, so we could not strictly rule out that the observed phenotype was not due to an off-target effect. To corroborate our hypothesis about the role of GPR56 in MES differentiation, we performed additional loss-of-function experiments using an alternative method to shRNA-mediated knockdown: CRISPR/Cas9-mediated knockout (KO). Furthermore, to broaden the role of GPR56 in regulating MES differentiation to other molecular subtypes besides PN-GICs, we set out to study the role of GPR56 in CL subtype-GICs.

4.2.1 GPR56 controls mesenchymal differentiation of PN-GICs

4.2.1.1 Generation of GPR56-KO GICs

The Clustered Regularly Interspaced Short Palindromic Repeats (CRISPR) and CRISPR-associated protein (Cas9) system is an adaptive immune response defence mechanism used by archaea and bacteria for the degradation of foreign genetic material (Hsu, Lander, & Zhang, 2014; Van Der Oost, Westra, Jackson, & Wiedenheft, 2014). This mechanism can be repurposed for other functions, including genomic engineering for mammalian systems, such as gene knockout (KO) (Cong et al., 2013; Ran et al., 2013; Shalem et al., 2014).

CRISPR/Cas9 KO Plasmid products enable the identification and cleavage of specific genes by utilizing guide RNA (gRNA) sequences. The RNA-guided CRISPR/Cas9 consists of a small guide RNA (sgRNA) in complex with Cas9 nuclease and whose pairing with the target DNA induces a single Cas9-dependent double-strand breaks (DSBs) (Figure 4.21).

DNA containing double-strand breaks (DSB) created by the CRISPR/Cas9 system can be repaired by either the non-homologous end-joining (NHEJ) or the homology-

directed repair (HDR) pathway. The NHEJ repair pathway introduces non-specific insertions or deletions at the cleavage site, whereas the HDR pathway allows for precise gene editing at the DSB site, in the presence of a donor-corrected HDR template (Ran et al., 2013; Shalem et al., 2014). Target-specific HDR Plasmids provide a DNA repair template for a DSB and, when co-transfected with CRISPR/Cas9 KO Plasmids, enable the insertion of specific selection markers where Cas9-induced DNA cleavage has occurred (Figure 4.21).

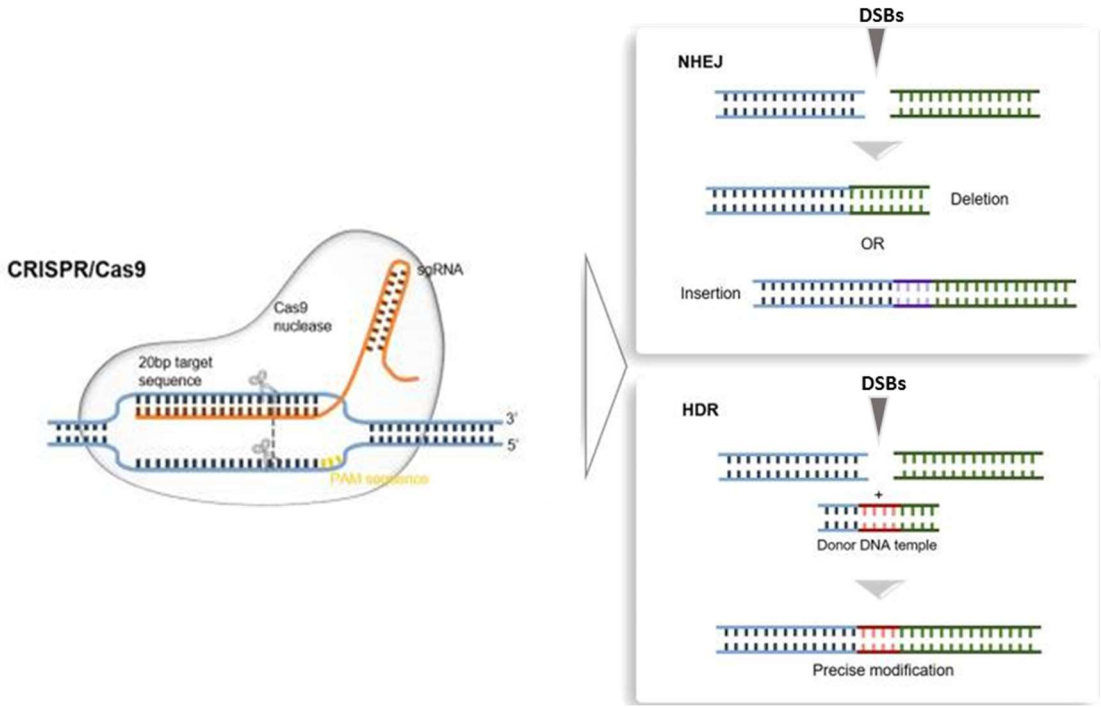

Figure 4.21: Gene editing mechanism of CRISPR/Cas9. *Genome editing nucleases (Cas9 nuclease) induce double-strand breaks (DSBs) at targeted sites, guided by small guide RNA (sgRNA). DSBs can be repaired by non-homologous end-joining NHEJ or, in the presence of a donor template, by homology-directed repair (HDR). In NHEJ, protein factors re-ligate the broken DNA strand either directly or by including nucleotide insertions or deletions (indels). This process occurs without a homologous DNA template, regularly leading to mutations and deletions in the repaired strand. In the presence of a donor-corrected HDR template, HDR gene correction or gene addition induces a DSB at the desired locus. (Adapted from H. Li et al., 2020)*

To obtain GPR56 knockout in PN-GICs, we used CRISPR/Cas9-mediated gene editing in GIC7 (PN-GICs). GPR56 CRISPR/Cas9 KO Plasmid is designed to disrupt gene expression by causing a DSB in a 5' constitutive exon within the human GPR56 gene. Briefly, a pool of three GPR56 KO plasmids (sc-406370; Santa Cruz Biotechnology) (Figure 4.22A), each of which encode for a GPR56-specific 20 nt gRNA together with the Cas9 ribonuclease, were co-electroporated along with a GPR56-HDR plasmid, which encodes for a puromycin resistance gene (Figure 1.22B) for drug selection of cells containing a successful CRISPR/Cas9 double-strand breaks followed by homologous recombination (sc-406370-HDR; Santa Cruz Biotechnology). The HDR plasmid also incorporates Red Fluorescent Protein (RFP) to visually confirm cells that have been efficiently recombined (Figure 4.22B).

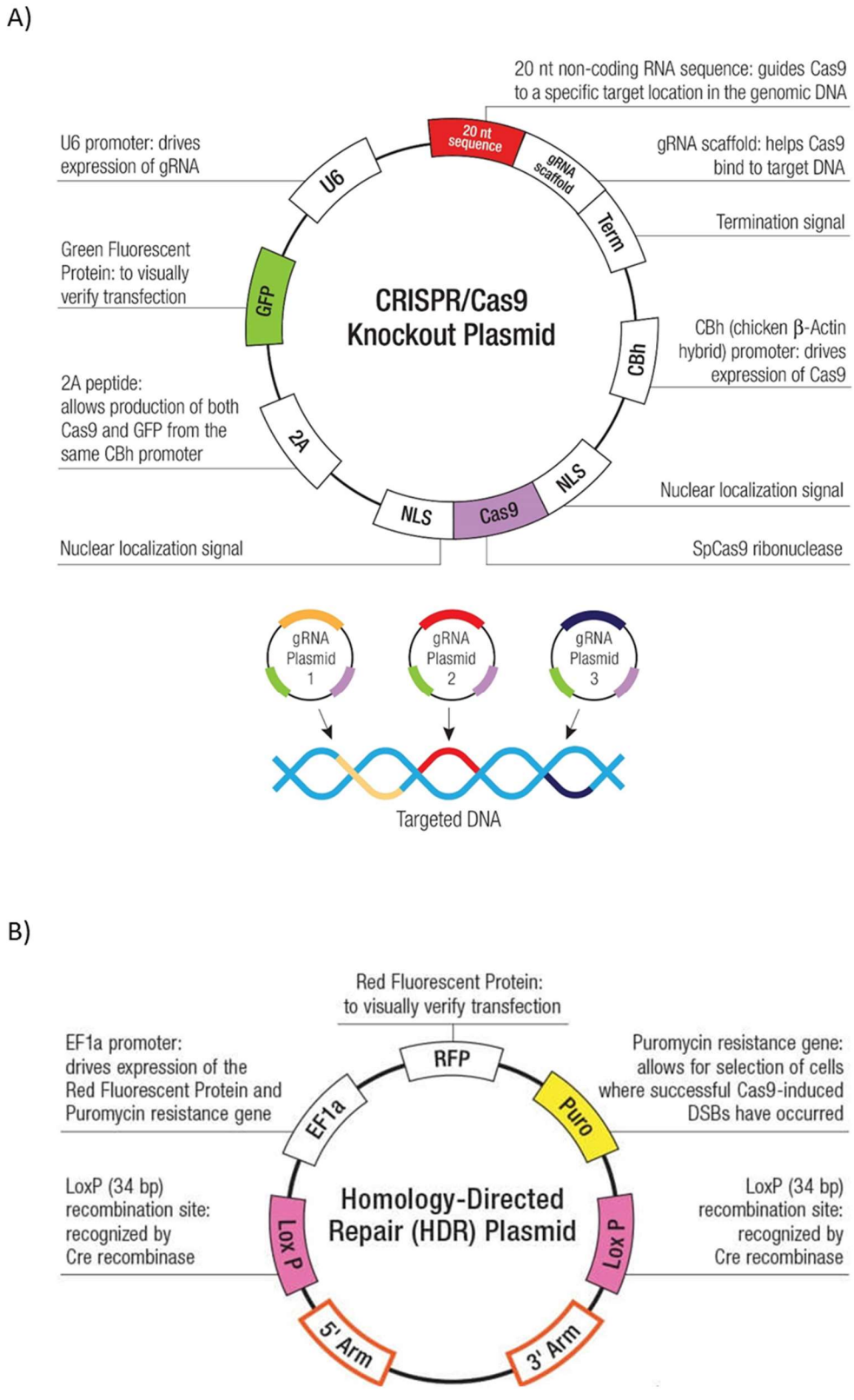

Figure 4.22: Plasmids used in CRISPR/Cas9-mediated gene editing. *(A) GPR56 CRISPR/Cas9 KO Plasmid human (human) designed to disrupt gene expression by causing a DSB in the GPR56 gene. (B) Target-specific HDR plasmid with Red Fluorescent Protein (RFP) sequence and puromycine resistance gene.*

We co-electroporated the CRISPR/Cas9 KO plasmids together with the HDR plasmid to obtain cells with DSB in GPR56 gene and expression of puromycin resistance gene to a posterior selection of KO-GICs by puromycin (Figure 4.23). Different concentrations of plasmids were tested to find the best combination in terms of both efficiency and toxicity. After electroporation in cell suspension, GICs were seeded at low density to eventually isolate individual cells to generate cell lines from clones.

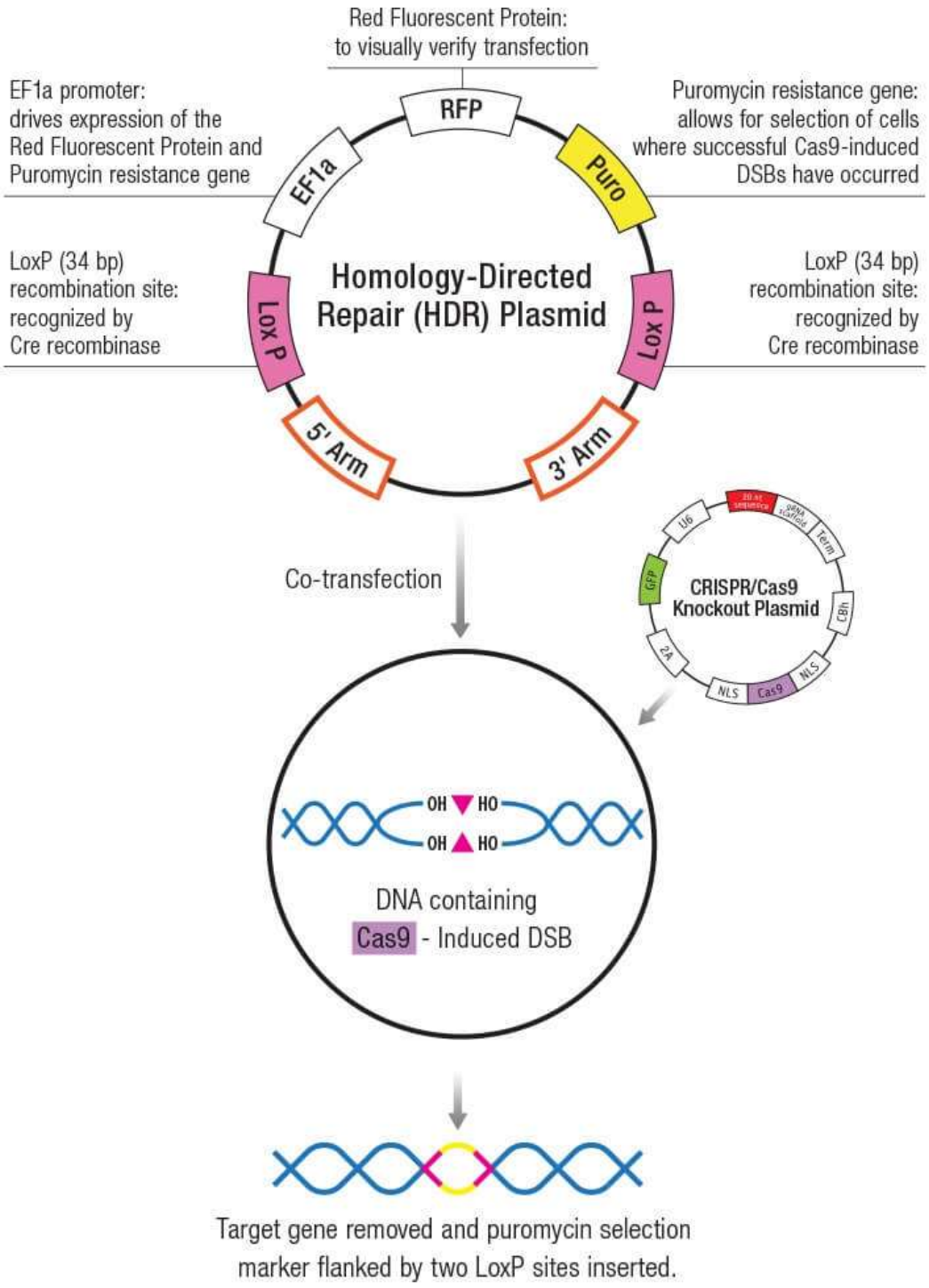

Figure 4.23: CRISPR/Cas9-mediated gene editing process by co-electroporation of CRISPR/Cas9 and HDR plasmids. *DNA containing double-strand breaks (DSB) created by the CRISPR/Cas9 system can be repaired by HDR pathway. HDR Plasmids provide a DNA repair template for a DSB enabling the insertion of specific puromycin selection gene where Cas9-induced DNA cleavage has occurred.*

We tested three different combinations of plasmid DNA for the electroporations: $4 \cdot 10^{-6}$g ($1 \cdot 10^{-6}$g of HDR single plasmid + $3 \cdot 10^{-6}$g CRISPR/Cas9 KO Plasmid), $6 \cdot 10^{-6}$g ($3 \cdot 10^{-6}$g of HDR pool-plasmid + $3 \cdot 10^{-6}$g of CRISPR/Cas9 KO Plasmid) and $6 \cdot 10^{-6}$g total DNA($1{,}5 \cdot 10^{-6}$g HDR single plasmid + $4{,}5 \cdot 10^{-6}$g CRISPR/Cas9 KO Plasmid). We found that all of these combinations were within the correct range because all samples were successfully electroporated and the viability was very similar between all electroporated cells.

We used electroporated GIC7 (PN-GICs) without any plasmid as a negative control. These cells suffered the same process than the CRISPR/Cas9-HDR-electroporated GIC7 with the difference that we did not add any plasmid in the electroporation process. We seeded two wells with control GIC7, one well was used as a control of electroporation (Parental-GICs) and the other one was used as a puromycin control, which was grown with puromycin in the medium during the selection process.

The sequence of RFP in the HDR plasmid allowed us to visually confirm that electroporation was successful, by observing RFP^+ cells under the fluorescence microscope. Next, cells were selected using $2 \cdot 10^{-6}$ g/mL of puromycin for 5 days to select for drug-resistant GPR56-KO cells.

After puromycin selection, individual cells were collected to generate cell lines of clones. We isolated and re-seeded 12 cells into 12 different wells and we continued the puromycin selection. Some GPR56-KO-GICs did not survive to puromycin selection, such as the KO1, KO2 and KO9 cells. Therefore, we continued the experiments with the other GPR56-KO-GIC cell lines (KO3, KO4, KO5, KO6, KO7, KO8, KO10, KO11 and KO12) (Figure 4.24).

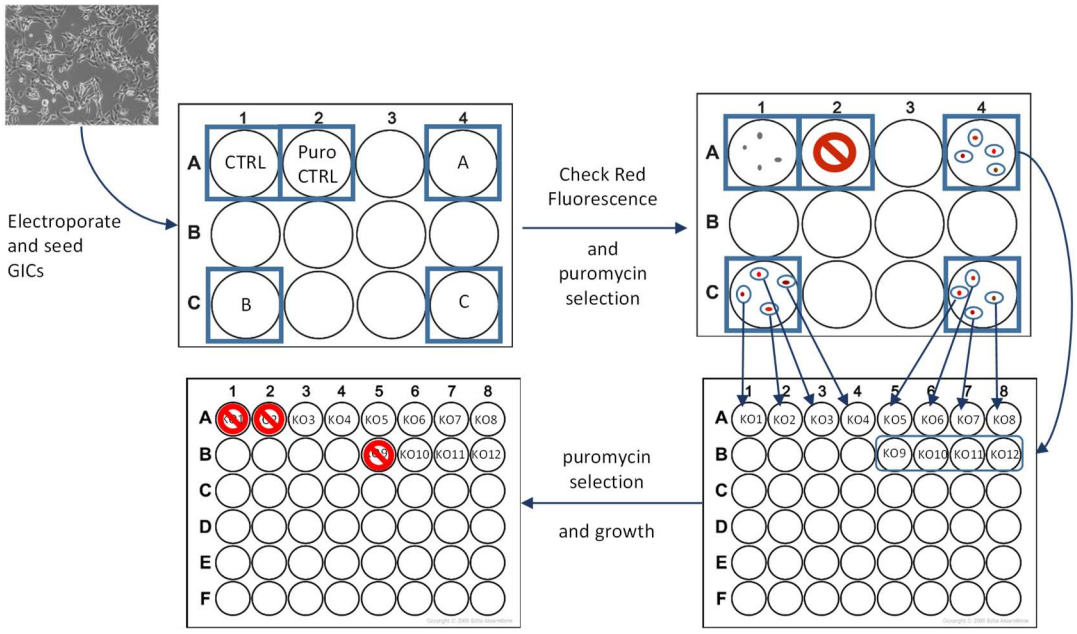

Figure 4.24: Experimental design to generation of GPR56-KO GICs. *GIC7s were electroporated with different concentration of plasmids and seeded in 12MW plate. "A" well was electroporated with $4{\cdot}10^{-6}$g ($1{\cdot}10^{-6}$g of HDR single plasmid + $3{\cdot}10^{-6}$g CRISPR/Cas9 KO Plasmid) of DNA, "B" well was electroporated $6{\cdot}10^{-6}$g ($3{\cdot}10^{-6}$g of HDR pool-plasmid + $3{\cdot}10^{-6}$g of CRISPR/Cas9 KO Plasmid) of DNA and "C" well was electroporated $6{\cdot}10^{-6}$g ($1{,}5{\cdot}10^{-6}$g HDR single plasmid + $4{,}5{\cdot}10^{-6}$g CRISPR/Cas9 KO Plasmid) of DNA. The Red protein fluorescence expression was checked by fluorescence microscopy to confirm the successful electroporation. Next, cells were selected by puromycin and the alive cells were isolated and re-seeded to growth and generate cell lines from clones. The selection by puromycin was continued a few days more. Three of twelve GPR56-KO-GICs did not survive to the puromycin selection (KO1, KO2 and KO9). The control of electroporation was the GIC7 seeded after electroporation without plasmids and grew without puromycin (CTRL). The control of puromycin was the GIC7 electroporated without plasmids and grew with puromycin (Puro CTRL).*

After puromycin selection and expansion of the CRISPR/Cas9-edited cell clones, GPR56 mRNA levels were studied by RT-qPCR. Some GPR56-KO-GIC clones, specifically the KO5 and KO8 cell lines, had lower expression of GPR56 mRNA than Parental cells (control). In contrast, other GPR56-KO-GICs, such as KO4, did not have lower GPR56-mRNA levels (Figure 4.25).

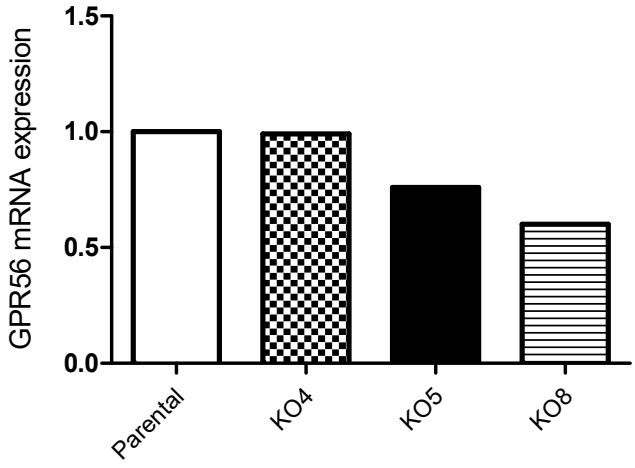

Figure 4.25: RT-qPCR of Parental cells (control) and GPR56-KO GICs determining GPR56 mRNA levels*. GPR56 mRNA expression was lower in GPR56-KO5-GICs (KO5) cells and in GPR56-KO8-GICs (KO8). In contrast, GPR56-KO4-GICs (KO4) expressed similar levels of GPR56 than control.*

These results suggest that at least two cell lines with lower mRNA expression of GPR56 were obtained by CRISPR/Cas9 gene editing. However, a complete GPR56 knockout was not obtained in any of the tested GICs, because we observed residual mRNA expression of GPR56 in all GICs.

Next, GPR56 protein levels were determined by western blotting analysis to study whether the decrease in GPR56 mRNA expression in GPR56-KO-GICs (KO5 and KO8) would also translate into lower GPR56 protein levels. As expected, both KO5 and KO8 expressed lower levels of GPR56 protein than control cells (Figure 1.26B). Additionally, GPR56 protein expression was also determined in the other GPR56-KO cell lines. In almost all GPR56-KO-GICs, with the exception of KO11, we observed very low levels of GFPR56 protein, which were nearly undetectable in the case of KO5 and KO8 (Figure 4.26).

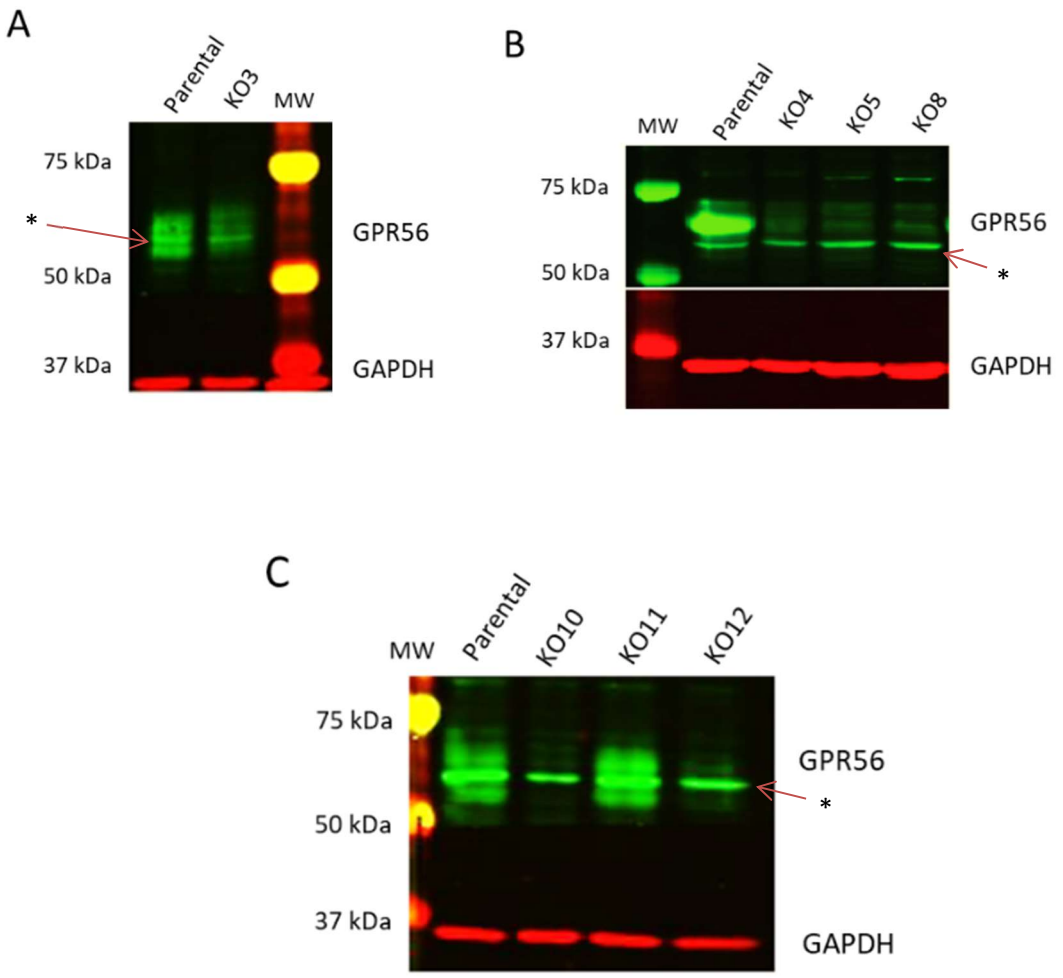

Figure 4.26: Western blot of Parental cells (control) and GPR56-KO-GICs determining GPR56 expression*. GPR56-KO-GICs (KO3, KO4, KO5, KO8, KO10 and KO12) had decreased GPR56 protein expression. However, KO11 had similar protein expression of GPR56 than the Parental GICs. GAPDH was used as a loading control. (* unspecific band)*

We observed a residual signal in the immunoblot in the expected molecular weight of GPR56 in GPR56-KO-GICs (KO3, KO4, KO5, KO8, KO10 and KO12) (Figure 1.26). This residual signal might be due to a GPR56 heterozygous deletion (deleted only one of the two GPR56 alleles). Nevertheless, the difference in GPR56 protein levels between GPR56-KO-GICs (KO3, KO4, KO5, KO8, KO10 and KO12) and Parental cells was highly significant (Figure 4.26). Therefore, even though we may not have obtained full GPR56 KO-cells, we proceeded to characterize the GPR56-KO-PN-GICs to study the effect of loss of GPR56 expression in PN-GICs.

On the other hand, GPR56-KO6-GIC (KO6) and GPR56-KO7-GIC (KO7) also expressed lower levels of GPR56 protein compared with the Parental GICs (data not shown). However, the residual signal in the GPR56's weight was more evident.

Therefore, we can conclude that we have been able to generate GPR56 KO-GICs using CRISPR/Cas9 gene editing, at least for one of the GPR56 alleles. Nevertheless, the system used was not 100% efficient, since one of the GPR56 KO-cell lines (KO11) had similar levels of GPR56 than control cells (Figure 4.26C) and a residual expression of GPR56 was observed in the majority of GPR56 KO-GICs, regarding both RT-qPCR and Western Blotting results. Although a full KO of GPR56 was not obtained, we kept naming these cell lines GPR56 KO-GICs, to differentiate them from the GPR56 knockdown-GICs. According to our results, we decided to further characterize KO5- and KO8-GICs, which had the lowest expression of GPR56, both at the mRNA and protein level.

4.2.1.2 Loss of GPR56 expression promotes MES differentiation in GICs

To study the role of GPR56 in mesenchymal differentiation, which is one of the molecular mechanism that confers resistance to therapy to glioblastoma (Mao et al., 2013; Y. Piao et al., 2013), we used two GPR56-KO-GICs the KO5- and the KO8-GICs. We analysed the mRNA expression of several GBM subtype markers by RT-qPCR and by microarray analysis. Next, a flow cytometry assay was performed to study the expression of CD44 protein, which is a marker of mesenchymal differentiation in GBM (Bhat et al., 2013).

4.2.1.2.1 Mesenchymal differentiation studied by RT-qPCR and microarray analysis

We analysed the mRNA levels of several mesenchymal markers (CD44, TGFb1, FN1, CTGF, ZEB1, TIMP1, SERPINE1, MCAM, SNAI1, SNAI2, TAZ, TGFbI and CHI3L1) in GPR56-KO-GICs and Parental GICs by RT-qPCR (Figure 4.27). We observed a tendency to increase the expression of mesenchymal markers upon GPR56 knockout, especially in KO5, although the differences between Parental and GPR56-KO-GICs were not significant for the majority of genes. Therefore, our mesenchymal

marker analysis by RT-qPCR was not sufficient to confirm a molecular subtype transition. Next, we analysed mRNA expression profiles in Parental- versus GPR56-KO-GICs by microarray analysis and performed a gene set enrichment analysis (GSEA) (Subramanian et al., 2005) using two previously published PN and MES signatures.

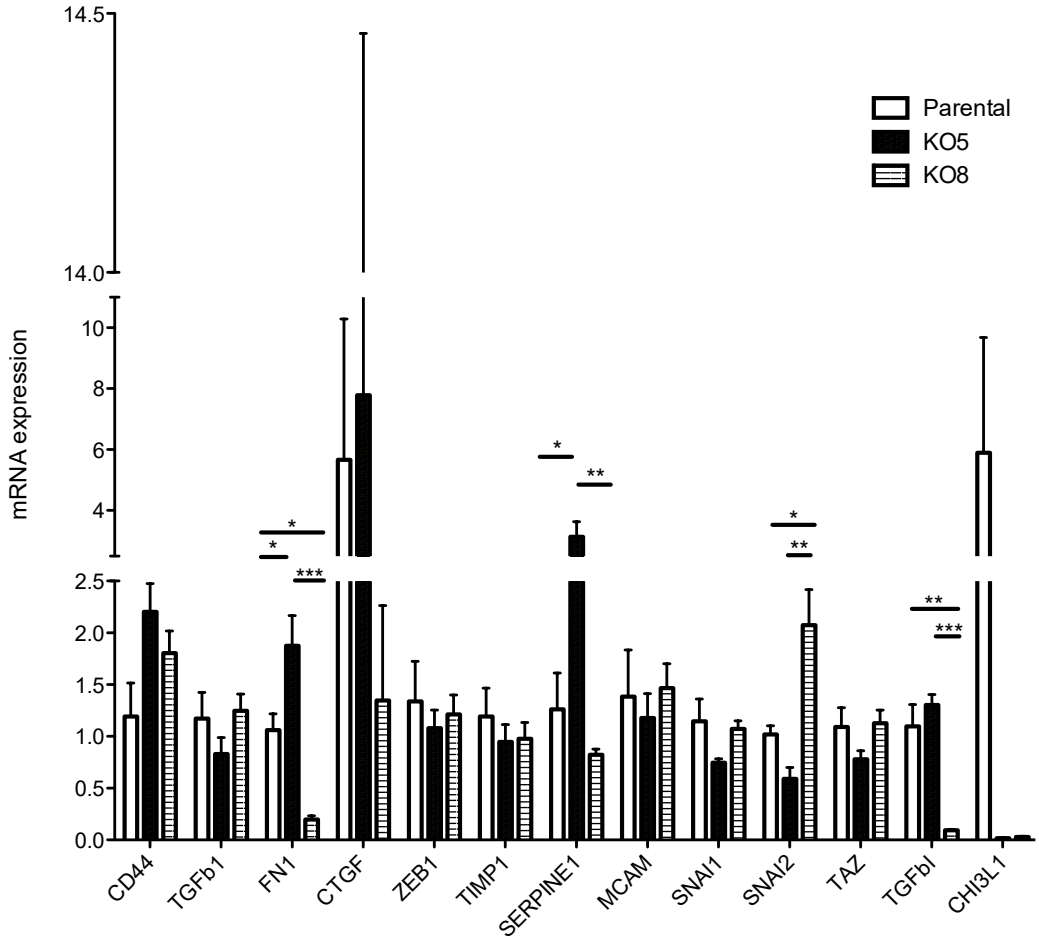

Figure 4.27: The expression of MES markers in Parental- or GPR56 knockout-GICs (clones KO5 and KO8) was assessed by RT-qPCR. *CD44 was increased in KO5 and KO8 GICs, but without significant difference. FN1 and SERPINE were significantly increased in KO5-GICs, but decreased in KO-GICs, with and without significant difference respectively, when they were compared with the Parental-GICs.SNAI2 was significantly increased in KO8-GICs versus KO5- and Parental-GICs. TGFbI was significantly decreased in KO8 compared with KO5 and Parental GICs. The other genes had not significant differences. Data are represented as mean ± SEM of at least three independent experiments. (ANOVA test, *p < 0.05, **p < 0.01, ***p<0.00).*

To further characterize the global MES transcriptional program induced by GPR56 knockout, we performed a whole-genome microarray analysis of gene expression in GPR56 knockout-GICs (KO5) versus control GICs (Parental). By GSEA using two previously published PN and MES signatures (Noushmehr et al., 2010; Phillips et al., 2006), we observed that GPR56 knockout-GICs were positively enriched for genes in the MES gene sets and, conversely, negatively enriched in PN genes (Figure 4.28).

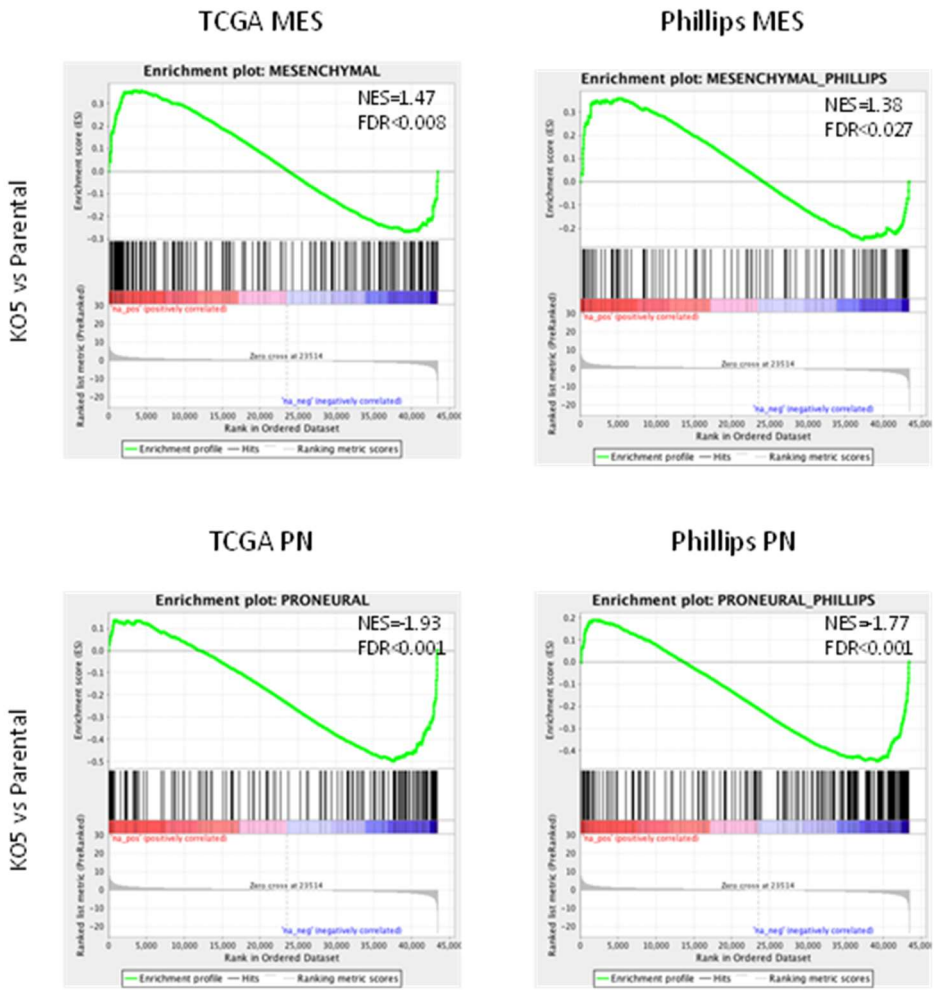

Figure 4.28: GSEA enrichment plots of MES and PN signatures (TCGA-Verhaak (left) and Phillips (right) signatures) in GPR56 knockout versus Parental GICs. *GPR56-KO5-PN-GICs (KO5) were positively enriched for MES gene signature (top) (TGCA signature (left) and Phillips signature (right)), whereas Parental PN-GICs (Parental) were positively enriched for PN gene signature (bottom) (TGCA signature (left) and Phillips signature (right). The normalized enrichment scores (NES) and the FDR values are shown for each plot.*

Taken together, our results suggest that GPR56 might be regulating the mesenchymal differentiation process, since we observed a gain of mesenchymal markers both by RT-qPCR analysis and GSEA. These results corroborate our previous analyses in the context of GPR56 knockdown-GICs.

4.2.1.2.2 Analysis of the CD44^{+} population of GPR56-KO-GICS by Flow Cytometry

CD44 is one of the most robust MES markers in GBM. By RT-qPCR, we had observed an increase in CD44 mRNA expression in KO-GICs, although this difference was not significant. To test if the tendency observed by RT-qPCR in the levels of CD44 mRNA, was also detected at the protein level, we performed a flow cytometry assay to study CD44 protein expression.

Both GPR56-KO5-GIC and GPR56-KO8-GIC displayed an increase in the percentage of CD44^{+} cells compared with control cells (Figure 4.29). The difference was only significant when we compared the percentage of cells with high expression of CD44 (CD44^{high} population), thereby suggesting that our GIC cell lines are highly heterogeneous and that Parental GICs express low levels of CD44 protein, even though they belong to the PN-subtype. In spite of that, the results obtained by flow cytometry suggest that loss of GPR56 expression promotes an increase in the CD44^{high} population. These results suggest that GPR56 might be involved in the mesenchymal differentiation of GICs.

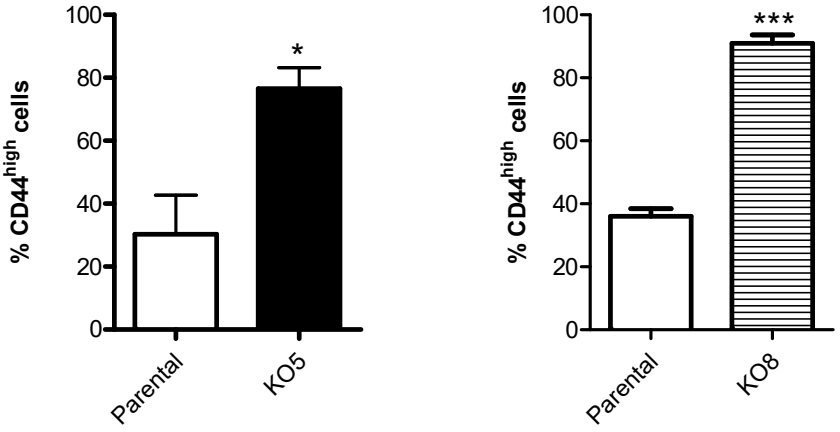

Figure 4.29: FACS analysis of the percentage of CD44^{high} cells in GPR56 knockout or Parental GIC7. *Loss of GPR56 promotes the upregulation of the CD44 expression, enriching significantly the percentage of CD44^{high} cells population. Data are represented as means ± SEMs of three independent experiments (t test, *p < 0.05).*

Additionally, we studied CD44 expression in GPR56-KO-GICs versus control GICs with and without TNFα stimulus. TNFα activates the NF-κB pathway, which promotes mesenchymal differentiation (Bhat et al., 2011). As we expected, Parental GICs significantly increased CD44^{high} population after TNFα stimulus, probably due to TNF-mediated mesenchymal differentiation. Regarding GPR56-KO-GICs, both KO5 and KO8 did not show a significant change in the levels of CD44^{high} cells either with or without TNFα. In any case, we observed a tendency in GPR56-KO-GICs towards higher levels of CD44^{high} cells after TNFα stimulus (Figure 4.30) which may be due to the heterogeneous population, also observed in the other approaches. The residual expression of GPR56, observed by RT-qPCR and Western Blotting analysis in GPR56-KO-GICs, might account for the increase in the percentage of CD44^{high} population after TNFα treatment.

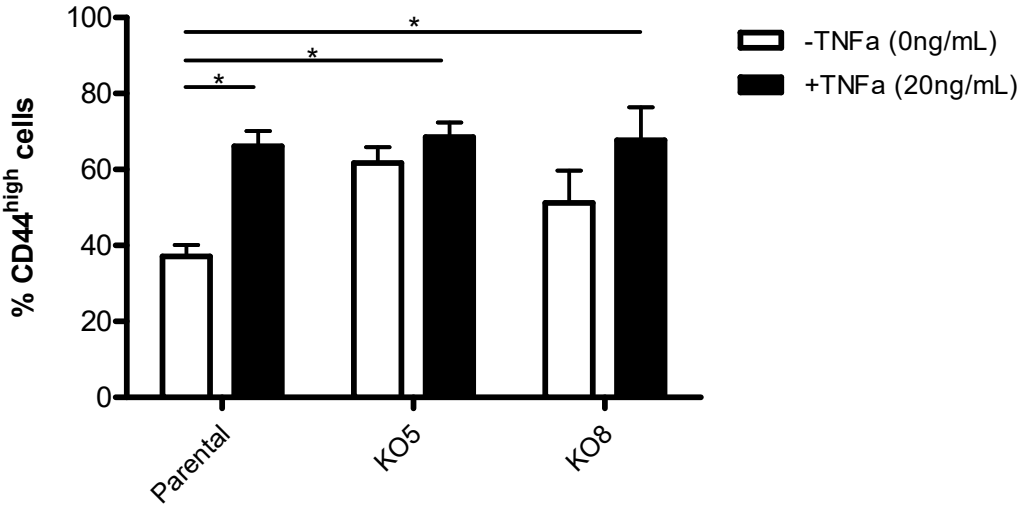

Figure 4.30: FACS analysis of CD44^{high} cells in GPR56 knockout GIC treated with or without TNFα for 4 days. *Parental GICs gained CD44^{high} cells after TNFα stimulus, due to mesenchymal differentiation promoted by TNFα. KO5 and KO8, which had more percentage of CD44^{high} population than control, also increased the percentage of CD44^{high} population, but this increase was not significant. Data are represented as mean ± SEM of at least three independent experiments (ANOVA test, *p < 0.05).*

Taken together, our results suggest that GPR56 may be inhibiting the mesenchymal differentiation of GICs. Therefore, when the levels of GRP56 decrease in PN-GICs, this might trigger a transition into a mesenchymal phenotype.

4.2.2 GPR56 is involved in the mesenchymal differentiation of CL-GICs

Next, we asked whether CL subtype GICs also undergo MES differentiation upon loss of GPR56 gene expression. To test this hypothesis, we used shRNA-mediated knockdown of GPR56 in CL-GICs (GSC6-27).

The knockdown of GPR56 in GCS6-7 was confirmed by analysis of GPR56 mRNA expression by RT-qPCR (Figure 4.31). Then, the expression of mesenchymal marker genes, the same genes used in our analyses of GPR56-KO-GICs, was analysed by RT-qPCR. We observed an increase in the expression of mesenchymal genes, which was more robust than in GPR56-KO-GICs. The expression of CD44 and SERPINE1

mRNA was significantly increased in GPR56 knockdown-GSC6-27 (sh#5) with respect to the control (Figure 4.31). These results suggest that GPR56 may also be regulating the classical to mesenchymal differentiation.

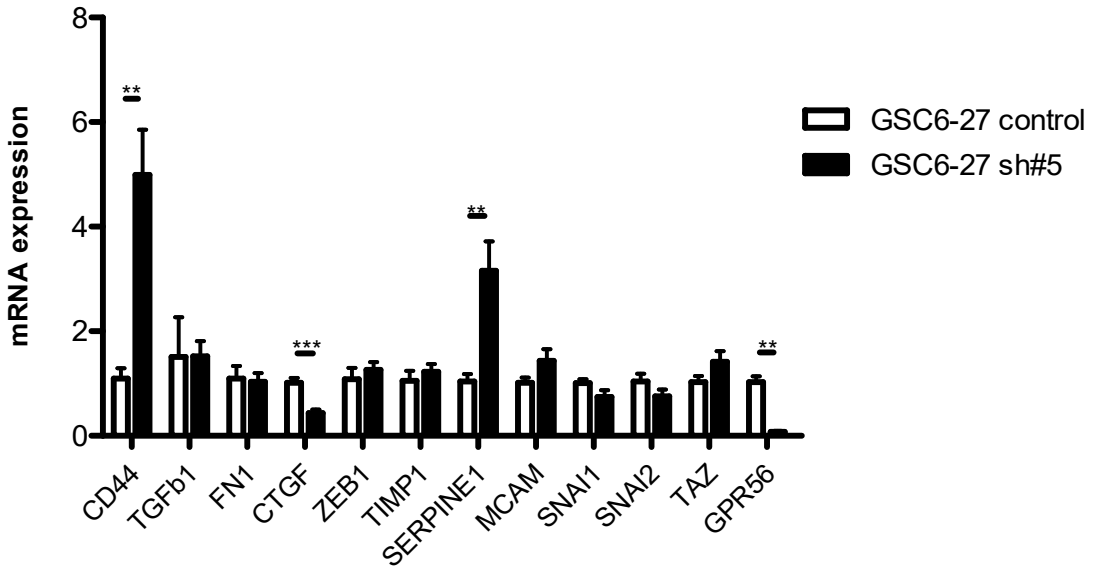

Figure 4.31: MES signature in control- or GPR56 knockdown-classical-GICs was assessed by RT-qPCR. *Data are represented as mean ± SEM of at least three independent experiments (t-test, *p < 0.05).*

Furthermore, a flow cytometry assay was performed to study the expression of CD44 protein in GPR56 knockdown-GSC6-27. The percentage of $CD44^+$ cells was significantly increased in GPR56 knockdown-GSC6-27 compared to control GICs (Figure 4.32), suggesting that classical GICs may differentiate into a mesenchymal subtype when GPR56 expression is downregulated. Taken together, these results suggest that GPR56 might also be regulating the classical to MES differentiation.

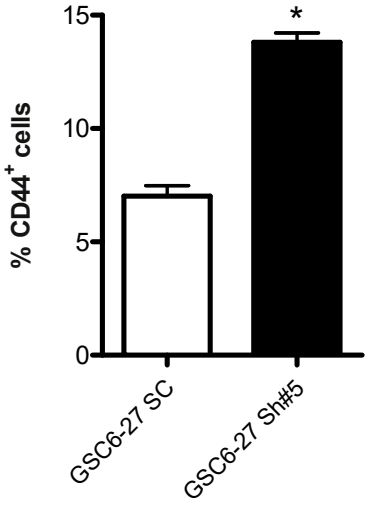

Figure 4.32: Percentage of CD44⁺ cells in control- or GPR56 knockdown-classical-GICs measured by FACS analysis. *GSC6-27 sh#5 had significantly increased the percentage of CD44⁺ population versus the control. Data are represented as mean ± SEM of three independent experiments (t.test, *p < 0.05)*

Altogether, our results suggest that GPR56 may be involved in the regulation of MES differentiation of non-MES GICs, including PN- and CL-GICs. GPR56 may have an inhibitory role, which might trigger the mesenchymal differentiation of PN or CL-GICs when GPR56 is downregulated. This mesenchymal differentiation may be linked to increased resistance to therapy.

5 DISCUSSION

GBM remains one of the most challenging tumours to understand and treat. The median survival time of GBM patients is 15 months and despite huge efforts to improve the outcome of this deadly tumour, mostly all GBM patients relapse (Furnari et al., 2007). In spite of our efforts to comprehend the biology of GBM to improve the treatment in the patients, the findings have not yet been relevant to clinical practice.

One of the characteristics of GBMs that makes this cancer very difficult to treat is its intra- and inter-tumoural heterogeneity. Despite all GBMs having similar anatomopathological characteristics, these tumours are very different at the molecular level from one patient to another. Adult GBM can be classified according to their gene expression and epigenetic profiles into four different subtypes: glioma-CpG island methylator phenotype (G-CIMP) and three non-G-CIMP subtypes termed proneural (PN), classical (CL), and mesenchymal (MES) (Brennan et al., 2013; Noushmehr et al., 2010; Verhaak et al., 2010; Q. Wang, Hu, Hu, Sulman, et al., 2017). Several studies have correlated the molecular subtypes with genetic alterations and different clinical features, such as the correlation of G-CIMP$^+$ patients (Bhat et al., 2013; Mao et al., 2013; Moreno, et al., 2017; Segerman et al., 2016). Furthermore, different subpopulations of cells within the tumour bulk and transitions from one GBM molecular subtype to another have been described in several studies, increasing the heterogeneity that characterizes these tumours (Campbell & Polyak, 2007; Plaks et al., 2015; Reya et al., 2001; Rich, 2016).

In GBM only a small fraction of cells within the tumour bulk that possess stem-like properties, known as glioma initiating cells (GIC), is considered to be the tumour driver cells (Fomchenko & Holland, 2005; Piccirillo et al., 2009). GICs share a huge number of similar characteristics with neural stem cells, such as asymmetric cell division, self-renewal and pluripotency (Fomchenko & Holland, 2005). This cell population has the ability to initiate and propagate the tumour as well as to display resistance to conventional therapies. Besides, GICs might be classified into molecular subtypes, maintaining the patient phenotype, and undergo transitions from one subtype to another, especially in response to inflammation or after therapy. Therefore,

understanding the biology of this cell population will help us to develop specific therapies targeting GICs and decrease the probability of relapse after treatment.

The main goal of this PhD thesis was to identify molecular mechanisms involved in resistance to therapy in GBM, in order to find actionable targets for a more effective anti-GBM therapy. This PhD thesis was divided into two separate projects. In the first project, using a candidate approach after an in silico analysis of RNA-sequencing data of GBM specimens, we identified novel lncRNAs that regulate the self-renewal capacity of GICs, which is one of the properties of GICs that confers to them the capacity to relapse the tumour in patients. In the second project, based on previous findings in our laboratory we have confirmed the role of GPR56 in the mesenchymal differentiation of GICs, which is another molecular mechanism of resistance to therapy in GBMs.

5.1 LNCRNAS INVOLVED IN RESISTANCE TO THERAPY IN GBM

In the first project, we analysed the expression patterns of lncRNAs using RNAseq data of GBM specimens to identify lncRNAs that might be involved in any molecular mechanism of resistance to therapy, such as the self-renewal capacity of GICs or their mesenchymal differentiation. After several bioinformatic analyses, we identified several candidate lncRNAs that we further functionally characterized in GICs in cell culture.

In mammals, lncRNAs participate in regulating important physiological processes such as neural development (Andersen & Lim, 2018), cell cycle (Sun et al., 2018), cell protection (Ma et al., 2018), and tumour development and metastasis (Dhamija & Diederichs, 2016). Therefore, we hypothesized that lncRNAs might also be involved in resistance to therapy in GBM.

First, we analysed the expression of total RNA of FFPE GBM specimens obtained from GBM patients treated homogeneously with radiotherapy and temozolomide after surgery (Stupp Regimen). After quality control (QC) of the RNAseq results, reliable data were obtained for 124 GBM samples of 236 FFPE GBM samples

submitted to RNA-sequencing. During QC the expression of mitochondrial RNA was taken into account. There is an extensive literature on the relationship between mtDNA, mitochondrially localized proteins, mitochondrial RNA, and cell death (Detmer & Chan, 2007; Galluzzi, Kepp, & Kroemer, 2012). When the cell membrane is broken, cytoplasmic RNA will be lost, but RNAs enclosed in the mitochondria will be retained. Thus, high levels of mitochondrial RNA might be characteristic for low-quality samples (Ilicic et al., 2016; Osorio & Cai, 2020). That is why we excluded the samples with >5% mitochondrial counts during the QC process, in order to yield genuine, biologically meaningful results. In this PhD thesis, we present several bioinformatic analyses of this RNAseq dataset. Of note, the weighted gene co-expression network analysis (WGCNA) to identify gene networks among molecular subtypes, was performed only on 36 out of 124 specimens, because at the time of analysis RNAseq data from these 36 samples was available. Therefore, the candidate lncRNAs were obtained from these 36 tumour specimens to posterior functional characterization.

Next, the patients were classified according to the G-CIMP status into G-CIMP positive or negative and according to gene expression into PN, CL and MES molecular subtype using support vector machines (svm, also support vector networks) algorithm. Svm is highly suitable for a limited training set size compared with other algorithms (Blumenthal et al., 2017; Thanh Noi & Kappas, 2017). Once the samples in our dataset were classified into subtypes, we applied weighted gene co-expression network analysis (WGCNA) and we compared RNA expression between the different subtypes in order to identify the networks of genes, including lncRNAs, enriched in one subtype or the other. Interestingly, although the majority of lncRNAs are expressed at lower levels than mRNAs, our WGCNA showed that some lncRNAs with a very high kin value (Table 4.1 and Table 4.2), suggesting that lncRNAs have a main role in the module expressed. Kin value is equivalent to the k-ME value that can be interpreted as a measure of module membership or intramodular connectivity (Dong & Horvath, 2007; Horvath & Dong, 2008). Genes with high connectivity are hubs or central genes, which are natural targets for testing hypotheses about modular function (Oldham et al., 2008). Thus, lncRNAs with a high kin value might be important in the module where they are expressed and might be regulating the expression of the other genes in the module.

Next, we selected different lncRNAs, from the bioinformatic analyses, with a high level of mRNA expression, with a high kin value, and co-expressed in modules with main genes for GBM subtypes, such as STAT3, PDGFRA, PAX6 and C/EBPβ. Furthermore, additional information about lncRNAs was searched in the bibliography. However, lncRNAs are still little studied and almost of pre-selected lncRNAs had no additional information. Among those pre-selected lncRNAs, PROCAR, PAUPAR and LINC00941 were correlated with some cancer and cellular processes that might be involved in resistance to therapy in cancer. PROCAR might be correlated with microRNA 219, which inhibits proliferation, migration, and invasion of epithelial ovarian cancer cells (Wei et al., 2017). PAUPAR might be involved in the tumourigenesis process, regulating the self-renewal capacity of neuroblastoma cells (Pavlaki et al., 2018) and LINC00941 is enriched in HCC patients and it was correlated with poor survival of HCC (X. Yan et al., 2017).

5.1.1 Limitations of lncRNA knockdown generation

To study if the candidate lncRNAs are involved in some molecular mechanism of resistance to therapy of GICs, we performed loss-of-function studies by inducing shRNA-mediated knockdown of our candidate lncRNAs in different GIC cell lines. Although we had successfully used shRNA to induce knockdown of protein-coding RNAs in our laboratory, it was the first time that we tested this strategy for lncRNAs.

Some lncRNAs are difficult to suppress due to their localization (nuclear or cytoplasmic or dual) or their structure, among others. shRNAs are less effective against nuclear-localized lncRNA targets, which are more easily suppressed using RNase-H activate antisense oligonucleotides (ASOs) since RNase H is predominantly found in the nucleus (Vickers & Crooke, 2015; Zeng & Cullen, 2002). However, some lncRNAs might be refractory to knockdown by both methods if the subcellular localization of the lncRNA is not accessible to either RNase H or the RNAi machinery (used in the shRNAs method). It could also occur if the lncRNA is highly structured or structurally blocked due to excessive protein binding or hybridizing to other nucleic acids. In these circumstances, using a technique such as CRISPR/Cas9 genome editing might be necessary (Goyal et al., 2016). Nevertheless, making a small indel in the targeted lncRNA most likely will not disrupt transcription

(S.-R. Kim et al., 2016). Besides, transcribed lncRNAs containing introduced indels may retain functional domains and/or binding sites. Therefore, depending on lncRNA localization, lncRNA transcript (in)accessibility to enzymes, and their transcriptional landscape, the knockdown of lncRNA will be successful or not. Additionally, many of the annotated lncRNAs have not been characterized and thus, we do not know many of the above-mentioned characteristics. All of these points might complicate knockdown of lncRNAs, compared to knockdown of protein-coding RNAs.

In this study, we successfully generated shRNA-mediated knockdown of two different lncRNAs in GICs: PAUPAR and LINC00941, thereby demonstrating that shRNA-mediated knockdown of lncRNAs may be achieved in these cells (Figure 4.8A-B). In addition, we obtained knockdown of LINC00941 in two MES-GIC cell lines, with three plasmids with different sequences against the lncRNA. However, we only obtained knockdown of PAUPAR in one of the two CL-GICs tested. The second CL-GICs infected with shRNA-encoding lentiviruses did not repeatedly survive any of the two infections that we performed. This might due to the important role of PAUPAR in the self-renewal capacity of CL-GICs. Similar results were observed in PN-GICs infected with shPROCAR-encoding lentiviruses, which had to be infected twice because in the first infection all cells died. At the second round of infection, only two out of three plasmid shRNA-infected GIC7 and GIC2 survived, which turned out to be cells that did not express lower levels of PROCAR (Figure 4.8C). Since no PROCAR knockdown cells were ever detected, this might be due to an important role of PROCAR in the survival of GICs. Another explanation might be that the localization of PROCAR or its transcriptional landscape might make it difficult for this lncRNA to be accessed by the RNAi machinery. In the subsequent functional characterization of lncRNA knockdown-GICs we only characterized the GICs with a successful knockdown of our candidate lncRNAs.

5.1.2 Role of lncRNAs in the stem cell-like properties of GICs

Cancer stem cells (CSCs), such as GICs, are suggested to be responsible for therapeutic resistance and cancer relapse due in part to their ability to self-renew and differentiate into heterogeneous lineages of cancer cells (J. Chen et al., 2012; Dean et al., 2005; A. Singh & Settleman, 2010; Thi et al., 2018). CSCs are able to undergo

cell cycle arrest and enter a quiescent state that would support their ability to become resistant to chemo- and radiotherapy (J. Chen et al., 2012; Cojoc, Mäbert, Muders, & Dubrovska, 2015; Shlush et al., 2017). Common chemotherapeutic agents target proliferating cells to lead to their apoptosis. Although a successful cancer therapy might abolish the bulk of proliferating tumour cells, a subset of remaining quiescent CSCs might survive and promote cancer relapse due to their ability to initiate and propagate the tumour again (Shlush et al., 2017; Z. J. Yang & Wechsler-Reya, 2007). It has been found that some lncRNAs regulate the self-renewal capacity of stem cells, such as Terra, AK028326 and AK141205 (Mohamed, Gaughwin, Lim, Robson, & Lipovich, 2010; X. Xu, Guo, Zhang, & Ye, 2018). Terra is regulated by the WNT/β-catenin pathway and upon overexpression it promotes self-renewal (Xu, Guo, Zhang, & Ye, 2018). AK028326 (Oct4-activated) and AK141205 (Nanog-repressed) inhibit the differentiation of mESC, regulating the expression of TF involved in this process, such as Oct4 and Nanog, respectively (Mohamed, Gaughwin, Lim, Robson, & Lipovich, 2010). Because of that, we hypothesized that lncRNAs might be regulating the self-renewal property of GICs, which may be a molecular mechanism of resistance to therapy and relapse of GBMs.

Our results in neurosphere formation assay suggest that both PAUPAR and LINC00941 promote the self-renewal capacity of GICs. The number of primary and secondary neurospheres, formed by a single cell, was decreased in knockdown-GICs with respect to control-GICs (Figure 4.15). In the case of PAUPAR, since knockdown was only obtained for one CL-GIC (GSC6-27), the number of secondary neurospheres was also analysed in order to corroborate the phenotype observed in primary neurospheres. Although only one CL-GIC line with knockdown of the PAUPAR lncRNA was obtained, for this cell line we obtained three independent PAUPAR knockdown-GSC6-27, suggesting that the results obtained in the neurosphere formation assay are specific for the decrease in PAUPAR expression.

In agreement with our results, Vance et al. showed that PAUPAR maintains the self-renewal property of neuroblastoma cells. Vance et al. suggested that PAUPAR might be involved in the tumourigenesis process, maintaining the dedifferentiated state of neuroblastoma cells and regulating their self-renewal capacity (Vance et al., 2018). In contrast, Ding et al. found that the expression of PAUPAR was significantly lower

in uveal melanoma tissues compared with normal tissues and that PAUPAR lncRNA inhibits the cell migration and suppresses tumour formation in vitro and in vivo uveal melanoma models (Ding et al., 2016). These results suggest that PAUPAR might have different roles depending on the tissue where it is expressed.

On the other hand, as it has been mentioned before, lncRNAs regulate gene expression during the differentiation process (Fatica & Bozzoni, 2014; Hong et al., 2020; Ju et al., 2019; Q. Yang et al., 2018). This is why we hypothesized that candidate lncRNAs might also be modulating gene expression of the molecular subtypes and hence, they might be regulating transitions between GBM subtypes. Vance et al. showed that knockdown of PAUPAR disrupts the normal cell cycle profile of neuroblastoma cells and induces neural differentiation (Keith W. Vance et al., 2014). In addition, the proximity of the PAUPAR gene to PAX6 suggests that it may be involved in the spatiotemporal control of PAX6 expression and, thus, that it may be important for nervous system development and neuronal cell subtype specification (Ding et al., 2016). Vance et al. showed that PAUPAR knockdown in neuroblastoma cells leads to an increase in PAX6 expression (Keith W. Vance et al., 2014), as we observed in our three PAUPAR knockdown-GICs, although the decrease in PAX6 mRNA expression was statistically significant only in two cases (Figure 4.13B). Concerning to the other subtype markers studied by RT-qPCR, we observed an increase in OLIG2 mRNA expression in the three PAUPAR knockdown-GICs, an increase in SOX2 mRNA in two of the three knockdown-CL-GICs and a reduction of SERPINE mRNA in two of the three shPAUPAR-GICs. However, the decrease in SERPINE mRNA and the increase of mRNA expression of SOX2 in shPAUPAR-CL-GICs were not statistically different compared to the control-GICs (Figure 4.13B). In addition, CD44 levels were not significantly altered upon PAUPAR knockdown (Figure 4.13A). Therefore, these results suggest that PAUPAR is not involved in transitions between GBM subtypes.

Liu et al. suggested that LINC00941 might be an essential regulator of tumour metastasis and cancer cell proliferation because they showed that silencing of LINC00941 significantly inhibited proliferation ability of gastric cancer (H. Liu et al., 2019). Similarly, we found that LINC00941 knockdown-GICs had a lower number of primary neurospheres with respect to control-GICs (Figure 4.12),

suggesting that LINC00941 has an important role in maintaining the self-renewal capacity of GICs.

On the other hand, Yan et al. showed that overexpression of LINC00941 in hepatocellular carcinoma promotes epithelial-to-mesenchymal transition (EMT) (X. Yan et al., 2017). However, LINC00941 knockdown-GICs changed neither the mRNA expression of subtype markers (Figure 4.10) nor CD44 protein analysed by flow cytometry (Figure 4.9), suggesting that there are not transition from MES subtype to another upon LINC00941 knockdown.

Taken together, our results suggest that LINC00941 and PAUPAR might be promoting the self-renewal capacity of GICs, but might not regulate the transition between GBM subtypes. The self-renewal capacity of GICs is prominent to initiate and propagate the tumour. Therefore, these lncRNAs might be involved in the relapse of GBM by maintaining the self-renewal capacity of GICs within tumour, allowing the progression or the acquisition of resistance to therapy in GBMs. These lncRNAs may be good targets to develop novel GIC-specific treatments that inhibit their self-renewal capacity, thereby avoiding the relapse and progression of GBM. More importantly, in the case of these two lncRNAs their inhibition would not promote any GBM-subtype transition, thus avoiding the resistance to therapy acquired by mesenchymal differentiation.

lncRNAs can be targeted by multiple approaches: generate knockdowns by creating steric inhibition of RNA-protein interactions or by using siRNAs or antisense oligonucleotides (ASOs) and modulate lncRNA genes by steric blockade of the promoter or by using genome-editing techniques (Arun, Diermeier, & Spector, 2018). Most of the toxic effects that could be observed with all oligonucleotide antisense technologies, maybe due to protein binding (Bennett & Swayze, 2010) and the activation of the immune system (Senn, Burel, & Henry, 2005). Oligonucleotides also have the potential to hybridize both on- or off-target, which can result in unwanted and unanticipated events. Off-target toxicity is difficult to control, although it is possible to predict some nonspecific hybridization events using bioinformatics tools (Wahlestedt, 2013). The field of regulatory lncRNAs is quite young and the modes of action of these molecules are still poorly understood. Therefore, a large amount of work is required to more fully assess their potential as therapeutic targets.

5.1.3 New lncRNA-based molecular classification of GBMs

The molecular classification of tumours is of crucial interest for clinical diagnostic, as well as to predict response to treatments and eventually develop patient-tailored therapies. The Cancer Genome Atlas (TCGA) project identified four distinct molecular subgroups in GBM. However, there was not a significant correlation between patient survival and gene expression subtype (Noushmehr et al., 2010; Verhaak et al., 2010). The epigenetic G-CIMP phenotype was the only molecular classification predictive of survival (Noushmehr et al., 2010). Therefore, it was necessary to refine the molecular classification of GBM to find another classification that would better correlate molecular determinants with clinical features.

In this Ph. D. thesis, we have been able to classify GBM specimens according to lncRNA expression into two different molecular subtypes by using NMF (Figure 4.19). Comparing our new classification with PN, CL and MES classification, we found that cluster 1 is enriched in PN subtypes, whereas MES specimens are clustered in Cluster 2. CL subtype samples are present in both clusters. This suggests that lncRNAs found in cluster 1 or in cluster 2 might be regulating some main genes for the PN or MES subtypes. Interestingly, two of the lncRNA candidates that we identified by WGCNA in the previous section are part of the metagene signature of each of the two clusters: PROCAR (MIR219A2) and LINC00941. This points at them as hub genes with an important role in the pathogenesis of their corresponding subtype-GBM.

Next, we asked if this new classification might be correlated with patient survival. Unfortunately, we found no difference in patient overall survival between the two lncRNA-based clusters (Figure 4.20). Further analysis should be done to study if the new classification by lncRNAs correlates with other clinical features, such as progression-free survival, response/resistance to therapy or even some radiological features.

5.2 GPR56 IS INVOLVED IN RESISTANCE TO THERAPY IN GBM

In the second project of this PhD thesis, we have studied the role of GPR56 in MES differentiation of PN and CL GICs. In previous studies in our laboratory, we showed that inhibition of GPR56, which was enriched in the PN-subtype, promotes MES differentiation and radioresistance of PN-GICs, while its expression correlates with longer survival.

As we mentioned before, GBMs are highly plastic and have an inherent tendency to transition from one subtype to another (Bhat et al., 2013; F. Lu et al., 2016; Mao et al., 2013). This transcriptional plasticity empowers GBMs with the capability to adapt to treatment and develop resistance to therapy. The identification of the molecular mechanisms that control transitions from one subtype to another is crucial to understand GBM natural evolution and acquired resistance to therapy. In this study, we corroborate the role of GPR56/ADGRG1 as an inhibitor of the MES differentiation in GICs. GPR56 is an adhesion GPCR with a prominent role in NSC and OPC proliferation and differentiation (Ackerman et al., 2015; Bae et al., 2014) and is highly expressed in PN and CL GBMs (Moreno, Pedrosa, Paré, Pineda, Bejarano, Martínez, Balasubramaniyan, Ezhilarasan, Kallarackal, Kim, Wang, Audia, Marín, et al., 2017).

Alterations in several classes of adhesion molecules have been implicated in the progression of various forms of cancers (Colpaert, Vermeulen, Van Marck, & Dirix, 2001; Reticker-Flynn et al., 2012). An essential step in tumour progression is the interaction of tumour cells with extracellular matrix (ECM) leading to its destruction and the tumour cells' invasive behaviour (Belkin, 2011). Cell adhesion receptors and their ligands provide traction, repulsion and stimulus for tumour cell migration. The modulation of therapeutic targets involved in tumour cell invasion and adhesion has great potential for the treatment of cancer (Haier, Goldmann, Hotz, Runkel, & Keilholz, 2002). GPR56 likely plays a role in cell adhesion and migration due to its co-localization with a-actin, which has a demonstrated role in this process (Shashidhar et al., 2005). Furthermore, GPR56 has been described up-regulated in some types of cancers such as breast, ovarian and pancreatic cancers, suggesting that

GPR56 might function as an oncogene (Ke et al., 2007; Shashidhar et al., 2005; Sud et al., 2006).

The functional relationship between GPCR signalling and EMT has been extensively described. In cancer, deregulation of GPCR signalling has been implicated in cell migration, invasion and metastasis (Sahai & Marshall, 2002; X. Tang et al., 2013; T. Wang et al., 2005; M. P. Wu et al., 2013). Bing Ji et al. showed that GPR56 induces epithelial-mesenchymal transition phenotypes in colorectal cancer cells (Ji et al., 2018). Moreover, previous results from our laboratory revealed that MES-GBMs express lower levels of GPR56 compared with other GBM subtypes. Additionally, GPR56 is co-expressed with PN markers and negatively correlated with MES markers and GPR56 is downregulated during the mesenchymal differentiation (Moreno, Pedrosa, Paré, Pineda, Bejarano, Martínez, Balasubramaniyan, Ezhilarasan, Kallarackal, Kim, Wang, Audia, Marín, et al., 2017). In functional assays, knockdown of GPR56 in PN-GICs triggers mesenchymal differentiation in these cells. Therefore, GPR56 may have an inhibitory role in the PN to MES differentiation of GICs.

In this Ph. D. thesis, we corroborated the above results by inducing KO of GPR56 in PN-GICs and knockdown of GPR56 in CL-GICs. GPR56-KO-PN-GICs and shGPR56-CL-GICs display an increase in the expression of MES genes. We show that CD44 protein expression is increased upon knockdown and knockout of GPR56, in CL- and PN-GICs (Figure 4.32 and Figure 4.29), respectively, suggesting that GPR56 has a role in MES differentiation. However, during the analysis of mRNA expression of different MES markers, we observed high variance in mRNA levels and the results were not so clear (Figure 4.31 and Figure 4.27). It may be due to that the mRNA is not as stable as protein and it might be fluctuant during cells passages. Despite that, we observed a tendency to gain of MES markers, regarding RT-qPCR assay (Figure 4.31 and Figure 4.27). Additionally, a GSEA analysis of microarray data was performed to study the expression of MES and PN signatures in GPR56-KO-PN-GICs with respect to control-PN-GICs. GSEA showed that GPR56-KO-GICs were positively enriched for MES genes and negatively enriched for PN genes (Figure 4.28). Taken together, our results suggest that GPR56 is inhibiting the mesenchymal differentiation of GICs. Altogether, our results suggest that GPR56 is

involved in the MES differentiation of non-MES GICs including PN- and CL-GICs (Figure 5.1). Therefore, when PN or CL-GICs downregulate GPR56 expression, this might trigger their MES differentiation and gain of resistance to therapy.

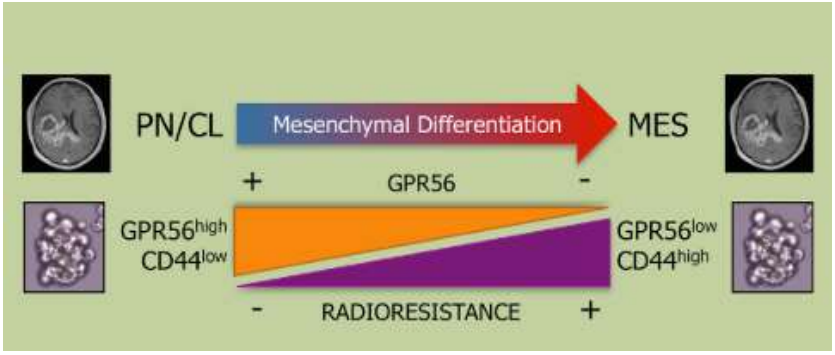

Figure 5.1: Features of mesenchymal differentiation in GICs. *Upon NF-κB pathway activation, PN and CL GICs undergo mesenchymal differentiation. This process is characterized by upregulation of MES genes, such as CD44, and downregulation of PN and CL genes, such as GPR56, accompanied by gain of radioresistance. (Moreno et al., 2017)*

5.3 CONCLUDING REMARKS

In this Ph. D. thesis, we have identified several molecular mechanisms that may confer resistance to therapy and allow the progression of GBM. On the one hand, we have identified two lncRNAs that might regulate the self-renewal capacity of GICs present within the tumour bulk in GBMs. This property of GICs may allow them to propagate the tumour after treatment and promote the progression of glioblastoma. On the other hand, we have identified GPR56/ADGRG1 as an inhibitor of MES differentiation in GICs. GBMs are highly plastic and have an inherent tendency to transition from one subtype to another. This transcriptional plasticity empowers GBMs with the capability to adapt to treatment and develop resistance to therapy. More specifically, MES differentiation has been shown to confer resistance to chemo- and radiotherapy.

For this reason, both lncRNAs identified in this study as well as GPR56 may be new therapeutic targets for the treatment of GBMs. In the case of PAUPAR or LINC00941, one therapeutic strategy might be to downregulate their expression using gene-editing therapies to inhibit the self-renewal capacity of GICs. Regarding GPR56, one might use an agonist of the receptor to prevent resistance to chemo- or radiotherapy associated to MES differentiation of GICs.

Finally, GPR56 and our lcnRNAs might also be used as new prognostic biomarkers. The presence of high levels of PAUPAR or LINC00941 in a given GBM patient might be suggestive of a tumour with a high ratio of sel-renwal. This might be a marker of bad prognosis. Conversely, the absence/low levels of GPR56 in a tumour might indicate resistance to therapy. Therefore, understanding the biology of GICs is important to identify the molecular mechanisms that may be involved in resistance to therapy in glioblastoma and to develop new therapies and/or find new prognostic biomarkers for this devastating disease.

6 CONCLUSIONS

- Identification of novel lncRNAs involved in the stem-like properties of GICs
    - Network analysis of RNAseq data from GBM specimens using WGCNA allowed us to identify several lncRNA candidates to regulate the stem-like properties of GICs.
    - We were able to obtain shRNA-mediated knockdown in GICs of two of the selected lncRNAs: PAUPAR and LINC00941.
    - Loss-of-function analyses show that PAUPAR and LINC00941 promote the self-renewal capacity of GICs
    - Knockdown of PAUPAR and LINC00941 do not induce any transition between GBM subtypes.
    - Clustering analysis of RNAseq data using NMF shows that GBMs may be classified into two different molecular subtypes according to the expression of lncRNAs independent of the mRNA-based classification into PN, CL and MES.
    - There is no difference in patient overall survival between the two lncRNA-based clusters.
- Role of GPR56 in mesenchymal differentiation of GICs
    - We generated PN- and CL-GICs with lowered expression of GPR56 using CRISPR/Cas9 and shRNA techniques, respectively. The GPR56-KO-GICs obtained are not full knockouts and maintain basal expression of GPR56.
    - Downregulation of GPR56 promotes mesenchymal differentiation in proneural- and classical-GICs.

BIBLIOGRAPHY

Ackerman, S. D., Garcia, C., Piao, X., Gutmann, D. H., & Monk, K. R. (2015). The adhesion GPCR Gpr56 regulates oligodendrocyte development via interactions with Gα12/13 and RhoA. *Nature Communications*, *6*, 6122. https://doi.org/10.1038/ncomms7122

Agnihotri, S., Burrell, K. E., Wolf, A., Jalali, S., Hawkins, C., Rutka, J. T., & Zadeh, G. (2013). Glioblastoma, a brief review of history, molecular genetics, animal models and novel therapeutic strategies. *Archivum Immunologiae et Therapiae Experimentalis*, *61*(1), 25–41. https://doi.org/10.1007/s00005-012-0203-0

Alison, M. R., Lim, S. M. L., & Nicholson, L. J. (2011). Cancer stem cells: Problems for therapy? *Journal of Pathology*, *223*(2), 148–162. https://doi.org/10.1002/path.2793

Andersen, R. E., & Lim, D. A. (2018, January 1). Forging our understanding of lncRNAs in the brain. *Cell and Tissue Research*, Vol. 371, pp. 55–71. https://doi.org/10.1007/s00441-017-2711-z

Andre Gerhard Wolff. (2020). *GPCRs: Structure, Function, and Drug Discovery*. Elsevier.

Andriani, F., Bertolini, G., Facchinetti, F., Baldoli, E., Moro, M., Casalini, P., … Roz, L. (2016). Conversion to stem-cell state in response to microenvironmental cues is regulated by balance between epithelial and mesenchymal features in lung cancer cells. *Molecular Oncology*, *10*(2), 253–271. https://doi.org/10.1016/j.molonc.2015.10.002

Appin, C. L., Gao, J., Chisolm, C., Torian, M., Alexis, D., Vincentelli, C., … Brat, D. J. (2013). Glioblastoma with Oligodendroglioma Component (GBM-O): Molecular Genetic and Clinical Characteristics. *Brain Pathology*, *23*(4), 454–461. https://doi.org/10.1111/bpa.12018

Arun, G., Diermeier, S. D., & Spector, D. L. (2018, March 1). Therapeutic Targeting of Long Non-Coding RNAs in Cancer. *Trends in Molecular Medicine*, Vol. 24, pp. 257–277. https://doi.org/10.1016/j.molmed.2018.01.001

Bae, B. Il, Tietjen, I., Atabay, K. D., Evrony, G. D., Johnson, M. B., Asare, E., … Walsh, C. A. (2014). Evolutionarily dynamic alternative splicing of GPR56 Regulates regional cerebral cortical patterning. *Science*, *343*(6172), 764–768. https://doi.org/10.1126/science.1244392

Balic, M., Lin, H., Young, L., Hawes, D., Giuliano, A., McNamara, G., … Cote, R. J. (2006). Most early disseminated cancer cells detected in bone marrow of breast cancer patients have a putative breast cancer stem cell phenotype. *Clinical Cancer Research*, *12*(19), 5615–5621. https://doi.org/10.1158/1078-0432.CCR-06-0169

Bao, S., Wu, Q., McLendon, R. E., Hao, Y., Shi, Q., Hjelmeland, A. B., … Rich, J. N. (2006). Glioma stem cells promote radioresistance by preferential activation of the DNA damage response. *Nature*, *444*(7120), 756–760. https://doi.org/10.1038/nature05236

Belkin, A. M. (2011, December). Extracellular TG2: Emerging functions and regulation. *FEBS Journal*, Vol. 278, pp. 4704–4716. https://doi.org/10.1111/j.1742-4658.2011.08346.x

Bennett, C. F., & Swayze, E. E. (2010). RNA Targeting Therapeutics: Molecular Mechanisms of Antisense Oligonucleotides as a Therapeutic Platform. *Annual Review of Pharmacology and Toxicology*, *50*(1), 259–293. https://doi.org/10.1146/annurev.pharmtox.010909.105654

Bhat, K. P. L., Balasubramaniyan, V., Vaillant, B., Ezhilarasan, R., Hummelink, K., Hollingsworth, F., … Aldape, K. (2013). Mesenchymal Differentiation Mediated by NF-κB Promotes Radiation Resistance in Glioblastoma. *Cancer Cell*, *24*(3), 331–346. https://doi.org/10.1016/j.ccr.2013.08.001

Bhat, K. P. L., Salazar, K. L., Balasubramaniyan, V., Wani, K., Heathcock, L., Hollingsworth, F., … Aldape, K. D. (2011). The transcriptional coactivator TAZ regulates mesenchymal differentiation in malignant glioma. *Genes and Development*, *25*(24), 2594–2609. https://doi.org/10.1101/gad.176800.111.6

Birney, E., Stamatoyannopoulos, J. A., Dutta, A., Guigó, R., Gingeras, T. R., Margulies, E. H., … De Jong, P. J. (2007). Identification and analysis of functional elements in 1% of the human genome by the ENCODE pilot project. *Nature*, *447*(7146), 799–816. https://doi.org/10.1038/nature05874

Blumenthal, D. T., Artzi, M., Liberman, G., Bokstein, F., Aizenstein, O., & Ben Bashat, D. (2017). Classification of high-grade glioma into tumor and nontumor components using support vector machine. *American Journal of Neuroradiology*, *38*(5), 908–914. https://doi.org/10.3174/ajnr.A5127

Brennan, C. W., Verhaak, R. G. W., McKenna, A., Campos, B., Noushmehr, H., Salama, S. R., … McLendon, R. (2013). The somatic genomic landscape of glioblastoma. *Cell*, *155*(2), 462. https://doi.org/10.1016/j.cell.2013.09.034

Brodie, S., Lee, H. K., Jiang, W., Cazacu, S., Xiang, C., Poisson, L. M., … Brodie, C. (2017). The novel long non-coding RNA TALNEC2, regulates tumor cell growth and the stemness and radiation response of glioma stem cells. *Oncotarget*, *8*(19), 31785–31801. https://doi.org/10.18632/oncotarget.15991

Bruna, A., Darken, R. S., Rojo, F., Ocaña, A., Peñuelas, S., Arias, A., … Seoane, J. (2007). High TGFβ-Smad Activity Confers Poor Prognosis in Glioma Patients and Promotes Cell Proliferation Depending on the Methylation of the PDGF-B Gene. *Cancer Cell*, *11*(2), 147–160. https://doi.org/10.1016/j.ccr.2006.11.023

Brunet, J. P., Tamayo, P., Golub, T. R., & Mesirov, J. P. (2004). Metagenes and molecular pattern discovery using matrix factorization. *Proceedings of the National Academy of Sciences of the United States of America*, *101*(12), 4164–4169. https://doi.org/10.1073/pnas.0308531101

Cabrera, M. C. (2015). Cancer stem cell plasticity and tumor hierarchy. *World Journal of Stem Cells*, *7*(1), 27. https://doi.org/10.4252/wjsc.v7.i1.27

Cai, T., Liu, Y., & Xiao, J. (2018). Long noncoding RNA MALAT1 knockdown reverses chemoresistance to temozolomide via promoting microRNA-101 in glioblastoma. *Cancer Medicine*, *7*(4), 1404–1415. https://doi.org/10.1002/cam4.1384

Campbell, L. L., & Polyak, K. (2007). Breast tumor heterogeneity: Cancer stem cells or clonal evolution? *Cell Cycle*, *6*(19), 2332–2338. https://doi.org/10.4161/cc.6.19.4914

Carro, M. S., Lim, W. K., Alvarez, M. J., Bollo, R. J., Zhao, X., Snyder, E. Y., … Iavarone, A. (2010). The transcriptional network for mesenchymal transformation of brain tumours. *Nature*, *463*(7279), 318–325. https://doi.org/10.1038/nature08712

Chalei, V., Sansom, S. N., Kong, L., Lee, S., Montiel, J. F., Vance, K. W., & Ponting, C. P. (2014). The long non-coding RNA Dali is an epigenetic regulator of neural differentiation. *ELife*,

3(e04530), 1–24. https://doi.org/10.7554/eLife.04530

Chen, J., Li, Y., Yu, T. S., McKay, R. M., Burns, D. K., Kernie, S. G., & Parada, L. F. (2012). A restricted cell population propagates glioblastoma growth after chemotherapy. *Nature*, *488*(7412), 522–526. https://doi.org/10.1038/nature11287

Chen, Y., Li, Z., Dong, Z., Beebe, J., Yang, K., Fu, L., & Zhang, J. T. (2017). 14-3-3σ contributes to radioresistance by regulating DNA repair and cell cycle via PARP1 and CHK2. *Molecular Cancer Research*, *15*(4), 418–428. https://doi.org/10.1158/1541-7786.MCR-16-0366

Chen, Z. Z., Huang, L., Wu, Y. H., Zhai, W. J., Zhu, P. P., & Gao, Y. F. (2016). LncSox4 promotes the self-renewal of liver tumour-initiating cells through Stat3-mediated Sox4 expression. *Nature Communications*, *7*(12598), 1–13. https://doi.org/10.1038/ncomms12598

Cojoc, M., Mäbert, K., Muders, M. H., & Dubrovska, A. (2015, April 1). A role for cancer stem cells in therapy resistance: Cellular and molecular mechanisms. *Seminars in Cancer Biology*, Vol. 31, pp. 16–27. https://doi.org/10.1016/j.semcancer.2014.06.004

Colpaert, C., Vermeulen, P., Van Marck, E., & Dirix, L. (2001). The presence of a fibrotic focus is an independent predictor of early metastasis in lymph node-negative breast cancer patients - [2]. *American Journal of Surgical Pathology*, Vol. 25, pp. 1557–1558. https://doi.org/10.1097/00000478-200112000-00016

Cong, L., Ran, F. A., Cox, D., Lin, S., Barretto, R., Habib, N., … Zhang, F. (2013). Multiplex genome engineering using CRISPR/Cas systems. *Science*, *339*(6121), 819–823. https://doi.org/10.1126/science.1231143

Cromie, G. A., Connelly, J. C., & Leach, D. R. F. (2001). Recombination at double-strand breaks and DNA ends: Conserved mechanisms from phage to humans. *Molecular Cell*, *8*(6), 1163–1174. https://doi.org/10.1016/S1097-2765(01)00419-1

Daga, A., Bottino, C., Castriconi, R., Gangemi, R., & Ferrini, S. (2011). New Perspectives in Glioma Immunotherapy. *Current Pharmaceutical Design*, *17*(23), 2439–2467. https://doi.org/10.2174/138161211797249206

Daniel D. Lee, & H. Sebastian Seung. (1999). Learning the parts of objects by non-negative matrix factorization. *Nature*, *401*, 788–791. Retrieved from www.nature.com

Dean, M., Fojo, T., & Bates, S. (2005, April). Tumour stem cells and drug resistance. *Nature Reviews Cancer*, Vol. 5, pp. 275–284. https://doi.org/10.1038/nrc1590

Detmer, S. A., & Chan, D. C. (2007, November). Functions and dysfunctions of mitochondrial dynamics. *Nature Reviews Molecular Cell Biology*, Vol. 8, pp. 870–879. https://doi.org/10.1038/nrm2275

Devarajan, K. (2008). Nonnegative Matrix Factorization: An Analytical and Interpretive Tool in Computational Biology. *PLoS Computational Biology*, *4*(7), e1000029. https://doi.org/10.1371/journal.pcbi.1000029

Dhamija, S., & Diederichs, S. (2016). From junk to master regulators of invasion: lncRNA functions in migration, EMT and metastasis. *International Journal of Cancer*, *139*(2), 269–280. https://doi.org/10.1002/ijc.30039

Digby, G. J., Lober, R. M., Sethi, P. R., & Lambert, N. A. (2006). Some G protein heterotrimers

physically dissociate in living cells. *Proceedings of the National Academy of Sciences of the United States of America*, *103*(47), 17789–17794. https://doi.org/10.1073/pnas.0607116103

Dillman, R. O., Duma, C. M., Schiltz, P. M., DePriest, C., Ellis, R. A., Okamoto, K., … Chico, S. (2004). Intracavitary placement of autologous lymphokine-activated killer (LAK) cells after resection of recurrent glioblastoma. *Journal of Immunotherapy*, *27*(5), 398–404. https://doi.org/10.1097/00002371-200409000-00009

Ding, X., Wang, X., Lin, M., Xing, Y., Ge, S., Jia, R., … Li, J. (2016). *PAUPAR* lncRNA suppresses tumourigenesis by H3K4 demethylation in uveal melanoma. *FEBS Letters*, *590*(12), 1729–1738. https://doi.org/10.1002/1873-3468.12220

Dong, J., & Horvath, S. (2007). Understanding network concepts in modules. *BMC Systems Biology*, *1*. https://doi.org/10.1186/1752-0509-1-24

Duan, H., Li, X., Chen, Y., Wang, Y., & Li, Z. (2019). LncRNA RHPN1-AS1 promoted cell proliferation, invasion and migration in cervical cancer via the modulation of miR-299–3p/FGF2 axis. *Life Sciences*, *239*(116856). https://doi.org/10.1016/j.lfs.2019.116856

Fanale, D., Castiglia, M., Bazan, V., & Russo, A. (2016). Involvement of non-coding RNAs in chemo- and radioresistance of colorectal cancer. *Advances in Experimental Medicine and Biology*, *937*, 207–228. https://doi.org/10.1007/978-3-319-42059-2_11

Fatica, A., & Bozzoni, I. (2014). Long non-coding RNAs: New players in cell differentiation and development. *Nature Reviews Genetics*, *15*(1), 7–21. https://doi.org/10.1038/nrg3606

Fedele, M., Cerchia, L., Pegoraro, S., Sgarra, R., & Manfioletti, G. (2019). Proneural-Mesenchymal Transition: Phenotypic Plasticity to Acquire Multitherapy Resistance in Glioblastoma. *International Journal of Molecular Sciences*, *20*(11). https://doi.org/10.3390/ijms20112746

Feng, S., Yao, J., Chen, Y., Geng, P., Zhang, H., Ma, X., … Yu, X. (2015). Expression and Functional Role of Reprogramming-Related Long Noncoding RNA (lincRNA-ROR) in Glioma. *Journal of Molecular Neuroscience*, *56*(3), 623–630. https://doi.org/10.1007/s12031-014-0488-z

Fomchenko, E. I., & Holland, E. C. (2005). Stem cells and brain cancer. *Experimental Cell Research*, *306*(2), 323–329. https://doi.org/10.1016/j.yexcr.2005.03.007

Friedman, H. S., Prados, M. D., Wen, P. Y., Mikkelsen, T., Schiff, D., Abrey, L. E., … Cloughesy, T. (2009). Bevacizumab alone and in combination with irinotecan in recurrent glioblastoma. *Journal of Clinical Oncology*, *27*(28), 4733–4740. https://doi.org/10.1200/JCO.2008.19.8721

Fu, W. M., Lu, Y. F., Hu, B. G., Liang, W. C., Zhu, X., Yang, H. Di, … Zhang, J. F. (2016). Long noncoding RNA hotair mediated angiogenesis in nasopharyngeal carcinoma by direct and indirect signaling pathways. *Oncotarget*, *7*(4), 4712–4723. https://doi.org/10.18632/oncotarget.6731

Furnari, F. B., Fenton, T., Bachoo, R. M., Mukasa, A., Stommel, J. M., Stegh, A., … Cavenee, W. K. (2007, November 1). Malignant astrocytic glioma: Genetics, biology, and paths to treatment. *Genes and Development*, Vol. 21, pp. 2683–2710. https://doi.org/10.1101/gad.1596707

Galluzzi, L., Kepp, O., & Kroemer, G. (2012, December 23). Mitochondria: Master regulators of danger signalling. *Nature Reviews Molecular Cell Biology*, Vol. 13, pp. 780–788.

https://doi.org/10.1038/nrm3479

Gerdes, M. J., Sood, A., Sevinsky, C., Pris, A. D., Zavodszky, M. I., & Ginty, F. (2014). Emerging understanding of multiscale tumor heterogeneity. *Frontiers in Oncology*, *4*(DEC). https://doi.org/10.3389/fonc.2014.00366

Goellner, E. M., Grimme, B., Brown, A. R., Lin, Y. C., Wang, X. H., Sugrue, K. F., … Sobol, R. W. (2011). Overcoming temozolomide resistance in glioblastoma via dual inhibition of NAD+ biosynthesis and base excision repair. *Cancer Research*, *71*(6), 2308–2317. https://doi.org/10.1158/0008-5472.CAN-10-3213

Goldstein, M., & Kastan, M. B. (2015). The DNA Damage Response: Implications for Tumor Responses to Radiation and Chemotherapy. *Annual Review of Medicine*, *66*(1), 129–143. https://doi.org/10.1146/annurev-med-081313-121208

Goyal, A., Myacheva, K., Groß, M., Klingenberg, M., Duran Arqú, B., & Diederichs, S. (2016). Challenges of CRISPR/Cas9 applications for long non-coding RNA genes. *Nucleic Acids Research*, *45*(3), 12. https://doi.org/10.1093/nar/gkw883

Guarino, M., Rubino, B., & Ballabio, G. (2007). The role of EMT in cancer pathology. *Pathology*, *39*(3), 305–318. https://doi.org/10.1080/00313020701329914

Guo, Q., Zhao, Y., Chen, J., Hu, J., Wang, S., Zhang, D., & Sun, Y. (2014). BRAF-activated long non-coding RNA contributes to colorectal cancer migration by inducing epithelial-mesenchymal transition. *Oncology Letters*, *8*(2), 869–875. https://doi.org/10.3892/ol.2014.2154

Guttman, M., Donaghey, J., Carey, B. W., Garber, M., Grenier, J. K., Munson, G., … Lander, E. S. (2011). LincRNAs act in the circuitry controlling pluripotency and differentiation. *Nature*, *477*(7364), 295–300. https://doi.org/10.1038/nature10398

Haier, J., Goldmann, U., Hotz, B., Runkel, N., & Keilholz, U. (2002). Inhibition of tumor progression and neoangiogenesis using cyclic RGD-peptides in a chemically induced colon carcinoma in rats. *Clinical and Experimental Metastasis*, *19*(8), 665–672. https://doi.org/10.1023/A:1021316531912

Hartmann, C., Hentschel, B., Wick, W., Capper, D., Felsberg, J., Simon, M., … Von Deimling, A. (2010). Patients with IDH1 wild type anaplastic astrocytomas exhibit worse prognosis than IDH1-mutated glioblastomas, and IDH1 mutation status accounts for the unfavorable prognostic effect of higher age: Implications for classification of gliomas. *Acta Neuropathologica*, *120*(6), 707–718. https://doi.org/10.1007/s00401-010-0781-z

Hong, S., Hu, S., Kang, Z., Liu, Z., Yang, W., Zhang, Y., … Chen, L. (2020). Identification of functional lncRNAs based on competing endogenous RNA network in osteoblast differentiation. *Journal of Cellular Physiology*, *235*(3), 2232–2244. https://doi.org/10.1002/jcp.29132

Horvath, S., & Dong, J. (2008). Geometric interpretation of gene coexpression network analysis. *PLoS Computational Biology*, *4*(8). https://doi.org/10.1371/journal.pcbi.1000117

Hsu, P. D., Lander, E. S., & Zhang, F. (2014). Development and applications of CRISPR-Cas9 for genome engineering. *Cell*, *157*(6), 1262–1278. https://doi.org/10.1016/j.cell.2014.05.010

Hu, W., Alvarez-Dominguez, J. R., & Lodish, H. F. (2012). Regulation of mammalian cell

differentiation by long non-coding RNAs. *EMBO Reports*, *13*(11), 971–983. https://doi.org/10.1038/embor.2012.145

Hyunsoo Kim, and H. P. (2007). Sparse non-negative matrix factorizations via alternating non-negativity-constrained least squares for microarray data analysis. *Bioinformatics*, 1495–1502. Retrieved from https://academic.oup.com/bioinformatics/article/23/12/1495/225472

Ilicic, T., Kim, J. K., Kolodziejczyk, A. A., Bagger, F. O., McCarthy, D. J., Marioni, J. C., & Teichmann, S. A. (2016). Classification of low quality cells from single-cell RNA-seq data. *Genome Biology*, *17*(1), 29. https://doi.org/10.1186/s13059-016-0888-1

Jackson, E. L., Garcia-Verdugo, J. M., Gil-Perotin, S., Roy, M., Quinones-Hinojosa, A., VandenBerg, S., & Alvarez-Buylla, A. (2006). PDGFRα-Positive B Cells Are Neural Stem Cells in the Adult SVZ that Form Glioma-like Growths in Response to Increased PDGF Signaling. *Neuron*, *51*(2), 187–199. https://doi.org/10.1016/j.neuron.2006.06.012

Jarroux, J., Morillon, A., & Pinskaya, M. (2017). Long Non Coding RNA Biology. In *Advances in experimental medicine and biology* (Vol. 1008). https://doi.org/10.1007/978-981-10-5203-3

Ji, B., Feng, Y., Sua, Y., Ji, D., Qian, W., Zhang, Z., … Sun, Y. (2018). GPR56 promotes proliferation of colorectal cancer cells and enhances metastasis via epithelial-mesenchymal transition through PI3K/AKT signaling activation. *Oncology Reports*, *40*(4), 1885–1896. https://doi.org/10.3892/or.2018.6582

Jin, C., Yan, B., Lu, Q., Lin, Y., & Ma, L. (2016). The role of MALAT1/miR-1/slug axis on radioresistance in nasopharyngeal carcinoma. *Tumor Biology*, *37*(3), 4025–4033. https://doi.org/10.1007/s13277-015-4227-z

Jing, L., Yuan, W., Ruofan, D., Jinjin, Y., & Haifeng, Q. (2015). HOTAIR enhanced aggressive biological behaviors and induced radio-resistance via inhibiting p21 in cervical cancer. *Tumor Biology*, *36*(5), 3611–3619. https://doi.org/10.1007/s13277-014-2998-2

Joyce, J. A., & Pollard, J. W. (2009). Microenvironmental regulation of metastasis. *Nature Reviews Cancer*, *9*(4), 239–252. https://doi.org/10.1038/nrc2618

Ju, C., Liu, R., Zhang, Y. W., Zhang, Y., Zhou, R., Sun, J., … Zhang, Z. (2019). Mesenchymal stem cell-associated lncRNA in osteogenic differentiation. *Biomedicine and Pharmacotherapy*, *115*(108912). https://doi.org/10.1016/j.biopha.2019.108912

Ke, N., Sundaram, R., Liu, G., Chionis, J., Fan, W., Rogers, C., … Li, Q. X. (2007). Orphan G protein-coupled receptor GPR56 plays a role in cell transformation and tumorigenesis involving the cell adhesion pathway. *Molecular Cancer Therapeutics*, *6*(6), 1840–1850. https://doi.org/10.1158/1535-7163.MCT-07-0066

Khalil, A. M., Guttman, M., Huarte, M., Garber, M., Raj, A., Morales, D. R., … Rinn, J. L. (2009). Many human large intergenic noncoding RNAs associate with chromatin-modifying complexes and affect gene expression. *Proceedings of the National Academy of Sciences of the United States of America*, *106*(28), 11667–11672. https://doi.org/10.1073/pnas.0904715106

Khanduja, J. S., Calvo, I. A., Joh, R. I., Hill, I. T., & Motamedi, M. (2016). Nuclear Noncoding RNAs and Genome Stability. *Molecular Cell*, *63*(1), 7–20. https://doi.org/10.1016/j.molcel.2016.06.011

Kim, J., Piao, H. L., Kim, B. J., Yao, F., Han, Z., Wang, Y., … Ma, L. (2018). Long noncoding RNA

MALAT1 suppresses breast cancer metastasis. *Nature Genetics*, *50*(12), 1705–1715. https://doi.org/10.1038/s41588-018-0252-3

Kim, S.-R., Ramos, J., Ashikari, M., Virk, P. S., Torres, E. A., Nissila, E., … Jena, K. K. (2016). Development and validation of allele-specific SNP/indel markers for eight yield-enhancing genes using whole-genome sequencing strategy to increase yield potential of rice, Oryza sativa L. *Rice*, *9*(1), 12. https://doi.org/10.1186/s12284-016-0084-7

Kiran, M., Chatrath, A., Tang, X., Keenan, D. M., & Dutta, A. (2018). A prognostic signature for lower-grade gliomas based on expression of long noncoding RNAs. *A Prognostic Signature for Lower Grade Gliomas Based on Expression of Long Non-Coding RNAs*, *56*(7), 4786–4798. https://doi.org/10.1101/442616

Kumabe, Sohma, Kayama, & Yoshimoto. (1992). Amplification of alpha-platelet-derived growth factor receptor gene lacking an exon coding for a portion of the extracellular region in a primary brain tumor of glial origin. *Oncogene*, *7*(4), 627–633.

Lander, E. S., Linton, L. M., Birren, B., Nusbaum, C., Zody, M. C., Baldwin, J., … Morgan, M. J. (2001). Initial sequencing and analysis of the human genome. *Nature*, *409*(6822), 860–921. https://doi.org/10.1038/35057062

Langfelder, P., & Horvath, S. (2007). Eigengene networks for studying the relationships between co-expression modules. *BMC Systems Biology*, *1*(1), 54. https://doi.org/10.1186/1752-0509-1-54

Langfelder, P., & Horvath, S. (2008). WGCNA: An R package for weighted correlation network analysis. *BMC Bioinformatics*, *9*(1), 559. https://doi.org/10.1186/1471-2105-9-559

Lewis-Tuffin, L. J., Rodriguez, F., Giannini, C., Scheithauer, B., Necela, B. M., Sarkaria, J. N., & Anastasiadis, P. Z. (2010). Misregulated E-Cadherin expression associated with an aggressive brain tumor phenotype. *PLoS ONE*, *5*(10), e13665. https://doi.org/10.1371/journal.pone.0013665

Li, D., Lu, J., Li, H., Qi, S., & Yu, L. (2019). Identification of a long noncoding RNA signature to predict outcomes of glioblastoma. *Molecular Medicine Reports*, *19*(6), 5406–5416. https://doi.org/10.3892/mmr.2019.10184

Li, H., Yang, Y., Hong, W., Huang, M., Wu, M., & Zhao, X. (2020). Applications of genome editing technology in the targeted therapy of human diseases: mechanisms, advances and prospects. *Signal Transduction and Targeted Therapy*, *5*(1), 1–23. https://doi.org/10.1038/s41392-019-0089-y

Li, T., Li, Z., Wan, H., Tang, X., Wang, H., Chai, F., … Wang, B. (2020). Recurrence-Associated Long Non-coding RNA LNAPPCC Facilitates Colon Cancer Progression via Forming a Positive Feedback Loop with PCDH7. *Molecular Therapy - Nucleic Acids*, *20*, 545–557. https://doi.org/10.1016/j.omtn.2020.03.017

Li, Z., Zhou, Y., Tu, B., Bu, Y., Liu, A., & Kong, J. (2017). Long noncoding RNA MALAT1 affects the efficacy of radiotherapy for esophageal squamous cell carcinoma by regulating Cks1 expression. *Journal of Oral Pathology & Medicine*, *46*(8), 583–590. https://doi.org/10.1111/jop.12538

Lin, N., Chang, K. Y., Li, Z., Gates, K., Rana, Z. A., Dang, J., … Rana, T. M. (2014). An evolutionarily conserved long noncoding RNA TUNA controls pluripotency and neural lineage commitment. *Molecular Cell*, *53*(6), 1005–1019.

https://doi.org/10.1016/j.molcel.2014.01.021

Liu, G., Yuan, X., Zeng, Z., Tunici, P., Ng, H., Abdulkadir, I. R., … Yu, J. S. (2006). Analysis of gene expression and chemoresistance of CD133+ cancer stem cells in glioblastoma. *Molecular Cancer*, *5*, 67. https://doi.org/10.1186/1476-4598-5-67

Liu, H., Wu, N., Zhang, Z., Zhong, X. D., Zhang, H., Guo, H., … Liu, Y. (2019). Long non-coding RNA LINC00941 as a potential biomarker promotes the proliferation and metastasis of gastric cancer. *Frontiers in Genetics*, *10*(JAN). https://doi.org/10.3389/fgene.2019.00005

Liu, M., Parker, R. M. C., Darby, K., Eyre, H. J., Copeland, N. G., Crawford, J., … Herzog, H. (1999). GPR56, a novel secretin-like human G-protein-coupled receptor gene. *Genomics*, *55*(3), 296–305. https://doi.org/10.1006/geno.1998.5644

Liu, W., Ma, J., Cheng, Y., Zhang, H., Luo, W., Zhang, H., … Yao, J. (2017). Knockdown of a DIS3l2 promoter upstream long noncoding RNA(AC105461.1) enhances colorectal cancer stem cell properties in vitro by down-regulating DIS3l2. *OncoTargets and Therapy*, *10*, 2367–2376. https://doi.org/10.2147/OTT.S132708

Liu, Y., Wang, Y., Yao, D., & Cui, D. (2018). LncSOX4 serves an oncogenic role in the tumorigenesis of epithelial ovarian cancer by promoting cell proliferation and inhibiting apoptosis. *Molecular Medicine Reports*, *17*(6), 8282–8288. https://doi.org/10.3892/mmr.2018.8892

Louis, D. N., Ohgaki, H., Wiestler, O. D., Cavenee, W. K., Burger, P. C., Jouvet, A., … Kleihues, P. (2007). The 2007 WHO classification of tumours of the central nervous system. *Acta Neuropathologica*, *114*(2), 97–109. https://doi.org/10.1007/s00401-007-0243-4

Louis, D. N., Perry, A., Reifenberger, G., Deimling, A. Von, Figarella, D., Webster, B., … Ellison, D. W. (2016). The 2016 World Health Organization Classification of Tumors of the Central Nervous System : a summary. *Acta Neuropathologica*, *131*(6), 803–820. https://doi.org/10.1007/s00401-016-1545-1

Lu, F., Chen, Y., Zhao, C., Canoll, P., Holland, E. C., Lu, Q. R., … He, X. (2016). Olig2-Dependent Reciprocal Shift in PDGF and EGF Receptor Signaling Regulates Tumor Phenotype and Mitotic Growth in Malignant Glioma Article Olig2-Dependent Reciprocal Shift in PDGF and EGF Receptor Signaling Regulates Tumor Phenotype and Mitotic Growth i. *Cancer Cell*, *29*(5), 669–683. https://doi.org/10.1016/j.ccell.2016.03.027

Lu, H., He, Y., Lin, L., Qi, Z., Ma, L., Li, L., & Su, Y. (2016). Long non-coding RNA MALAT1 modulates radiosensitivity of HR-HPV+ cervical cancer via sponging miR-145. *Tumor Biology*, *37*(2), 1683–1691. https://doi.org/10.1007/s13277-015-3946-5

Luo, C., Tao, Y., Zhang, Y., Zhu, Y., Minyao, D. N., Haleem, M., … Liao, Q. (2018). Regulatory network analysis of high expressed long non-coding RNA LINC00941 in gastric cancer. *Gene*, *662*, 103–109. https://doi.org/10.1016/j.gene.2018.04.023

Lynch, T. J., Bell, D. W., Sordella, R., Gurubhagavatula, S., Okimoto, R. A., Brannigan, B. W., … Haber, D. A. (2004). Activating Mutations in the Epidermal Growth Factor Receptor Underlying Responsiveness of Non-Small-Cell Lung Cancer to Gefitinib. *New England Journal of Medicine*, *350*(21), 2129–2139. https://doi.org/10.1056/NEJMoa040938

M, S., M, I., & S, G.-F. (2016). The Role of Long Non-Coding RNAs in Breast Cancer. *Archives of Iranian Medicine*, *19*(7), 508–517. https://doi.org/0161907/aim.0011

Ma, S. C., Li, Q., Peng, J. Y., Zhouwen, J. L., Zhang, D. N., Zhang, C. B., … Jia, W. (2018). CLDN5 affects IncRNAs acting as ceRNA dynamics contributing to regulating blood-brain barrier permeability in tumor brain metastasis. *Oncology Reports*, *39*(3), 1441–1453. https://doi.org/10.3892/or.2018.6208

Mao, P., Joshi, K., Li, J., Kim, S. H., Li, P., Santana-Santos, L., … Nakano, I. (2013). Mesenchymal glioma stem cells are maintained by activated glycolytic metabolism involving aldehyde dehydrogenase 1A3. *Proceedings of the National Academy of Sciences of the United States of America*, *110*(21), 8644–8649. https://doi.org/10.1073/pnas.1221478110

Mayes, D. A., Hu, Y., Teng, Y., Siegel, E., Wu, X., Panda, K., … Zhou, Y. H. (2006). PAX6 suppresses the invasiveness of glioblastoma cells and the expression of the matrix metalloproteinase-2 gene. *Cancer Research*, *66*(20), 9809–9817. https://doi.org/10.1158/0008-5472.CAN-05-3877

McLendon, R., Friedman, A., Bigner, D., Van Meir, E. G., Brat, D. J., Mastrogianakis, G. M., … Thomson, E. (2008). Comprehensive genomic characterization defines human glioblastoma genes and core pathways. *Nature*, *455*(7216), 1061–1068. https://doi.org/10.1038/nature07385

Meacham, C. E., & Morrison, S. J. (2013). Tumour heterogeneity and cancer cell plasticity. *Nature*, *501*(7467), 328–337. https://doi.org/10.1038/nature12624

Michor, F., & Polyak, K. (2010). The origins and implications of intratumor heterogeneity. *Cancer Prevention Research*, *3*(11), 1361–1364. https://doi.org/10.1158/1940-6207.CAPR-10-0234

Mikheeva, S. A., Mikheev, A. M., Petit, A., Beyer, R., Oxford, R. G., Khorasani, L., … Rostomily, R. C. (2010). TWIST1 promotes invasion through mesenchymal change in human glioblastoma. *Molecular Cancer*, *9*(1), 1–18. https://doi.org/10.1186/1476-4598-9-194

Mohamed, J. S., Gaughwin, P. M., Lim, B., Robson, P., & Lipovich, L. (2010). Conserved long noncoding RNAs transcriptionally regulated by Oct4 and Nanog modulate pluripotency in mouse embryonic stem cells. *RNA*, *16*(2), 324–337. https://doi.org/10.1261/rna.1441510

Moreno, M., Pedrosa, L., Paré, L., Pineda, E., Bejarano, L., Martínez, J., … de la Iglesia, N. (2017). GPR56/ADGRG1 Inhibits Mesenchymal Differentiation and Radioresistance in Glioblastoma. *Cell Reports*, *21*(8), 2183–2197. https://doi.org/10.1016/j.celrep.2017.10.083

Moreno, M., Pedrosa, L., Paré, L., Pineda, E., Bejarano, L., Martínez, J., … De la Iglesia, N. (2017). GPR56/ADGRG1 inhibits the Proneural-to-Mesenchymal Transition and Radioresistance in Glioblastoma. *Cell Reports*, *21*, 2183–2197. https://doi.org/10.1002/jcp.25597

Morrissey, E. R., & N Diaz-Uriarte, R. (2009). Pomelo II: finding differentially expressed genes. *Nucleic Acids Research*, *37*, 581–586. https://doi.org/10.1093/nar/gkp366

Murat, A., Migliavacca, E., Gorlia, T., Lambiv, W. L., Shay, T., Hamou, M.-F., … Hegi, M. E. (2008). Stem Cell–Related "Self-Renewal" Signature and High Epidermal Growth Factor Receptor Expression Associated With Resistance to Concomitant Chemoradiotherapy in Glioblastoma. *Journal of Clinical Oncology*, *26*(18), 3015–3024. https://doi.org/10.1200/JCO.2007.15.7164

Myung, J. K., Choi, S. A., Kim, S. K., Wang, K. C., & Park, S. H. (2014). Snail plays an oncogenic role in glioblastoma by promoting epithelial mesenchymal transition. *International Journal of Clinical and Experimental Pathology*, *7*(5), 1977–1987.

Natsume, A., Kinjo, S., Yuki, K., Kato, T., Ohno, M., Motomura, K., … Wakabayashi, T. (2011). Glioma-initiating cells and molecular pathology: Implications for therapy. *Brain Tumor Pathology*, *28*(1), 1–12. https://doi.org/10.1007/s10014-010-0011-3

Norden, A. D., Young, G. S., Setayesh, K., Muzikansky, A., Ciampa, A. S., Ebbeling, L. G., … Wen, P. Y. (2008). Bevacizumab for recurrent malignant gliomas: Efficacy, toxicity, and patterns of recurrencesymbol. *Neurology*, *70*(10), 779–787. https://doi.org/10.1212/01.wnl.0000304121.57857.38

Noushmehr, H., Weisenberger, D. J., Diefes, K., Phillips, H. S., Pujara, K., Berman, B. P., … Aldape, K. (2010). Identification of a CpG Island Methylator Phenotype that Defines a Distinct Subgroup of Glioma. *Cancer Cell*, *17*(5), 510–522. https://doi.org/10.1016/j.ccr.2010.03.017

O'Keefe, E. P. (2013). siRNAs and shRNAs: Tools for Protein Knockdown by Gene Silencing. *Materials and Methods*, *3*. https://doi.org/10.13070/mm.en.3.197

Ohgaki, H., Dessen, P., Jourde, B., Horstmann, S., Nishikawa, T., Di Patre, P. L., … Kleihues, P. (2004). Genetic pathways to glioblastoma: A population-based study. *Cancer Research*, *64*(19), 6892–6899. https://doi.org/10.1158/0008-5472.CAN-04-1337

Ohgaki, H., & Kleihues, P. (2013). The definition of primary and secondary glioblastoma. *Clinical Cancer Research*, *19*(4), 764–772. https://doi.org/10.1158/1078-0432.CCR-12-3002

Ohka, F., Natsume, A., & Wakabayashi, T. (2012). Current Trends in Targeted Therapies for Glioblastoma Multiforme. *Neurology Research International*, *2012*, 13. https://doi.org/10.1155/2012/878425

Oldham, M. C., Konopka, G., Iwamoto, K., Langfelder, P., Kato, T., Horvath, S., & Geschwind, D. H. (2008). Functional organization of the transcriptome in human brain. *Nature Neuroscience*, *11*(11), 1271–1282. https://doi.org/10.1038/nn.2207

Osorio, D., & Cai, J. (2020). Systematic determination of the mitochondrial proportion in human and mice tissues for single-cell RNA sequencing data quality control. *BioRxiv*, 2020.02.20.958793. https://doi.org/10.1101/2020.02.20.958793

Ostrom, Q. T., Gittleman, H., Farah, P., Ondracek, A., Chen, Y., Wolinsky, Y., … Barnholtz-sloan, J. S. (2013). CBTRUS Statistical Report : Primary Brain and Central Nervous System Tumors Diagnosed in the United States in 2006-2010. *Neuro-Oncology*, *16*(suppl_2), 1–56. https://doi.org/10.1093/neuonc/not151

P.Sulman, E., Guerrero, M., & Aldape, K. (2009). Beyond Grade: Molecular Pathology of Malignant Gliomas. *Seminars in Radiation Oncology*, *19*(3), 142–149.

Paatero, P., & Tapper, U. (1994). Positive matrix factorization: A non-negative factor model with optimal utilization of error estimates of data values. *Environmetrics*, *5*(2), 111–126. https://doi.org/10.1002/env.3170050203

Paralkar, V. R., & Weiss, M. J. (2013). Long noncoding RNAs in biology and hematopoiesis. *Blood*, *121*(24), 4842–4846. https://doi.org/10.1182/blood-2013-03-456111

Parsons, D. W., Jones, S., Zhang, X., Lin, J. C. H., Leary, R. J., Angenendt, P., … Kinzler, K. W. (2008). An integrated genomic analysis of human glioblastoma multiforme. *Science*, *321*(5897), 1807–1812. https://doi.org/10.1126/science.1164382

Pastori, C., Kapranov, P., Penas, C., Peschansky, V., Volmar, C. H., Sarkaria, J. N., … Roberts, T. C. (2015). The bromodomain protein BRD4 controls HOTAIR, a long noncoding RNA essential for glioblastoma proliferation. *Proceedings of the National Academy of Sciences of the United States of America*, *112*(27), 8326–8331. https://doi.org/10.1073/pnas.1424220112

Patel, A. P., Tirosh, I., Trombetta, J. J., Shalek, A. K., Gillespie, S. M., Wakimoto, H., … Bernstein, B. E. (2014). Single-cell RNA-seq highlights intratumoral heterogeneity in primary glioblastoma. *Science*, *344*(6190), 1396–1401. https://doi.org/10.1126/science.1254257

Pavlaki, I., Alammari, F., Sun, B., Clark, N., Sirey, T., Lee, S., … Vance, K. W. (2018). The long non-coding RNA Paupar promotes KAP 1-dependent chromatin changes and regulates olfactory bulb neurogenesis. *The EMBO Journal*, *37*(10). https://doi.org/10.15252/embj.201798219

Phillips, H. S., Kharbanda, S., Chen, R., Forrest, W. F., Soriano, R. H., Wu, T. D., … Aldape, K. (2006). Molecular subclasses of high-grade glioma predict prognosis, delineate a pattern of disease progression, and resemble stages in neurogenesis. *Cancer Cell*, *9*(3), 157–173. https://doi.org/10.1016/j.ccr.2006.02.019

Piao, X., Hill, S. S., Bodell, A., Chang, B. S., Basel-Vanagaite, L., Straussberg, R., … Walsh, C. A. (2004). G Protein-Coupled Receptor-Dependent Development of Human Frontal Cortex. *Science*, *303*(5666), 2033–2036. https://doi.org/10.1126/science.1092780

Piao, Y., Liang, J., Holmes, L., Henry, V., Sulman, E., & De Groot, J. F. (2013). Acquired resistance to anti-VEGF therapy in glioblastoma is associated with a mesenchymal transition. *Clinical Cancer Research*, *19*(16), 4392–4403. https://doi.org/10.1158/1078-0432.CCR-12-1557

Piccirillo, S. G. M., Combi, R., Cajola, L., Patrizi, A., Redaelli, S., Bentivegna, A., … Vescovi, A. L. (2009). Distinct pools of cancer stem-like cells coexist within human glioblastomas and display different tumorigenicity and independent genomic evolution. *Oncogene*, *28*(15), 1807–1811. https://doi.org/10.1038/onc.2009.27

Pietras, A., Katz, A. M., Ekström, E. J., Wee, B., Halliday, J. J., Pitter, K. L., … Holland, E. C. (2014). Osteopontin-CD44 signaling in the glioma perivascular niche enhances cancer stem cell phenotypes and promotes aggressive tumor growth. *Cell Stem Cell*, *14*(3), 357–369. https://doi.org/10.1016/j.stem.2014.01.005

Pisapia, D. J. (2017). The updated world health organization glioma classification: Cellular and molecular origins of adult infiltrating gliomas. *Archives of Pathology and Laboratory Medicine*, *141*(12), 1633–1645. https://doi.org/10.5858/arpa.2016-0493-RA

Plaks, V., Kong, N., & Werb, Z. (2015). The cancer stem cell niche: How essential is the niche in regulating stemness of tumor cells? *Cell Stem Cell*, *16*(3), 225–238. https://doi.org/10.1016/j.stem.2015.02.015

Pu, H., Zheng, Q., Li, H., Wu, M., An, J., Gui, X., … Lu, D. (2015). CUDR promotes liver cancer stem cell growth through upregulating TERT and C-Myc. *Oncotarget*, *6*(38), 40775–40798. https://doi.org/10.18632/oncotarget.5805

Qiu, K., Zheng, Z., & Huang, Y. (2020). Long intergenic noncoding RNA 00844 promotes apoptosis and represses proliferation of prostate cancer cells through upregulating GSTP1 by recruiting EBF1. *Journal of Cellular Physiology*, 1–14. https://doi.org/10.1002/jcp.29690

Quant, E. C., Norden, A. D., Drappatz, J., Muzikansky, A., Doherty, L., Lafrankie, D., … Wen, P.

Y. (2009). Role of a second chemotherapy in recurrent malignant glioma patients who progress on bevacizumab. *Neuro-Oncology*, *11*(5), 550–555. https://doi.org/10.1215/15228517-2009-006

Ran, F. A., Hsu, P. D., Wright, J., Agarwala, V., Scott, D. A., & Zhang, F. (2013). Genome engineering using the CRISPR-Cas9 system. *Nature Protocols*, *8*(11), 2281–2308. https://doi.org/10.1038/nprot.2013.143

Rand, V., Huang, J., Stockwell, T., Ferriera, S., Buzko, O., Levy, S., … Strausberg, R. L. (2005, October 4). Sequence survey of receptor tyrosine kinases reveals mutations in glioblastomas. *Proceedings of the National Academy of Sciences of the United States of America*, Vol. 102, pp. 14344–14349. https://doi.org/10.1073/pnas.0507200102

Ravasz, E., Somera, A. L., Mongru, D. A., Oltvai, Z. N., & Barabási, A. L. (2002). Hierarchical organization of modularity in metabolic networks. *Science*, *297*(5586), 1551–1555. https://doi.org/10.1126/science.1073374

Redza-Dutordoir, M., & Averill-Bates, D. A. (2016). Activation of apoptosis signalling pathways by reactive oxygen species. *Biochimica et Biophysica Acta - Molecular Cell Research*, *1863*(12), 2977–2992. https://doi.org/10.1016/j.bbamcr.2016.09.012

Reticker-Flynn, N. E., Malta, D. F. B., Winslow, M. M., Lamar, J. M., Xu, M. J., Underhill, G. H., … Bhatia, S. N. (2012). A combinatorial extracellular matrix platform identifies cell-extracellular matrix interactions that correlate with metastasis. *Nature Communications*, *3*. https://doi.org/10.1038/ncomms2128

Reya, T., Morrison, S. J., Clarke, M. F., & Weissman, I. L. (2001). Stem cells, cancer, and cancer stem cells. *Nature*, *414*(6859), 105–111. https://doi.org/10.1038/35102167

Rich, J. N. (2016). Cancer stem cells: Understanding tumor hierarchy and heterogeneity. *Medicine (United States)*, *95*(1), S2–S7. https://doi.org/10.1097/MD.0000000000004764

Rizvi, A. H., Camara, P. G., Kandror, E. K., Roberts, T. J., Schieren, I., Maniatis, T., & Rabadan, R. (2017). Single-cell topological RNA-seq analysis reveals insights into cellular differentiation and development. *Nature Biotechnology*, *35*(6), 551–560. https://doi.org/10.1038/nbt.3854

Sahai, E., & Marshall, C. J. (2002). RHO - GTPases and cancer. *Nature Reviews Cancer*, *2*(2), 133–142. https://doi.org/10.1038/nrc725

Salmena, L., Poliseno, L., Tay, Y., Kats, L., & Pandolfi, P. P. (2011, August 5). A ceRNA hypothesis: The rosetta stone of a hidden RNA language? *Cell*, Vol. 146, pp. 353–358. https://doi.org/10.1016/j.cell.2011.07.014

Sampson, J. H., Archer, G. E., Mitchell, D. A., Heimberger, A. B., Herndon, J. E., Lally-Goss, D., … Bigner, D. D. (2009). An epidermal growth factor receptor variant III-targeted vaccine is safe and immunogenic in patients with glioblastoma multiforme. *Molecular Cancer Therapeutics*, *8*(10), 2773–2779. https://doi.org/10.1158/1535-7163.MCT-09-0124

Sanai, N., Alvarez-Buylla, A., & Berger, M. S. (2005). Mechanisms of disease: Neural stem cells and the origin of gliomas. *New England Journal of Medicine*, *353*(8), 811–822. https://doi.org/10.1056/NEJMra043666

Sarkar, D., Leung, E. Y., Baguley, B. C., Finlay, G. J., & Askarian-Amiri, M. E. (2014). Epigenetic regulation in human melanoma: Past and future. *Epigenetics*, *10*(2), 103–121.

https://doi.org/10.1080/15592294.2014.1003746

Scherer, H. J. (1940). Cerebral astrocytomas and their derivatives. *American Journal of Cancer*, *40*(2), 159–198. https://doi.org/10.1158/ajc.1940.159

Schiöth, H. B., & Lagerström, M. C. (2008). Structural diversity of g proteincoupled receptors and significance for drug discovery. *Nature Reviews Drug Discovery*, *7*(4), 339–357. https://doi.org/10.1038/nrd2518

Schmitt, A. M., & Chang, H. Y. (2016). Long Noncoding RNAs in Cancer Pathways. *Cancer Cell*, *29*(4), 452–463. https://doi.org/10.1016/j.ccell.2016.03.010

Scott, B. J., Quant, E. C., McNamara, M. B., Ryg, P. A., Batchelor, T. T., Wen, P. Y., & Bjs, M. (2010). Bevacizumab salvage therapy following progression in high-grade glioma patients treated with VEGF receptor tyrosine kinase inhibitors. *Neuro-Oncology*, *12*(6), 603–607. https://doi.org/10.1093/neuonc/nop073

Segerman, A., Niklasson, M., Haglund, C., Bergström, T., Jarvius, M., Xie, Y., … Westermark, B. (2016). Clonal Variation in Drug and Radiation Response among Glioma-Initiating Cells Is Linked to Proneural-Mesenchymal Transition. *Cell Reports*, *17*(11), 2994–3009. https://doi.org/10.1016/j.celrep.2016.11.056

Senn, J. J., Burel, S., & Henry, S. P. (2005). Non-CpG-containing antisense 2′-methoxyethyl oligonucleotides activate a proinflammatory response independent of toll-like receptor 9 or myeloid differentiation factor 88. *Journal of Pharmacology and Experimental Therapeutics*, *314*(3), 972–979. https://doi.org/10.1124/jpet.105.084004

Shalem, O., Sanjana, N. E., Hartenian, E., Shi, X., Scott, D. A., Mikkelsen, T. S., … Zhang, F. (2014). Genome-scale CRISPR-Cas9 knockout screening in human cells. *Science*, *343*(6166), 84–87. https://doi.org/10.1126/science.1247005

Shashidhar, S., Lorente, G., Nagavarapu, U., Nelson, A., Kuo, J., Cummins, J., … Foehr, E. D. (2005). GPR56 is a GPCR that is overexpressed in gliomas and functions in tumor cell adhesion. *Oncogene*, *24*(10), 1673–1682. https://doi.org/10.1038/sj.onc.1208395

Sheng, S. R., Wu, J. S., Tang, Y. L., & Liang, X. H. (2017). Long noncoding RNAs: Emerging regulators of tumor angiogenesis. *Future Oncology*, *13*(17), 1551–1562. https://doi.org/10.2217/fon-2017-0149

Shlush, L. I., Mitchell, A., Heisler, L., Abelson, S., Ng, S. W. K., Trotman-Grant, A., … Dick, J. E. (2017). Tracing the origins of relapse in acute myeloid leukaemia to stem cells. *Nature*, *547*(7661), 104–108. https://doi.org/10.1038/nature22993

Singer, R. A., Arnes, L., Cui, Y., Wang, J., Gao, Y., Guney, M. A., … Sussel, L. (2019). The Long Noncoding RNA Paupar Modulates PAX6 Regulatory Activities to Promote Alpha Cell Development and Function. *Cell Metabolism*, *30*(6), 1091-1106.e8. https://doi.org/10.1016/j.cmet.2019.09.013

Singh, A., & Settleman, J. (2010). EMT, cancer stem cells and drug resistance: An emerging axis of evil in the war on cancer. *Oncogene*, Vol. 29, pp. 4741–4751. https://doi.org/10.1038/onc.2010.215

Singh, S. K., Clarke, I. D., Terasaki, M., Bonn, V. E., Hawkins, C., Squire, J., & Dirks, P. B. (2003). Identification of a cancer stem cell in human brain tumors. *Cancer Research*, *63*(18), 5821–

5828.

Smith, C., & Ironside, J. W. (2007). Diagnosis and pathogenesis of gliomas. *Current Diagnostic Pathology*, *13*(3), 180–192. https://doi.org/10.1016/j.cdip.2007.04.002

Stein-O'Brien, G., Arora, R., Culhane, A., Favorov, A., Garmire, L., Greene, C., … Fertig, E. (2017). Enter the matrix: factorization uncovers knowledge from omics Names/Affiliations. *BioRxiv*, 196915. https://doi.org/10.1101/196915

Steinbichler, T. B., Dudás, J., Skvortsov, S., Ganswindt, U., Riechelmann, H., & Skvortsova, I. I. (2018, December 1). Therapy resistance mediated by cancer stem cells. *Seminars in Cancer Biology*, Vol. 53, pp. 156–167. https://doi.org/10.1016/j.semcancer.2018.11.006

Stupp, R., Mason, W. P., Van Den Bent, M. J., Weller, M., Fisher, B., Taphoorn, M. J. B., … Mirimanoff, R. O. (2005). Radiotherapy plus concomitant and adjuvant temozolomide for glioblastoma. *New England Journal of Medicine*, *352*(10), 987–996. https://doi.org/10.1056/NEJMoa043330

Su, J., Zhang, E., Han, L., Yin, D., Liu, Z., He, X., … Shen, D. (2017). Long noncoding RNA BLACAT1 indicates a poor prognosis of colorectal cancer and affects cell proliferation by epigenetically silencing of p15. *Cell Death and Disease*, *8*(3), e2665–e2665. https://doi.org/10.1038/cddis.2017.83

Subramanian, A., Tamayo, P., Mootha, V. K., Mukherjee, S., Ebert, B. L., Gillette, M. A., … Mesirov, J. P. (2005). Gene set enrichment analysis: A knowledge-based approach for interpreting genome-wide expression profiles. *Proceedings of the National Academy of Sciences of the United States of America*, *102*(43), 15545–15550. https://doi.org/10.1073/pnas.0506580102

Sud, N., Sharma, R., Ray, R., Chattopadhyay, T. K., & Ralhan, R. (2006). Differential expression of G-protein coupled receptor 56 in human esophageal squamous cell carcinoma. *Cancer Letters*, *233*(2), 265–270. https://doi.org/10.1016/j.canlet.2005.03.018

Sulman, E., Aldape, K., & Colman, H. (2008). Brain Tumor Stem Cells. *Current Problems in Cancer*, *32*(3), 124–142. https://doi.org/10.1016/j.currproblcancer.2008.02.004

Sun, Q., Tripathi, V., Yoon, J.-H., Singh, D. K., Hao, Q., Min, K.-W., … Prasanth, K. V. (2018). MIR100 host gene-encoded lncRNAs regulate cell cycle by modulating the interaction between HuR and its target mRNAs. *Nucleic Acids Research*, *46*, 10405–10416. https://doi.org/10.1093/nar/gky696

Tamimi, A. F., & Juweid, M. (2017). Chaper 8: Epidemiology and Outcome of Glioblastoma. In *Glioblastoma* (pp. 143–153). https://doi.org/10.15586/codon.glioblastoma.2017.ch8

Tan, J., Qiu, K., Li, M., & Liang, Y. (2015). Double-negative feedback loop between long non-coding RNA TUG1 and miR-145 promotes epithelial to mesenchymal transition and radioresistance in human bladder cancer cells. *FEBS Letters*, *589*(20), 3175–3181. https://doi.org/10.1016/j.febslet.2015.08.020

Tan, S. K., Pastori, C., Penas, C., Komotar, R. J., Ivan, M. E., Wahlestedt, C., & Ayad, N. G. (2018). Serum long noncoding RNA HOTAIR as a novel diagnostic and prognostic biomarker in glioblastoma multiforme. *Molecular Cancer*, *17*(1), 74. https://doi.org/10.1186/s12943-018-0822-0

Tanaka, S., Louis, D. N., Curry, W. T., Batchelor, T. T., & Dietrich, J. (2013). Diagnostic and therapeutic avenues for glioblastoma: No longer a dead end? *Nature Reviews Clinical Oncology*, *10*(1), 14–26. https://doi.org/10.1038/nrclinonc.2012.204

Tang, X., Jin, R., Qu, G., Wang, X., Li, Z., Yuan, Z., … Luo, J. (2013). GPR116, an adhesion G-protein-coupled receptor, promotes breast cancer metastasis via the Gαq-p63 Rho GEF-Rho GTPase pathway. *Cancer Research*, *73*(20), 6206–6218. https://doi.org/10.1158/0008-5472.CAN-13-1049

Tang, X. L., Wang, Y., Li, D. L., Luo, J., & Liu, M. Y. (2012). Orphan G protein-coupled receptors (GPCRs): Biological functions and potential drug targets. *Acta Pharmacologica Sinica*, *33*(3), 363–371. https://doi.org/10.1038/aps.2011.210

Taslaman, L., & Nilsson, B. (2012). A Framework for Regularized Non-Negative Matrix Factorization, with Application to the Analysis of Gene Expression Data. *PLoS ONE*, *7*(11), e46331. https://doi.org/10.1371/journal.pone.0046331

Tay, Y., Kats, L., Salmena, L., Weiss, D., Tan, S. M., Ala, U., … Pandolfi, P. P. (2011). Coding-independent regulation of the tumor suppressor PTEN by competing endogenous mRNAs. *Cell*, *147*(2), 344–357. https://doi.org/10.1016/j.cell.2011.09.029

Terskikh, A. V., Easterday, M. C., Li, N., Hood, L., Kornblum, H. I., Geschwind, D. H., & Weissman, I. L. (2001). From hematopoiesis to neuropoiesis: Evidence of overlapping genetic programs. *Proceedings of the National Academy of Sciences of the United States of America*, *98*(14), 7934–7939. https://doi.org/10.1073/pnas.131200898

Thakkar, J. P., Dolecek, T. A., Horbinski, C., Ostrom, Q. T., Lightner, D. D., Barnholtz-Sloan, J. S., … Lee Villano, J. (2014). Epidemiologic and Molecular Prognostic Review of Glioblastoma. *Cancer Epidemiol Biomarkers Prev*, *23*(10), 1985–1996. https://doi.org/10.1158/1055-9965.EPI-14-0275

Thanh Noi, P., & Kappas, M. (2017). Comparison of Random Forest, k-Nearest Neighbor, and Support Vector Machine Classifiers for Land Cover Classification Using Sentinel-2 Imagery. *Sensors (Basel, Switzerland)*, *18*(1). https://doi.org/10.3390/s18010018

The Cancer Genome Atlas Program - National Cancer Institute. (n.d.). Retrieved July 13, 2020, from https://www.cancer.gov/about-nci/organization/ccg/research/structural-genomics/tcga

Thi, L., Phi, H., Sari, I. N., Yang, Y.-G., Lee, S.-H., Jun, N., … Kwon, H. Y. (2018). *Cancer Stem Cells (CSCs) in Drug Resistance and their Therapeutic Implications in Cancer Treatment*. https://doi.org/10.1155/2018/5416923

Thiery, J. P., Acloque, H., Huang, R. Y. J., & Nieto, M. A. (2009). Epithelial-Mesenchymal Transitions in Development and Disease. *Cell*, *139*(5), 871–890. https://doi.org/10.1016/j.cell.2009.11.007

Vallon, M., & Essler, M. (2006). Proteolytically processed soluble tumor endothelial marker (TEM) 5 mediates endothelial cell survival during angiogenesis by linking integrin αvβ3 to glycosaminoglycans. *Journal of Biological Chemistry*, *281*(45), 34179–34188. https://doi.org/10.1074/jbc.M605291200

Van Der Oost, J., Westra, E. R., Jackson, R. N., & Wiedenheft, B. (2014). Unravelling the structural and mechanistic basis of CRISPR-Cas systems. *Nature Reviews Microbiology*, *12*(7), 479–492. https://doi.org/10.1038/nrmicro3279

Vance, K. W., Sansom, S. N., Lee, S., Chalei, V., Kong, L., Cooper, S. E., … Ponting, C. P. (2014). The long non-coding RNA Paupar regulates the expression of both local and distal genes. *The EMBO Journal*, *33*(4), 296–311. https://doi.org/10.1002/embj.201386225

Vance, Keith W., Sansom, S. N., Lee, S., Chalei, V., Kong, L., Cooper, S. E., … Ponting, C. P. (2014). The long non-coding RNA paupar regulates the expression of both local and distal genes. *EMBO Journal*, *33*(4), 296–311. https://doi.org/10.1002/embj.201386225

Veeravagu, A., Liu, Z., Niu, G., Chen, K., Jia, B., Cai, W., … Chen, X. (2008). Integrin αvβ3-targeted radioimmunotherapy of glioblastoma multiforme. *Clinical Cancer Research*, *14*(22), 7330–7339. https://doi.org/10.1158/1078-0432.CCR-08-0797

Verhaak, R. G. W., Hoadley, K. A., Purdom, E., Wang, V., Qi, Y., Wilkerson, M. D., … Hayes, D. N. (2010). Integrated Genomic Analysis Identifies Clinically Relevant Subtypes of Glioblastoma Characterized by Abnormalities in PDGFRA, IDH1, EGFR, and NF1. *Cancer Cell*, *17*(1), 98–110. https://doi.org/10.1016/j.ccr.2009.12.020

Vickers, T. A., & Crooke, S. T. (2015). The rates of the major steps in the molecular mechanism of RNase H1-dependent antisense oligonucleotide induced degradation of RNA. *Nucleic Acids Research*, *43*(18), 8955–8963. https://doi.org/10.1093/nar/gkv920

Wahlestedt, C. (2013, June). Targeting long non-coding RNA to therapeutically upregulate gene expression. *Nature Reviews Drug Discovery*, Vol. 12, pp. 433–446. https://doi.org/10.1038/nrd4018

Wang, L., Zhao, H., Xu, Y., Li, J., Deng, C., Deng, Y., … Zhang, Y. (2019). Systematic identification of lincRNA-based prognostic biomarkers by integrating lincRNA expression and copy number variation in lung adenocarcinoma. *International Journal of Cancer*, *144*(7), 1723–1734. https://doi.org/10.1002/ijc.31865

Wang, Q., Hu, B., Hu, X., Kim, H., Squatrito, M., Scarpace, L., … Verhaak, R. G. W. (2017). Tumor Evolution of Glioma-Intrinsic Gene Expression Subtypes Associates with Immunological Changes in the Microenvironment. *Cancer Cell*, *32*(1), 42-56.e6. https://doi.org/10.1016/j.ccell.2017.06.003

Wang, T., Ward, Y., Tian, L., Lake, R., Guedez, L., Stetler-Stevenson, W. G., & Kelly, K. (2005). CD97, an adhesion receptor on inflammatory cells, stimulates angiogenesis through binding integrin counterreceptors on endothelial cells. *Blood*, *105*(7), 2836–2844. https://doi.org/10.1182/blood-2004-07-2878

Wei, C., Zhang, X., He, S., Liu, B., Han, H., & Sun, X. (2017). MicroRNA-219-5p inhibits the proliferation, migration, and invasion of epithelial ovarian cancer cells by targeting the Twist/Wnt/β-catenin signaling pathway. *Gene*, *637*, 25–32. https://doi.org/10.1016/j.gene.2017.09.012

Wen, P. Y., & Kesari, S. (2008). Malignant gliomas in adults. *New England Journal of Medicine*, *359*(5), 492–507. https://doi.org/10.1056/NEJMra0708126

Wu, M. P., Doyle, J. R., Barry, B., Beauvais, A., Rozkalne, A., Piao, X., … Gussoni, E. (2013). G-protein coupled receptor 56 promotes myoblast fusion through serum response factor- and nuclear factor of activated T-cell-mediated signalling but is not essential for muscle development in vivo. *FEBS Journal*, *280*(23), 6097–6113. https://doi.org/10.1111/febs.12529

Wu, X., Cao, Z., Chen, H., Ou, Q., Huang, X., & Wang, Y. (2020). Downregulation of Linc-RNA

activator of myogenesis lncRNA participates in FGF2-mediated proliferation of human periodontal ligament stem cells. *Journal of Periodontology*, *91*(3), 422–427. https://doi.org/10.1002/JPER.19-0317

Xu, C., Zhang, Y., Wang, Q., Xu, Z., Jiang, J., Gao, Y., … Liu, H. (2016). Long non-coding RNA GAS5 controls human embryonic stem cell self-renewal by maintaining NODAL signalling. *Nature Communications*, *7*. https://doi.org/10.1038/ncomms13287

Xu, Na, Papagiannakopoulos, T., Pan, G., Thomson, J. A., & Kosik, K. S. (2009). MicroRNA-145 Regulates OCT4, SOX2, and KLF4 and Represses Pluripotency in Human Embryonic Stem Cells. *Cell*, *137*(4), 647–658. https://doi.org/10.1016/j.cell.2009.02.038

Xu, Ningbo, Liu, B., Lian, C., Doycheva, D. M., Fu, Z., Liu, Y., … Guo, H. (2018). Long noncoding RNA AC003092.1 promotes temozolomide chemosensitivity through miR-195/TFPI-2 signaling modulation in glioblastoma. *Cell Death & Disease*, *9*(12), 1139. https://doi.org/10.1038/s41419-018-1183-8

Xu, X., Guo, M., Zhang, N., & Ye, S. (2018). Telomeric noncoding RNA promotes mouse embryonic stem cell self-renewal through inhibition of TCF3 activity. *American Journal of Physiology - Cell Physiology*, *314*(6), C712–C720. https://doi.org/10.1152/ajpcell.00292.2017

Yan, H., Parsons, D. W., Jin, G., McLendon, R., Rasheed, B. A., Yuan, W., … Bigner, D. D. (2009). *IDH1* and *IDH2* Mutations in Gliomas. *New England Journal of Medicine*, *360*(8), 765–773. https://doi.org/10.1056/NEJMoa0808710

Yan, X., Zhang, D., Wu, W., Wu, S., Qian, J., Hao, Y., … Fan, Z. (2017). Mesenchymal Stem Cells Promote Hepatocarcinogenesis via lncRNA-MUF Interaction with ANXA2 and miR-34a. *Cancer Research*, *77*(23), OF1–OF13. https://doi.org/10.1158/0008-5472.CAN-17-1915

Yang, Q., Wan, Q., Zhang, L., Li, Y., Zhang, P., Li, D., … Du, Q. (2018). Analysis of LncRNA expression in cell differentiation. *RNA Biology*, *15*(3), 413–422. https://doi.org/10.1080/15476286.2018.1441665

Yang, Z. J., & Wechsler-Reya, R. J. (2007, January 1). Hit 'Em Where They Live: Targeting the Cancer Stem Cell Niche. *Cancer Cell*, Vol. 11, pp. 3–5. https://doi.org/10.1016/j.ccr.2006.12.007

Ye, B., Liu, B., Yang, L., Zhu, X., Zhang, D., Wu, W., … Fan, Z. (2018). LncKdm2b controls self-renewal of embryonic stem cells via activating expression of transcription factor Zbtb3 . *The EMBO Journal*, *37*(8). https://doi.org/10.15252/embj.201797174

Yip, A. M., & Horvath, S. (2007). Gene network interconnectedness and the generalized topological overlap measure. *BMC Bioinformatics*, *8*(1), 22. https://doi.org/10.1186/1471-2105-8-22

Yuan, J. hang, Yang, F., Wang, F., Ma, J. zhao, Guo, Y. jun, Tao, Q. fei, … Sun, S. han. (2014). A Long Noncoding RNA Activated by TGF-β promotes the invasion-metastasis cascade in hepatocellular carcinoma. *Cancer Cell*, *25*(5), 666–681. https://doi.org/10.1016/j.ccr.2014.03.010

Zeng, Y., & Cullen, B. R. (2002). RNA interference in human cells is restricted to the cytoplasm. *RNA*, *8*(7), 855–860. https://doi.org/10.1017/S1355838202020071

Zhang, B., & Horvath, S. (2005). A general framework for weighted gene co-expression network analysis. *Statistical Applications in Genetics and Molecular Biology*, *4*(1).

https://doi.org/10.2202/1544-6115.1128

Zhang, D., Zhou, H., Liu, J., & Mao, J. (2019). Long Noncoding RNA ASB16-AS1 Promotes Proliferation , Migration , and Invasion in Glioma Cells. *BioMed Research International*, *2019*, 10. https://doi.org/10.1155/2019/5437531

Zhang, Lei, Xue, Z., Yan, J., Wang, J., Liu, Q., & Jiang, H. (2019). LncRNA Riken-201 and Riken-203 modulates neural development by regulating the Sox6 through sequestering miRNAs. *Cell Proliferation*, *52*(3). https://doi.org/10.1111/cpr.12573

Zhang, Lixing, Qiang, J., Yang, X., Wang, D., Rehman, A. ur, He, X., … Liu, S. (2020). IL1R2 Blockade Suppresses Breast Tumorigenesis and Progression by Impairing USP15-Dependent BMI1 Stability. *Advanced Science*, *7*(1). https://doi.org/10.1002/advs.201901728

Zhang, M., Gao, C., Yang, Y., Li, G., Dong, J., Ai, Y., … Li, W. (2018). Long noncoding RNA Crnde/PRC2 participated in the radiotherapy resistance of human lung adenocarcinoma through targeting P21 expression. *Oncology Research*, *26*(8), 1245–1255. https://doi.org/10.3727/096504017X14944585873668

Zhang, T., Hu, H., Yan, G., Wu, T., Liu, S., Chen, W., … Lu, Z. (2019). Long Non-Coding RNA and Breast Cancer. *Technology in Cancer Research & Treatment*, *18*. https://doi.org/10.1177/1533033819843889

Zhang, Y., He, Q., Hu, Z., Feng, Y., Fan, L., Tang, Z., … Zhang, L. (2016). Long noncoding RNA LINP1 regulates repair of DNA double-strand breaks in triple-negative breast cancer. *Nature Structural and Molecular Biology*, *23*(6), 522–530. https://doi.org/10.1038/nsmb.3211

Zhang, Z., Sun, L., Zhang, Y., Lu, G., Li, Y., & Wei, Z. (2018). Long non-coding RNA FEZF1-AS1 promotes breast cancer stemness and tumorigenesis via targeting miR-30a/Nanog axis. *Journal of Cellular Physiology*, *233*(11), 8630–8638. https://doi.org/10.1002/jcp.26611

Zhou, Y. H., Wu, X., Tan, F., Shi, Y. X., Glass, T., Liu, T. J., … Yung, W. K. A. (2005). PAX6 suppresses growth of human glioblastoma cells. *Journal of Neuro-Oncology*, *71*(3), 223–229. https://doi.org/10.1007/s11060-004-1720-4

Zhu, J., Chen, S., Yang, B., Mao, W., Yang, X., & Cai, J. (2019). Molecular mechanisms of lncRNAs in regulating cancer cell radiosensitivity. *Bioscience Reports*, *39*(8). https://doi.org/10.1042/BSR20190590

Zhuang, C., Yuan, Y., Song, T., Wang, H., Huang, L., Luo, X., … Zhang, T. (2017). miR-219a-5p inhibits breast cancer cell migration and epithelial-mesenchymal transition by targeting myocardin-related transcription factor A. *Acta Biochimica et Biophysica Sinica*, *49*(12), 1112–1121. https://doi.org/10.1093/ABBS/GMX114

LIST OF FIGURES

LIST OF TABLES